Master's thesis

NTNU
Norwegian University of Science and Technology
Faculty of Engineering
Department of Marine Technology

Nora Solheim Stuedal

Methods for Mapping of Zooplankton using Optical Sensor Technology

Master's thesis in Marine Technology
Supervisor: Asgeir J. Sørensen
Co-supervisor: Håvard S. Løvås, Emlyn J. Davies
June 2021

NTNU
Norwegian University of
Science and Technology

Nora Solheim Stuedal

Methods for Mapping of Zooplankton using Optical Sensor Technology

Master's thesis in Marine Technology
Supervisor: Asgeir J. Sørensen
Co-supervisor: Håvard S. Løvås, Emlyn J. Davies
June 2021

Norwegian University of Science and Technology
Faculty of Engineering
Department of Marine Technology

NTNU
Norwegian University of
Science and Technology

NTNU Trondheim
Norwegian University of Science and Technology
Department of Marine Technology

MASTER OF TECHNOLOGY THESIS DEFINITION (30 SP)

Name of the candidate:	Nora Solheim Stuedal
Field of study:	Marine Cybernetics
Thesis title (Norwegian):	Methods for mapping of zooplankton using optical sensor technology
Thesis title (English):	Metoder for kartlegging av dyreplankton ved bruk av optisk sensorteknologi

Background

Food production today is responsible for one-quarter of the world's greenhouse gas emissions, where one of the main reasons is that we harvest from the top of the food chain. Also, half of the world's habitable land is used for agriculture. The ocean, on the other hand, hosts a large number of species such as mesopelagic fish, krill, copepods, and others in the lower tropic levels, which are either not harvested or only marginally utilized. While these species can provide a huge potential for commercial harvesting they also play a key role in the marine ecosystems, and over-fishing and destruction of these ecosystems would have severe consequences. Hence, with the intention of sustainable harvesting of these species, proper knowledge about the amount, life cycles and their vulnerability need to be developed. As many of these species are found in huge spatial areas, as well as on large depths and in remote environments, new technology is necessary to obtain this knowledge. As a step towards future solutions, this project will be a part of NTNU AMOS and SFI Harvest in cooperation with SINTEF Ocean and industry partners to develop methods, sensors and sensor-carrying platforms for imaging and classifications of organisms, especially copepods, in the ocean.

Scope of Work

1. Present background material to provide information and relevant references on:
   - Zooplankton species *Eurasia superba* and *Calanus finmarchichus.*
   - Relevant sensor-carrying platforms for remote and in situ operations.
   - Optical imaging methods based Silhouette Camera (SilCam) and Hyperspectral Imaging (HSI) sensor technology. Their relevance, advantages, and disadvantages for mapping of small organisms such as krill and copepods should be addressed.
   - Theory of fundamentals of light and spectroscopy. This should build a foundation for planning and performing relevant experiments of optical imaging of zooplankton.
2. Propose a method to image copepods using a hyperspectral imager in a laboratory environment.
3. Perform the experiments with hyperspectral imaging of copepods. Analyze the resulting data using several approaches.
4. Report the results.

Specifications

The student shall at startup provide a maximum 2-page week plan of work for the entire project period, with main activities and milestones. This should be updated on a monthly basis in agreement with supervisor.

Every weekend throughout the project period, the candidate shall send a status email to the supervisor and co-advisors, providing two brief bulleted lists: 1) work done recent week, and 2) work planned to be done next week.

The scope of work may prove to be larger than initially anticipated. By the approval from the supervisor, described topics may be deleted or reduced in extent without consequences with regard to grading.

The candidate shall present personal contribution to the resolution of problems within the scope of work. Theories and conclusions should be based on mathematical derivations and logic reasoning identifying the steps in the deduction.

The report shall be organized in a logical structure to give a clear exposition of background, problem/research statement, design/method, analysis, and results. The text should be brief and to the point, with a clear language. Rigorous mathematical deductions and illustrating figures are preferred over lengthy textual descriptions. The report shall have

font size 11 pts., and it is not expected to be longer than 70 A4-pages, 100 B5-pages, from introduction to conclusion, unless otherwise agreed. It shall be written in English (preferably US) and contain the elements: Title page, abstract, preface (incl. description of help, resources, and internal and external factors that have affected the project process), acknowledgement, project definition, list of symbols and acronyms, table of contents, introduction (project background/motivation, objectives, scope and delimitations, and contributions), technical background and literature review, problem formulation, method, results and analysis, conclusions with recommendations for further work, references, and optional appendices. Figures, tables, and equations shall be numerated. The original contribution of the candidate and material taken from other sources shall be clearly identified. Work from other sources shall be properly acknowledged using quotations and a Harvard citation style (e.g. natbib Latex package). The work is expected to be conducted in an honest and ethical manner, without any sort of plagiarism and misconduct, which is taken very seriously by the university and will result in consequences. NTNU can use the results freely in research and teaching by proper referencing, unless otherwise agreed.

The thesis shall be submitted with an electronic copy to the main supervisor and department according to NTNU administrative procedures. The final revised version of this thesis definition shall be included after the title page. Computer code, pictures, videos, data series, etc., shall be included electronically with the report.

Start date: 15th of January 2021 **Due date:** 10th of June 2021

Supervisor: Professor Asgeir J. Sørensen
Co-advisor(s): Håvard S. Løvås, Emlyn J. Davies

Trondheim, 10.06.2021

Asgeir J. Sørensen
Supervisor

Preface

When Asgeir J. Sørensen proposed the opportunity to work with identification and mapping of microorganisms, I was inspired by the forward-looking and sustainable focus of the topic. With an interest in sustainability, I saw my opportunity to focus my degree towards developing technology for sustainable harvesting, which potentially could be of huge importance in the future. However, this opportunity meant leaving most of my previous knowledge from my studies behind and immersing myself in entirely new topics. As a result, I have discovered a new field of interest in the combination of biology and technology.

The main goal of the study is to explore how marine organisms in lower trophic levels can be mapped, identified, and controlled more accurately using imaging technology. The thesis can roughly be divided into two parts. The first part examines present sensor technologies, sensor-carrying platforms, and their future potential, from remote aerial imaging to *in situ* identification using underwater robotics. The second part is a research-based process, including several laboratory experiments and data analysis.

The Master's thesis completes the fulfillment of the Master's degree in Marine Technology, with a specialization in Marine Cybernetics, at the Norwegian University of Science and Technology (NTNU). It is the only work in the course TMR4930 of 30 ETC, and is to a large degree a continuation of the pre-work done in the Project thesis the previous fall. Simultaneously with writing the Project thesis, I took the two module courses *TMR09- Underwater Technology* and *TMR06- Autonomous Marine Systems* , which both provided knowledge and understanding of the task in general. Finally, with a lot of inspiration and guidance along the way, this thesis is now completed. The work presented is solely done by me, unless otherwise is stated in the text.

Trondheim, June 10, 2021

Nora Solheim Stuedal

Acknowledgements

When I first began my work for the Project thesis the previous fall, I had nearly no background knowledge about the topic and technology of my chosen thesis. Therefore, I would like to express my gratitude to my supervisor Professor Asgeir J. Sørensen, for giving me the confidence and trust to embrace the task. I highly appreciate his guidance throughout the semester and the drive and enthusiasm for the field he has shared with me.

I would also like to thank my co-supervisors, Ph.D. candidate Håvard S. Løvås and Dr. Emlyn J. Davies from SINTEF Ocean. Løvas has assisted me in organizing and conducting the laboratory experiments of the thesis and has always been available for help with data analysis and understanding of the general theory. Davies has shared with me his work of the SilCam development and connected me to relevant people and sources of information.

For the experiments to take place, several additional people were required. I would like to thank Dag Altin who provided copepods for both experiments and shared his expertise on the creatures. Thank you to Raghnild I. Jacobsen from Kavli Institute for Systems Neuroscience and Centre for Neural Computation, NTNU, for providing copepods from Trondheimsfjorden for the second experiment. I would also like to thank Ph.D. candidate David Williamson for his willingness to participate in the experiments and share his knowledge of the hyperspectral imager.

In the fall, I was given the opportunity to participate in a field trip to the Sletvik field station with a biology class. Here, I was introduced to Professor Geir Johnsen and Ph.D. candidate Aksel Alstad Mogstad, who shared with me their knowledge and enthusiasm for the biology-technology field. I would like to thank everyone who made this field trip possible for me.

Summary

Today, food production is responsible for one-quarter of the world's greenhouse gas emissions, much due to the harvesting from the top of the food chain. Harvesting in the lower trophic levels of the ocean could provide an enormous potential for sustainable harvesting. In the lower trophic levels, zooplankton such as *Eurasia superba* and *Calanus finmarchichus* are found, which are sought after for their high content of marine nutrients. However, these species hold a key role in their ecosystem, and close monitoring and increased knowledge are necessary to ensure sustainable harvesting. A solution for achieving good stock estimates over the vast ocean areas could be remote sensing followed by *in situ* observations performed by autonomous or remotely operated underwater vehicles.

This thesis aims to describe complementary technology for obtaining increased knowledge and mapping of zooplankton. This includes a review of already existing technology within sensors and sensor-carrying platforms and remote sensing by the sense of optical imaging. Optical imaging of the mentioned species is attractive due to their red color, which is a result of their high content of the red pigment *astaxanthin*. The report investigates if this red pigment makes the species recognizable through spectroscopy, which is the analysis of how light interacts with materials, measured in intensity over wavelengths. These studies of spectroscopy are performed through several laboratory experiments with hyperspectral imaging of alive individuals of *C.fimarchichus*, where the aim is to discover significant spectral signatures. These signatures can then be used as a "ground truth" for future remote sensing purposes.

The laboratory experiments are conducted with two different groups of *C.finmarchichus*. One group of individuals is obtained from a stock held at SINTEF's facilities in Trondheim, while the second group of individuals was isolated from Trondheimsfjorden a week before the last experiment took place. The different individuals are imaged with both backlighting and overhead lighting to obtain results of both transmittance and reflectance, respectively. The data analyzes are performed with two different methods. The first approach involves obtaining the spectral signature of selected parts of the individual. The second approach is to compute an average spectrum over each individual to provide a more realistic view for remote sensing of large patches of the species in the ocean.

The majority of the results show distinct spectral signatures that closely match the absorption spectrum of astaxanthin. Some areas of the individuals are especially consistent for nearly all examples, confirming the work's potential. However, larger variation is experienced in other areas, in addition to faint spectral signatures of the average spectra. This could result from inappropriate chosen imager settings or oversimplified analyzes of complicated 3D structures. Although the overall results were satisfactory, the study has room for improvement. Moreover, the general potential for future work is both large and exciting.

Sammendrag

Den Norske Regjering presenterte i 2017 en havstrategi for fremtidig bærekraftig verdiskaping av havets ressurser. Strategien beskriver det uutnyttede potensialet for høsting på lavere trofiske nivåer, som også er godt kjent i havforsknings- og fiskerimiljøet. Dyreplankton som *Eurasia superba* (Antarktisk krill) og *Calanus finmarchichus* (Raudåte) er ettertraktet for sitt høye innhold av marine næringsstoffer, og utgjør store potensialer for kommersielt fiske. Samtidig har disse artene en nøkkelrolle i sitt økosystem, henholdsvis Antarktis og Nord-Atlanteren, og overvåkning og økt kunnskap er nødvendig for å garantere bærekraftig fiske. En løsning for å oppnå gode bestandsestimater over de enorme havområdene, kan være fjernmåling etterfulgt av *in situ* observasjoner gjort av autonome eller fjernstyrte undervannsroboter.

Denne rapporten forsøker å beskrive komplementerende teknologi for å kartlegge og skaffe økt kunnskap om dyreplankton. Dette inkluderer en gjennomgang av allerede eksisterende teknologi innenfor sensorer og sensorbærende plattformer, og fjernmåling i form av optisk bildeteknologi. Optisk avbildning av de nevnte artene er attraktivt på grunn av den rødlige fargen de har, som kommer av et høyt innhold av det røde pigmentet *astaxanthin*. I rapporten undersøkes det om dette pigmentet gjør det mulig å gjenkjenne artene ved bruk av spektroskopi, som er en analyse av hvordan lys oppfører seg sammen med et materiale målt i intensitet over bølgelengder. Dette studiet utføres ved flere laboratorieforsøk med hyperspektral avbildning av levende raudåte, der målet er å avdekke signifikante spektrale signaturer, sammenlignbart med menneskers fingeravtrykk, som kan brukes som en "fasit" til fremtidige fjernmålingsformål.

Laboratorieeksperimentene er utført med to ulike grupper raudåte. En gruppe individer er fra en bestand som oppbevares på SINTEFs lokaler i Trondheim, mens den andre gruppen ble isolert fra Trondheimsfjorden en uke før det siste eksperimentet. De ulike individene er avbildet med både bakbelysning og overbelysning for å oppnå resultater for henholdsvis transmittans og reflektans. Dataanalysen fokuserer i hovedsak på to ulike metoder. Den ene er å finne spektralsignaturen for bestemte områder av raudåten, og sammenligne dette med absorbsjonsspekteret til astaxanthin. Den andre metoden er å beregne et gjennomsnittspekter over hver raudåte for å presentere et mer realistisk perspektiv for fjernmåling av store svermer i havet.

Stort sett viser resultatene tydelige spektrale signaturer som korresponderer svært bra med astaxanthins absorpsjonsspekter. Noen områder i raudåten er spesielt tydelige og konsekvente for nesten alle eksempler, noe som bekrefter potensialet ved arbeidet. Likevel observeres det også en del variasjon i andre områder, i tillegg til svake spektrale signaturer for gjennomssnittsspektrene. Dette kan være et resultat feil valg av kamerainnstillinger, eller en overforenklet analyse av kompliserte 3D strukturer. Selv om resultatene stort sett er tilfredsstillende, har arbeidet rom for forbedring. I tillegg er potensialet for fremtidig arbeid både stort og spennende.

Contents

List of Figures

List of Abbreviations

AUV	Autonomous Underwater Vehicle
HSI	Hyperspectral Imaging
OOI	Object Of Interest
ROV	Remotely Operate Vehicle
UAV	Unmanned Aerial Vehicle
UHI	Underwater Hyperspectral Imaging
UUV	Unmanned Underwater Vehicle

Chapter 1

Introduction

As a step towards future solutions for sustainable harvesting in lower trophic levels, this project will be a part of NTNU AMOS and SFI Harvest in cooperation with SINTEF Ocean and industry partners. The overall purpose which this thesis contributes to is to develop methods, sensors, and sensor-carrying platforms for mapping, monitoring, and classification to ensure sustainable harvesting.

This chapter addresses the "big picture" motivating the work of the thesis by explaining the background and surrounding topics. This is followed by a defined research question and an overview of the structure of the thesis.

1.1 Motivation

Today, food production is responsible for one-quarter of the world's greenhouse gas emissions (Ritchie, 2019a), much due to our harvesting from the top of the food chain. Furthermore, half of the world's habitable land is used for agriculture (Ritchie, 2019b). On the other hand, the ocean hosts a large number of species such as mesopelagic fish, krill, copepods, and others in the lower tropic levels, which are either not harvested or only marginally utilized. While these species can provide a huge potential for commercial harvesting, they also play a key role in the marine ecosystem, and over-fishing and destruction of these ecosystems could have catastrophic consequences. Hence, with the intention of sustainable harvesting of these species, proper knowledge about the amount, life cycles, and vulnerability of the species needs to be obtained. As many of these species are found in huge spatial areas, as well as on large depths and in remote environments, new technology is necessary to obtain this knowledge.

1.1.1 Marine Ecosystem

The ocean is the largest ecosystem on the planet, covering more than 99% of its habitable space (Oceana, n.d.). It can be argued that all species rely on this ecosystem, directly or indirectly, and that disrupting it can provide enormous consequences. As shown in Figure 1.1, the largest amount of energy is stored in the two bottom trophic levels. Nevertheless, humans harvest from the two top ones. Only 10 % of all energy is carried on to the next level in the ecosystem, which leaves 90 % unexploited.

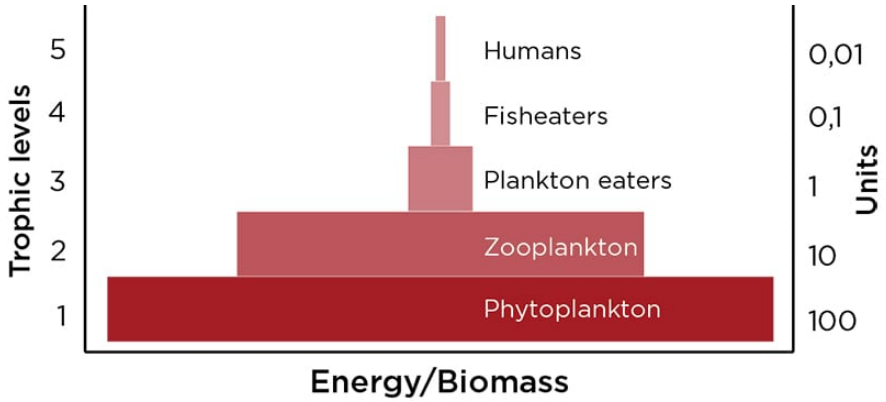

FIGURE 1.1: Distribution of energy/biomass over the ocean trophic levels. Courtesy of Calanus (n.d.).

Figure 1.1 illustrates how phytoplankton are the foundation of nearly all organic production in water (Throndsen, 2018). Because phytoplankton require sunlight to perform photosynthesis, they are found in the upper ocean, commonly known as the epipelagic zone. This zone extends from the surface to 200 meters and is also where most zooplankton are situated to feed on phytoplankton (Oceana, n.d.). Moreover, the entire ecosystem's depth is by scientists divided into zones based on how much light the zone receives. As the epipelagic zone only reaches 200 m, the vast majority of the ocean is entirely dark, except for light produced by living organisms, known as bioluminescence.

The amount of plankton in the ecosystem is strongly regulated by the seasons, where the most significant changes are due to the plankton bloom. A plankton bloom is a spontaneous increase in microalgae growth and often occurs in coastal waters in the spring. A bloom of zooplankton follows the phytoplankton bloom, and it is this production that forms the economic basis for the harvestable fishery resources.

Harvesting from lower trophic levels is not a new idea. Already in 1977, NASA published a forward-looking report called "The Role of Aerospace Technology in Agriculture" (McRee, 1977), mentioning harvesting of Antarctic krill; *Eurasia superba* as a solution to feed a ballooning world population. However, harvesting of zooplankton species has to a large degree been avoided. This is partly because of their lack of financial value and the general awareness of their importance in the ecosystem. Hence, from NASA's article in 1977 to today's reasons for minimal harvesting and strict quotas, the same statement is used; large-scale harvesting of species in lower trophic levels can not be conducted until adequate knowledge about the species' way of life is obtained.

1.1.2 Plastic Pollution

The problem of plastic pollution is well-known. Every year, 381 million tonnes of plastic are produced, and the production is projected to nearly double the next 10-15 years (Geyer et al., 2017). At least 8 million tonnes of these end up in the ocean (IUCN, n.d.) in a large variety of compositions and sizes. Many companies, organizations, and volunteers are eager to contribute by cleansing beaches and the large garbage patches of plastic floating around in the ocean. However, microplastics can not be cleaned this way. In 2014, Van Sebille et al. (2015) estimated that 15 to 51 trillion particles of

microplastics were hovering the seas. 80% of microplastics found in the ocean originates from human-made, land-based sources, such as bags and bottles (Jambeck et al., 2015). As microplastics are challenging to locate and clean, they will remain in the ocean, where the main issue is ingestion of marine biota. The small size of the microplastics means that they can be ingested by tiny organisms like zooplankton and further bio-accumulated through the trophic levels, affecting the larger species.

It is assumed that once the technology of remote hyperspectral imaging is well established, it can contribute in many areas, and detection of microplastics is one of them. Dahl et al. (2019) evaluates this by obtaining spectral signatures of different types of microplastics in a laboratory setting, which, for the same reason as proposed in this thesis, can facilitate a library of spectral signatures available for remote classification using hyperspectral imaging.

1.2 Related Work

As this project is a part of the NTNU AMOS and SINTEF Ocean community, several related projects contribute to a common goal of obtaining knowledge of the marine ecosystem in Norwegian waters. Underwater hyperspectral imaging (UHI) is often used, where hyperspectral imaging is used under water to capture spectral signatures of desired objects, mostly located at the sea-floor.

1.2.1 Sensor-Carrying Platforms and UHI

Further advancements of a UHI prototype developed in Johnsen et al. (2013) are described in Johnsen et al. (2016), where the use of UHI deployed on a remotely operated vehicle is tested. The method aims to obtain a more automated identification, mapping, and monitoring of bio-geo-chemical objects of interest (OOI). The information obtained by using this method is used to provide a photomosaic of the area of interest, where OOIs can be decided using machine learning technology, namely classification.

Pettersen et al. (2014) uses UHI to elucidate species-specific absorption and corresponding reflection signatures of marine organisms on the seafloor. By using an existing collection of signatures obtained in a laboratory setting, it can be shown that the absorption spectra and the hyperspectral reflection spectra are inversely related for the investigated organisms. These findings are highly relevant for this thesis, as the same method is applied with comparing copepods' spectra to the absorption spectrum of *astaxanthin*.

UHI has also successfully been applied to marine archeology. Ødegård et al. (2018) presents UHI as a new tool for marine archaeology, where spectral signatures representative of materials likely to be present at wreck sites are found. The study uses knowledge obtained in Ødegård et al. (2016), where unmanned underwater vehicles (UUV) and sensors are considered as capable for non-intrusive marine archaeology surveys. Similarly, Mogstad et al. (2020) presents a non-intrusive shipwreck survey using multiple complementary remote sensing techniques, including unmanned vehicles (UUV) and optical sensors. Detailed photogrammetry successfully provided a 3D model of the wreck, where UHI complemented the model with optical information combining archaeology and biology, as discovered in Ødegård et al. (2018).

1.2.2 Mapping of Plankton

Recently, there has been an increasing interest in using the mentioned studies' concepts also for investigation of plankton. NTNU has embraced this task with the AILARON project, led by Anette Stahl, NTNU. It is a multidisciplinary project focused on plankton-based imagery using advanced environmental- and optical sensors, machine learning, and hydrodynamics (NTNU, n.d.).

As a part of this project, an interdisciplinary group performed an excursion for estimating the amount of phytoplankton outside the island Mausund in Trøndelag during the plankton blooming in April 2021 (Bazilchuk, 2021). For this study, hyperspectral imagers were mounted on drones and small airplanes for aerial amount-estimations of phytoplankton, combined with satellite images for estimates of chlorophyll A. A lightweight autonomous underwater vehicle (LAUV) was used for gathering samples and following the blooming patches, which is done by the use of advanced technology of data processing and machine learning. The LAUV is the AILARON project's main tool, and it is continuously improved for future adaptive sampling purposes.

Outside the NTNU environment, there are also recent related developments. One example is the Mesobot, developed by Yoerger et al. (2018). It is an autonomous underwater vehicle (AUV) developed for observing slow-moving targets in the midwater ocean, including zooplankton. Using stereo cameras, lights, and on-board computing resources, the vehicle is designed to image and follow animals and particles to a depth of 1000 meters. This makes the concepts of the *Mesobot* highly relevant for further investigation within this field. Figure 1.2 shows a typical operation of the *Mesobot*, where it is teleoperated through a tether by a human pilot until locating a suitable target. Then, the tether is released and the vehicle tracks the target autonomously.

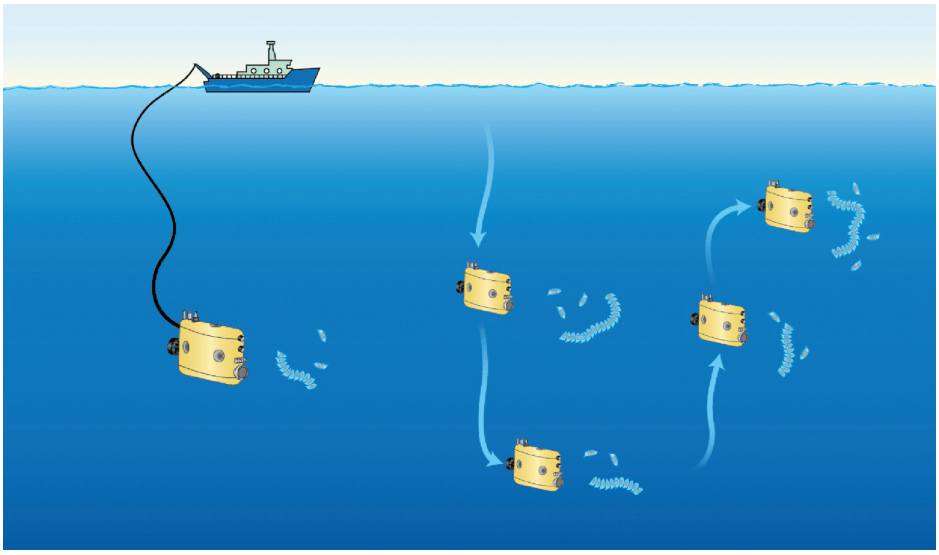

FIGURE 1.2: A typical *Mesobot* tracking mission. Courtesy of Yoerger et al. (2018).

1.3 Field Trials at Slettvik

In the course BI3070 - "Enabling technology for marine ecological studies and marine science", led by Professor Geir Johnsen, NTNU, a field trip was arranged as a part of the lecture plan to give the students an insight into planning, preparation, and execution of marine operations using advanced sensor technology and underwater vehicles. This field trip covered several of the prospects in this thesis, and for increased motivation and understanding of the task, I was allowed to participate.

The excursion was located at Sletvik Field Station in Hopavågen, Agdenes. It is situated beside a semi-enclosed lagoon which is sheltered from wind and waves. As a result, the lagoon becomes a mesocosm, which is an outdoor experimental system for studying the natural environment under controlled conditions, ideal for studying interrelations between physical, chemical, and biological processes.

Several physical operations were conducted in the lagoon. Ph.D. candidates Håvard S. Løvås, Aksel Mogstad, and Jens E. Bremnes had designed a mini remotely operated vehicle (ROV) consisting of two BluEye ROVs (BluEye, n.d.) and several sensors, including a hyperspectral imager. Their goal was to perform UHI of the sea bottom. Being the first time they tried their ROV in an *in situ* operation, a couple of days were used to fix errors and unforeseen issues, but the mapping operations were successfully conducted in the end. Figure 1.3 shows some images taken during the operation.

(A) Bremnes controlling the mini ROV.

(B) Mogstad monitoring the UHI data flow

FIGURE 1.3: UHI mapping using a mini ROV.

The biology class went snorkeling to find different species from the lagoon for analysis in the saltwater laboratory. Here, a spectrometer was used to obtain their spectral signatures to use these as "ground truths" for further work with the UHI. The goal, in the end, is to be able to recognize and identify these species remotely. Figure 1.4 shows how the different species were stored and analyzed with a spectrometer.

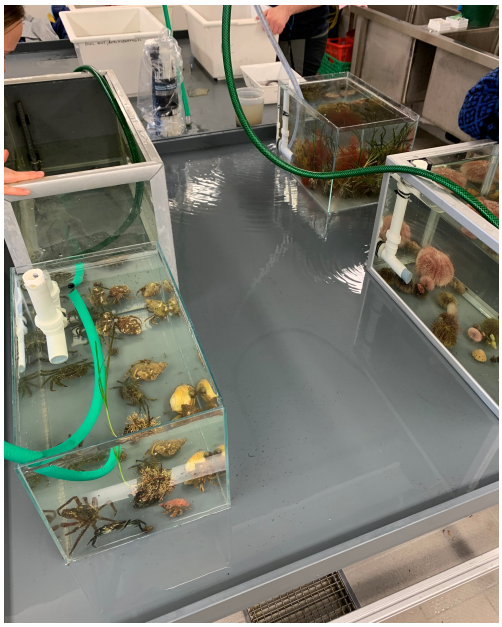

(A) Aquariums with a flow of saltwater containing different species.

(B) Mogstad obtaining spectral signatures with a spectrometer.

FIGURE 1.4: Images from the saltwater laboratory.

For the aim of my thesis, I wanted to embrace the opportunity and find some individuals of *C.finmarchichus* in the tidal current at the entrance of Hopavågen. This was done by placing a plankton net in the current. The current was strong and most of the water flushed out of the net through the "entrance" and not through the filter. Therefore, only a few very tiny individuals were captured and taken to the laboratory for inspection under the microscope.

(A) Plankton net

(B) Collecting individuals of *Calanus finmarchichus* in the current.

FIGURE 1.5: Attempt of collecting *C.finmarhichus* individuals.

Although the field trip did not provide any results for the thesis, it was an educational and motivating experience. I was introduced to several fieldwork concepts, including

long working days, continuous flow of operations, changed schedules, failed attempts, and teamwork towards success. This experience provided knowledge of the complexity of field trials and *in situ* operations that I would not have obtained otherwise.

1.4 Research Question

The aim of this thesis is to answer the following question: *What methods can be used for obtaining more information about zooplankton such as Eurasia superba and Calanus finmarchichus?* This will be studied through the more specific objectives listed below,

1. What optical sensors and sensor-carrying platforms can be used for imaging and mapping of zooplankton?
2. How can further utilizing the fundamentals of light increase the information obtained by the optical sensors?

1.5 Main Contributions

The experimental contribution of this thesis is a thorough analysis of the spectra of *Calanus finmarchichus* in different light settings, contributing to a library of spectral signatures which can be useful for future purposes. However, the thesis also describes and compares several existing technologies for remote and *in situ* imaging. The reader can find information about the following,

- A description of the optical sensors Silhuette Camera (SilCam) and hyperspectral imager, and a brief explanation of how they can be used in their respective type of operation, being *in situ* and remote sensing.
- A description of several sensor-carrying platforms and a brief explanation of how they are suited for the purpose of the thesis.
- A description of the fundamentals of light and how light can be utilized to a greater extent with a focus on spectroscopy.

1.6 Thesis Outline

The chapters in this thesis are structured as follows:

CHAPTER 2

Chapter 2 provides background information of zooplankton with a focus on *E.superba* and *C.finmarchichus*. The overall goal of the chapter is to inform the reader about why it is desired to establish harvesting of zooplankton, and why technology for increased knowledge is necessary to make the industry sustainable.

CHAPTER 3

Chapter 3 elucidates on existing technology of remote and *in situ* sensors and sensor-carrying platforms. The concepts presented are all performing different types of operations and complement each other with the complex goal of mapping and monitoring zooplankton.

CHAPTER 4

Chapter 4 covers the fundamentals of light and spectroscopy. As optical imaging is a large part of the thesis, understanding of light conditions are crucial for obtaining satisfactory data both over and under water.

CHAPTER 5

Chapter 5 presents the technology of hyperspectral imaging. It addresses both the system optics of a spectrometer and the imaging method it uses.

CHAPTER 6

Chapter 6 describes the experimental approach of the study. This includes several laboratory experiments and how the data retrieved from the measurements are processed and analyzed.

CHAPTER 7

Chapter 7 presents the results obtained from the laboratory experiments. They are structured by the approaches described in Chapter 6, and contain small comments of the observations.

CHAPTER 8

Chapter 8 discusses the experimental approach of the thesis. This includes a thorough discussion of the laboratory experiments, data analyzes, and the obtained results.

CHAPTER 9

Chapter 9 provides a conclusion of the performed work and closes the circle by answering the thesis' research question. It also proposes ideas and recommendations for further work on the topic.

Chapter 2

Zooplankton

Food webs consist of several trophic levels, where animals are ranked based on how many steps they are above the primary producers at the web base. The primary producers are usually phytoplankton, fed on by zooplankton in the next level. Zooplankton include all marine animals that roam freely in the water masses, but often with a vertical diel migration depending on the light conditions.

This chapter presents the two species *Eurasia Superba*, Latin for Antarctic krill, and *Calanus finmarchichus* (in Norwegian called *Raudåte*). These species have many similarities in both biology and distribution, as well as being harvested for the same commercial reasons. From the point of view where large-scale harvesting of these species is considered, the techniques presented in this thesis are highly relevant for them both. Common to these species is that they are a pivotal species in their respective ecosystems, providing energy for larger predators from microscopic algae. Hence, overfishing or interrupting the natural ecosystem could cause huge consequences, and increased knowledge of both species is vital if large-scale fishing is intended.

Krill are shrimp-like, planktonic crustaceans, averaging at about 3,5 cm in length (Repstad, 2019). Krill are found in all oceans, but the Antarctic krill is assumed to be the most abundant species and is hence the species objected to most research and exploitation.

C.finmarchichus is a key species in the ecosystem of the North Atlantic, frequently constituting more than 50 % of the mesozooplankton biomass (Melle et al., 2014). It is a large copepod in the Calanus genus, and of the four Calanus species in Norwegian waters, *C.finmarchichus* is the most dominating (Borge, 2017). For the laboratory experiment of this thesis, *C.finmarchichus* individuals are used, and represent the main focus of this thesis.

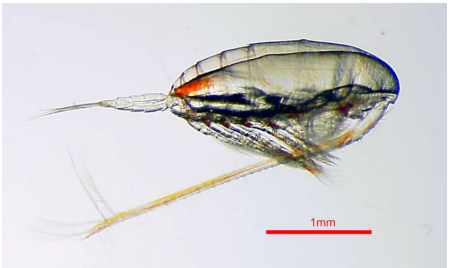

(A) Image of *C.finmarchichus*. Courtesy of Dag Altin, SINTEF

(B) Image of *Eurasia superba*l. Courtesy of Krafft (2019)

FIGURE 2.1: *C.finmarchichus* and *Eurasia superba*

2.1 Distribution

Both krill and *C.finmarhichus* are gregarious and found for most of their lives in pelagic swarms or schools. It is this swarming habit that has made them attractive to commercial fisheries (Nicol et al., 1987). Their appearance in the surface areas depends on the wind and currents, ebb and flow, and the time of day as they perform dial migration driven by the light and climate. Diel migration is a common movement for zooplankton, where they come up to the surface in the dusk and go back deeper in the morning to protect themselves from predators. For both species, the abundance is highly variable between and within years, increasing the complexity of obtaining a sufficient understanding. There is today an insufficient amount of knowledge to provide a certain number of the total biomass of either species. Because of their swarming behavior, obtaining more precise mapping methods is crucial before increased fishing occurs. With increased knowledge, harvesting can be more effective and with a decreased possibility of accidents, bi-catch, and non-sustainable fishing.

2.1.1 Distribution of Antarctic Krill

Historically, the primary krill habitat was thought to be within the top 200 m of the water column; however, there is increasing evidence of krill regularly occurring near the seafloor at abyssal depth. Technological developments are making it possible to reveal evidence of a vast amount of krill biomass in places scientists never suspected. It is yet to understand the dynamics and extent of those deep krill and their relation to the surface population (Jones et al., 2015).

The yearly variability of the amount of krill is driven mostly by how many young krill enter the population each year, which can be affected by the amount of sea ice. Hence, with the ongoing climate change, the sea-ice amount and other ecological changes in the Antarctic environment must be evaluated and controlled closely for harvesting to be sustainable. On average, the biomass in the Antarctic has been suggested to fall within the range of 60 to 420 million tonnes, with a current best estimate of 389 million tonnes (Jones et al., 2015). However, some sources claim far higher estimates, with numbers between 125 million and 6 billion tonnes in the waters around Antarctica (National Geographic, n.d.). Figure 2.2 is presented by Cuzin-Roudy et al. (2014). The figure represents the probability of the presence of krill based on the environment. Inside this generally suitable habitat, krill may show even higher preferences for some areas depending on other factors such as currents, gyres, and sea-ice.

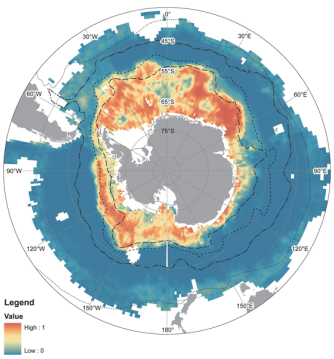

FIGURE 2.2: Probability of presence of Antarctic krill in the Southern ocean. Courtesy of Cuzin-Roudy et al. (2014).

2.1.2 Distribution of *Calanus finmarchichus*

The Norwegian Institute of Marine Research (Havforskningsinstituttet) has computed that there is at any time at least 33 million tons *C.finmarchichus* in the Norwegian sea. However, when the production is at its top during the summer, this production exceeds 300 million tonnes. In comparison, the Norweigan fish farming industry produces just below 1,4 million tonnes of fish (Borge, 2017). Hence, in addition to being the principal pray for some of the world's largest fish stocks, such as mackerel, herring (Wiborg et al., 1974), and larvae of Northeast Arctic cod (Melle et al., 2014), *C.finmarchichus* serves a huge potential for commercial harvesting.

C.finmarchichus is widely distributed and normally predominant in the southern and western parts of the Barents sea; that is, in the Atlantic waters south of the polar front (Sakshaug et al., 2009). Similar to the Antarctic krill, there is a large seasonal variability, as the ocean seems to be free of *C.finmarchihus* during the winter. The remaining individuals spend the winter in the deep, at depths between 600 and 1000 meters (Broms et al., 2016), with no reproduction, often found in high-density stock centers or layers, and move towards surface areas to spawn in the spring, where they stay until autumn. During this period, there are found examples of up to 50 grams of copepods per m^3 near the coast (Wiborg et al., 1974).

2.2 Sampling and Harvesting

Harvesting of zooplankton is a widely debated subject because of its important role in the ecosystem. Harvesting of Antarctic Krill is today an established industry, and hence attracts the most recognition, both positively and negatively. On the other hand, harvesting of *C.finmarchichus* has just begun.

2.2.1 Sampling and Harvesting of Antarctic Krill

While the industry of harvesting Antarctic Krill is portraying itself as one of the world's most sustainable fisheries, critics such as Greenpeace are raising concerns about ongoing harvesting in critical areas and so-called ocean sanctuaries. These areas are protected to help the marine ecosystems build resilience to the combined impacts of climate change, pollution, and fishing. One of their biggest concerns is related to accidents, which may cause substantial environmental consequences (Greenpeace International, 2018). Figure 2.3 displays the critical role of the krill in the Antarctic ecosystem and how most Antarctic life depends on it.

Significant sampling of Antarctic krill began in 1925 with the Discovery investigations. At that time, net sampling was the primary way of obtaining information on distribution, abundance, population demography, and behavior of the krill (Everson, 2008). The use of acoustics in recent years has provided a much more detailed picture of both local and large scale distribution and abundance of krill (Miller et al., 1989). However, the acoustic techniques still require methods to identify the proportion of the acoustic signal that can be attributed to krill and scale the signal to generate krill density. This is usually done by conducting trawlers along with a ship that utilizes echo-sounds to discover the krill (Jones et al., 2015).

All commercial harvesting of krill in the Southern sea over the last 50 years has been, and is, regulated by the international "Commission for the Conservation of Antarctic

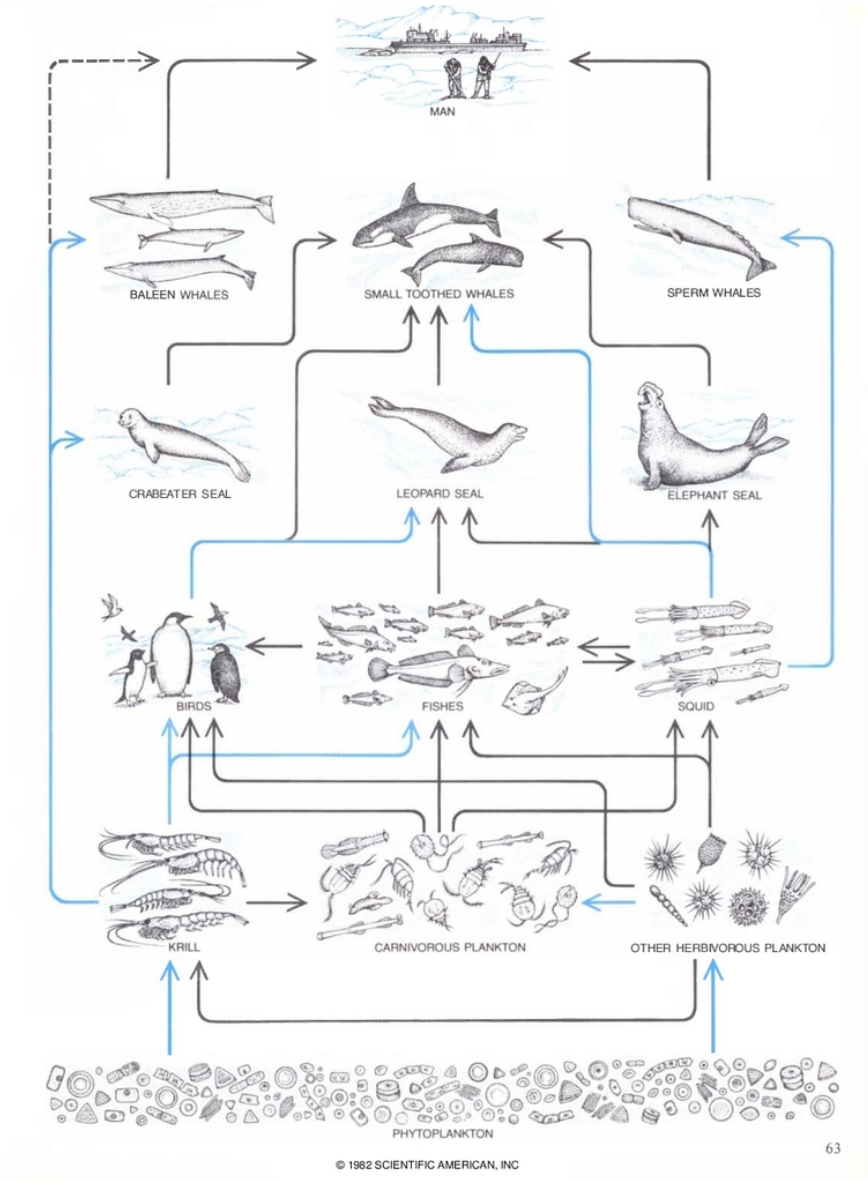

FIGURE 2.3: Food pyramid in the Antarctic waters. Courtesy of Beddington et al. (1982)

Marine Living Resources" (CCAMLR) (Giske, 2018). CCAMLR was established in 1980 amid concerns that an expanding krill fishery could have a significant impact on the ecosystem of the Southern Ocean (Jones et al., 2015). As the harvesting should be far below the risk of ecological effects, CCAMLR has put a limitation of 620.000 tonnes annual harvest until the knowledge is more expansive than what it is today (Giske, 2018). These limits are based on mathematical models and simulation studies of krill populations, where effects of fishery can be implemented to determine how much krill can be taken out without having an unsustainable impact on the population (Jones et al., 2015). As the United Nations (UN) considers quotas within 10 percent of the fish population as sustainable fishing, today's limitation is rigorous to guarantee sustainability. Scientists have, however, previously estimated that it is possible to harvest 5,3 million tonnes of krill annually without harming the natural ecosystem (Ytreberg, 2019).

2.2.2 Sampling and Harvesting of *C.finmarchichus*

Harvesting of *C.finmarchichus* has been of interest since 1950, and it was considered as an interest for fish-farming feed already in 1990. However, all fishing of zooplankton was banned in Norwegian waters due to lack of knowledge. One wanted to have a wider understanding of the resource, as well as a sustainable regulation in order before harvesting took place (Borge, 2017). The bio-marine industrial company Calanus AS has since 2003 been the only company to harvest copepods with an annual quota of 5000 tonnes in coastal accordance with the trial permits of the Norwegian authorities (Borge, 2017). However, until 2015, the annual harvested amount was about 513 tonnes. The Norwegian Ministry of Climate and Environment (NMCE) has established a fishing quota for *C.finmarchichus* inspired by CCAMLR for krill (Prado-Cabrero et al., 2021), and in 2019 the government approved for commercial harvesting with a quota of up to 254,000 tonnes (Myrbakken, 2021). The quota is based on data from the zooplankton monitoring program of the Norwegian Institute of Marine Research, *Havforskningsinstituttet*, which includes estimation models with samples collected from all Norwegian ocean areas where the *C.finmarchichus* is widespread. Samples are collected using plankton nets and towing optical plankton counters through the water masses.

In addition to the concerns of interrupting the *C.finmarchichus* stock, one major issue is by-catch when harvesting. Using plankton nets with small mesh sizes, fish eggs, larvae, post-larvae and early juveniles are included in the nets. Fishers are also afraid that harvesting on a larger scale will reduce the food base for the larger predators. Hence, it is wanted that, if large scale commercial harvesting of *C. finmarchichus* is planned, that this is extended to areas further away from the coastal areas (Borge, 2017). To do so, new technology and knowledge about the availability of larger ocean areas, including the Arctic Ocean, are necessary. Basedow et al. (2019) presented in 2019 a research of remote sensing of zooplankton swarms, focusing on *C.finmarchichus* in Norwegian coastal areas. They used satellite images for mapping of large stocks of *C.finmarchichus* for the first time, which shows the great abundance of the stocks in and outside the coastal areas of Norway. This research is further mentioned in Section 3.1.1. Working with this type of technology can be the solution for both obtaining more control of the *C.finmarchichus* stock, and also locate swarms further away from the critical coastal areas to avoid critical bi-catch.

2.3 Fishery and Potential Uses

Both krill and *C.finmarchichus* are small in size, and in general, not intended as a direct food source for people (krill are used somewhere - e.g., as the Japanese dish *Okiami* (Swerdloff, 2016)), but most wanted for agricultural feeding. It is their nutritional content that is highly sought-after both for fish and human health, and scientists have found that including these species in the feeding has a positive effect on the health and well-being of the salmon, as well as improving the quality of the fish (fishfarmingExpert, 2020). More than 70 % of fish feed today is plant-based (Borge, 2017), which in addition to lacking the optimal marine nutrients, contributes to rain-forest cuttings for space for agricultural farming. Hence, using more krill and *C.finmarchichus* in the diet could contribute to getting feeding back into balance (Giske, 2018).

As well as for the fish, krill and *C.finmarchichus* serve as a healthy option for humans. They contain nutrients such as wax esters, natural antioxidants, and most importantly,

desirable long-chained omega-3 fatty acids (Pedersen, 2007). Only 3 percent of the world population have adequate levels of omega-3. Omega-3 fatty acids, namely EPA (eiocosapentaenoc acid) and DHA (docosahecaenoic), are acids that humans and many other vertebrates are unable to produce in sufficient quantities to maintain normal physiological processes (NTNU, 2020). These acids are assumed to prevent several diseases, improve cardiovascular health, as well as to have a positive impact on the immune system (Shahidi et al., 2018). Hence, in addition to including more of these species in the feed of farmed fish, they can be used in supplements as an easy solution to reach optimal levels of omega-3 fatty acids (Aker Biomarine, n.d.).

The red color of krill and *C.finmarchichus* comes as these species contain high concentrations of red carotenoid pigments, where *astaxanthin* can constitute 85-80 % of the total carotenoid amount (Funk et al., 1991; Lotocka et al., 2001). As fish feed is either land-based or based on white fish, synthetic astaxanthin is added to the feed to give salmon the desirable red color and increase the meat quality. Using krill and *C.finmarchichus* in the fish feed, optimal color and meat quality can be obtained naturally. However, in the essence of mapping and remote imaging, this red color is of much greater importance than coloring the fish meat- it is why the swarms can be observed and controlled remotely and will be thoroughly discussed further in the thesis.

From a biological point of view, *C.finmarchicus* is challenging to distinguish from some other copepods, and DNA analysis are often the only solution. Therefore, in *in situ* operations, it is difficult to be certain of the sort of copepod observed. For simplicity, the term copepod will hence be used further on in this thesis, but the reader should keep in mind that it is *C.finmarchichus* it is referred to.

Chapter 3

Remote- and *in situ* Sensors and Sensor-Carrying Platforms

For the most accurate mapping and monitoring, a combination of remote and *in situ* imaging should be used. Remote sensing is effective for its ability to cover large areas. However, for accurate measurements, *in situ* observations would be necessary to confirm the objects of interest.

In order to recognize and classify organisms, data must be collected. This is done using sensors, and this chapter describes the optical sensor technologies of SilCam and hyperspectral imaging. The sensors need to be carried, and different sensor-carrying platforms are also briefly described and compared in this chapter. Finally, the idea of adaptive sampling is presented.

3.1 Remote Sensing

Remote sensing is usually performed by aerial or space imaging. In the context of this thesis, it is done to observe large patches of changes in the color of the ocean surface, such as phytoplankton spring blooms. Zooplankton are likely to appear in massive swarms that can be seen from space or air and can be located by using optical imaging sensors. It is a commonly used technique in ecological research, land management, conservation, tactical planning, defense and surveillance (Asner et al., 2007; Mahmoud et al., 2021). Using aerial imaging for underwater purposes, on the other hand, is challenging. Light rays, which can be considered as waves of energy, are quickly absorbed in water and can only image the very upper layer of the water column. Considering zooplankton, only top layers of the swarm can be observed and further exploration of deeper sites requires the use of underwater platforms.

3.1.1 Sensor-Carrying Platforms

Sensor-carrying platforms in air and space are typically satellites, Unmanned Aerial Vechiles (UAVs), and airplanes. One great advantage they have compared to underwater platforms is that communication and navigation are much easier as the information travels through air and not water. There is hence no need to connect the platforms to the observers with wires or cables. This advantage lets the platforms perform 2D mapping with unique capabilities when it comes to range and coverage, as well as reaching areas with limited accessibility with other platforms (Sørensen et al., 2020).

UAV

UAVs, or more commonly called drones, are air-crafts with no human pilot on-board. They are either operated under remote control by a human operator or with various degrees of autonomy. They are categorized based on several terms, commonly weight, altitude, endurance, and autonomy. There is, however, no official standard for the classification of UAVs as it is unlikely that rules can be developed that fit all UAVs (Dalamagkidis, 2015).

UAVs are used for many reasons and hence have large variations, from micro UAVs of less than 5 kg to today's largest UAV, Ravn X, with a weight of nearly 25 tonnes. In between these UAVs are many classes, but worth mentioning are the concepts of low-altitude, low-endurance (LALE), medium-altitude, long-endurance (MALE), and high-altitude, low-endurance (HALE) (Dalamagkidis, 2015). Costs of deployment and operations naturally vary with the classes, but UAVs are often more manageable, cheap, and effective for scientific purposes compared to airplanes and satellites. One major limiting factor of UAVs is weather conditions, where wind and icing can lead to problems with controlling the vehicle or loss of the vehicle (Sørensen et al., 2020).

Satellites

Satellites are objects that orbit the earth, with sizes ranging from a few grams to many tonnes. They are used for many different purposes and often placed in one of three categories; communication and navigation, science and transport, or remote sensing. Remote sensing is frequently used to identify and monitor an area's physical features by measuring the reflected and emitted radiation. This allows a satellite to gather information on the area's weather and natural resources (USGS, n.d.). Satellites for remote sensing are often placed in the Low Earth Orbit (LEO) with a height between 200 and 1200 km from the earth (Birkeland, 2009). A typical plankton sensing image is provided in Figure 3.1, which shows the plankton bloom around the island Gotland in Østersjøen in 2019. The image is taken by Sentinel-3, which is an Earth observation satellite developed by the European Space Agency (ESA) as a part of the Copernicus Programme. Its main objective is to measure sea-surface topography, sea and land surface temperature, and ocean and land surface color with high accuracy (ESA, n.d.). Plankton bloom helps understand ocean currents, as the plankton moves with the larges currents all over the ocean. It is this kind of information one is eager to obtain of also zooplankton.

FIGURE 3.1: Phytoplankton by Gotland in the Baltic sea, seen by Sentinel-3 in July 2019. Image courtesy of Copernicus.

When large patches of zooplankton are gathered at the surface, they can be remotely viewed and identified based on the red color they obtain from the astaxanthin pigment mentioned in Section 2.3. In the mentioned study by Basedow et al. (2019), satellite imaging is followed by *in situ* sampling. Figure 3.2 shows one of their resulting composites, with Visible/Infrared Imaging Radiometer Suite (VIIRS) images obtained over a week in the spring close to the coast of northern Norway. The red-colored areas are assumed to represent large swarms of *C.finmarchichus*, while the yellow and blue lines illustrate *in situ* sampling using towed optical plankton counters.

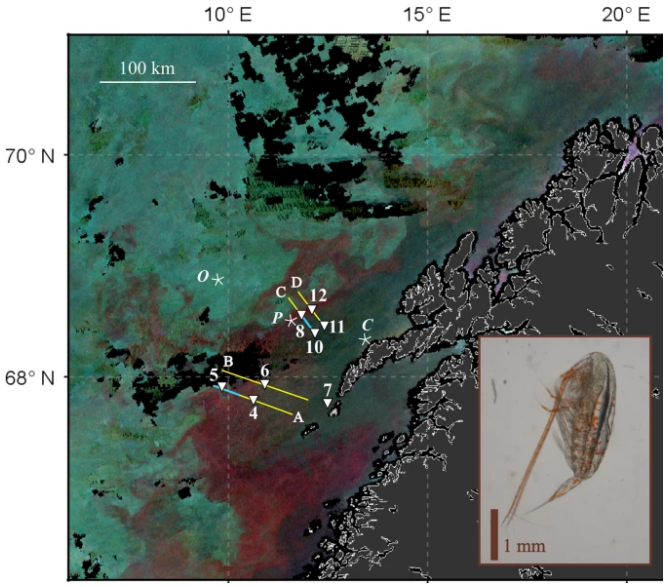

FIGURE 3.2: Satellite observations of swarms of copepods. Courtesy of Basedow et al. (2019).

Similarly with the UAVs, satellite imaging has several issues when it comes to imaging. Satellites orbit the earth and are not directly subjected to weather conditions, but are still affected by these because the imaging requires a clear sky and visibility. There is also a risk when it comes to loss of data and the vehicle, and when this happens, the vehicle is considered as lost and keeps orbiting as space garbage. The cost of the satellites, in addition to the complexity of the deployment, makes losses critical. For example, the Sentinel-3 series mentioned earlier contracted its satellites for between 225 and 520 million euros (Selding, 2016). However, these are satellites that continually image the surface for many years and provide many different types of data necessary for different purposes. This data is obtained using different payload sensors.

3.1.2 Payload Sensors

The satellites used for remote sensing, which are the focus of this report, can carry many different payload sensors. An overview of these can be found at NASA (n.d.). In general, it is divided between active and passive sensors. Active sensors provide their own energy source to illuminate objects on the earth and then measures the radiation that is backscattered or reflected from the target. These concepts of radiation are further described in Chapter 4. Passive sensors detect the natural radiation that is emitted from the earth's surface or specific object. The most common source of natural radiation is reflected sunlight (NASA, n.d.).

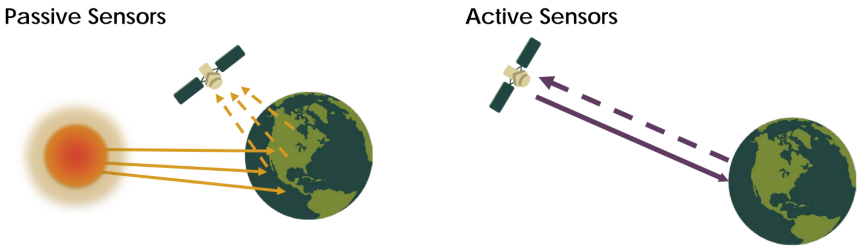

FIGURE 3.3: Passive and active sensors on satellites. Courtesy of NASA (n.d.)

This thesis will, however, focus on one specific type of sensor for remote sensing, the hyperspectral imager. Hyperspectral imagers mounted on satellites are usually passive sensors, meaning that it detects the radiation emitted from the earth. Based on NASA (n.d.) there are at least 14 satellites carrying hyperspectral instruments in current missions. These are used for various missions, but they all measure some radiation to gain information about atmospheric conditions and solar emissions. Hyperspectral imagers have also been mounted on both UAVs, small airplanes, and underwater robotics (Bazilchuk, 2021; Johnsen et al., 2016; Ødegård et al., 2018). For underwater robotics operating in an unsatisfactory amount of natural light, artificial lighting is often necessary, making the hyperspectral imagers active sensors. How a hyperspectral imager works is described in detail in Chapter 5, and the laboratory experiment using a hyperspectral imager is described in detail in Chapter 6.

3.2 *In situ* Imaging

As mentioned, *in situ* imaging is necessary for confirming the object of interest (OOI) observed remotely. Recent advancements in underwater robotics, mentioned in Section 1.2, make it possible for the underwater vehicles to follow, e.g., patches of plankton through the water masses based on inputs from sensor data. This section describes some of the sensor-carrying platforms used for this purpose and the technology of the SilCam optical sensor. The concept of adaptive sampling is also included.

3.2.1 Sensor-Carrying Platforms

The following paragraphs are largely inspired by Sørensen et al. (2020).

As mentioned, the swarms of krill and copepods are most likely to be found in or close to the polar areas of the world. These areas are characterized as remote and harsh environments for scientific operations, and the darkness of the Polar Night makes it even more demanding. The spatial and seasonal variability, as well as variability over years, makes it difficult to obtain good scientific data upon which one can draw a conclusion. Hence, if it is ever wanted to explore and understand these areas, superior and reliable technology and adaptable operational procedures over a long time may be the only solution to do so.

ROV

Remotely Operated Vehicles (ROV) are common in most industries regarding underwater operations and are used for various missions. They are divided into several classes

that differ in size, range, and work performance. The different sizes carry different amounts of sensors, but it is in general possible to obtain detailed mapping and sampling of a specific area with high-resolution data. ROVs can be operated from land and floating platforms, but most commonly from a ship, where they are connected to the operator or control room through an umbilical cord. The umbilical cord often provides unlimited electrical power as well as high bandwidth communication, but ship motions may degrade the obtained data quality due to environmental forces or ROV motions due to hydrodynamic forces on the umbilical. Moreover, if the goal is to cover larger spatial areas, the umbilical cord is limiting the operation. Therefore, an AUV can be more suitable for this type of mission.

AUV

Autonomous Underwater Vehicles (AUVs) are as well as ROVs used for a variety of tasks. However, the independence of an umbilical cord lets the AUV perform operations in, e.g., remote areas with limited or no accessibility like under ice. Seabed mapping using AUVs is a well-known field. It has provided impressive results within the offshore oil and gas industry (Hegrenæs et al., 2010) with inspection of underwater structures, search for sunken ships or airplanes, and underwater research of marine habitats, geology, and biology (Kebkal et al., 2017).

New science and improved technology open up for increasingly complex uses of AUVs. However, there are several issues with AUVs that need to be solved to perform complex surveys. These issues include the concept of underwater navigation and communication, the risk and possible hazards of the AUV, and the AUV's capability to carry payload sensors and electrical power for surveys. On the other hand, the opportunities for AUVs when the main issues are handled, are unbounded. With increasing situational awareness, adaptive sampling, and the ability to learn, AUVs will provide an essential contribution to understanding the ocean.

Glider

A Glider is a type of AUV that employs a propulsion system based on variable buoyancy rather than a propelled propulsion system. Hence, the Glider follows the large ocean current systems and has a very high spatial and temporal coverage compared to AUVs and ROVs. A Glider can operate for months without human intervention and obtain sensor data from the water column of huge areas. The information collected is usually ocean environmental data and not of living organisms. Some disadvantages connected to this type of vehicle include limited power, limited speed, limited payload capacity, and decreasing navigation and data accuracy.

3.2.2 Physical Effects of Sensor-Carrying Platforms in Water

An important aspect to consider for *in situ* imaging with artificial lighting, is how the environment reacts to this foreign object and unnatural illumination. This is investigated in Berge et al. (2020). Here, it is experienced that the organisms usually seen as prey quickly disappear when they are exposed to light, as this naturally makes them vulnerable for predators . Accordingly, copepods, krill and other species in the lower parts of the food chain will naturally flee the illuminated area, which is a problem that has to be overcome for satisfactory mapping results.

The pressure field generated by the UUVs are also causing issues for underwater robotics. The zooplankton have very limited vision, and will sense danger or predators rather then seeing them. Hence, a swarm of zooplankton will likely flee the imaging area of the UUV regardless of the artificial lighting. This is a highly relevant issue to consider when true measurements are wanted. The imaging area of an AUV with a mounted SilCam is shown in Figure 3.6.

3.2.3 SilCam

The chapters regarding SilCam are based on the information from the SilCam Github repository, in addition to several publications on the technique. Davies et al. (2017) is a publication describing the main principles of the technology, close related to the information on the website, and is hence the article which most of this chapter is based on.

SilCam is a holographic imaging system developed by SINTEF. It was developed to measure particle pollutants in seawater, and has been utilized in experiments with subsea releases of oil and gas. It has also been used to quantify distributions of organic material in the water column, such as copepods and zooplankton in general, phytoplankton, mineral grain, and marine snow. The imaging system operates using the principle of backlighting to create quasi-silhouettes of particles between the light and the camera.

System Configuration

As mentioned, SilCam uses the principle of backlighting, which means that when there are no particles present, the obtained image only contains the direct source illumination, which is a large, high-power LED array. This illumination is homogeneous and clean, which is important to simplify data treatment and increase accuracy and reliability of measurements. The source light passes through a holographic diffuser in order to reduce radial variance surrounding the center of the LED cluster before entering the sample volume. Further on it enters the near-side housing window and the telecentric receiving optics, which is attached to a color CCD (Charge-Coupled Device) camera. The configuration can be seen in Figure 3.4.

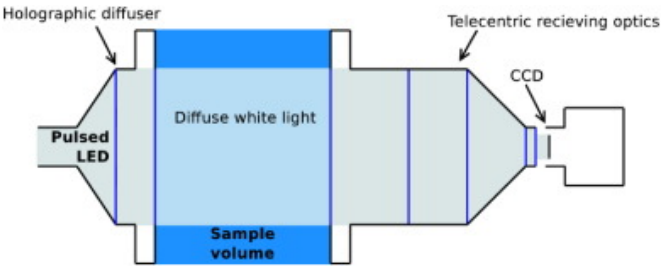

FIGURE 3.4: Schematic illustration of the optical configuration of the silhouette system. Courtesy of Davies et al. (2017).

SilCam uses telecentric receiving optics with a depth-of-field equal to- or wider than the instrument path length, which is the gap between the illumination source and the camera housing window. The telecentric receiving optics receive only collimated light rays, whereas mentioned in Section 5.2, the incoming light is aligned in a parallel fashion. This results in that all objects in the sample volume are in focus, and errors due to out-of-focus particles are removed. They also remove parallax effects, which is an apparent displacement or difference of orientation of an object associated with

conventional lenses. Parallax effects result in objects that lie close to the camera appear relatively larger than similar objects further away. The result of removing this effect is ergo that the OOIs of the same size appear as the same size independent of their location in the sample volume relative to the camera-end.

Method and Data Processing

When particles are introduced, their sample volume attenuates the backlight, and the silhouettes of them are obtained by measuring how much light of different wavelengths is blocked. As a result of this technique, however, the surface texture of the particles is not easily resolved as it is based on obtaining high-resolution silhouettes from backlighting and not on analyzing the reflected light. An example of this is shown in Figure 3.5, where details and the body internals of a copepod are satisfactorily resolved for biometrical characterization. This can be promising for further classification.

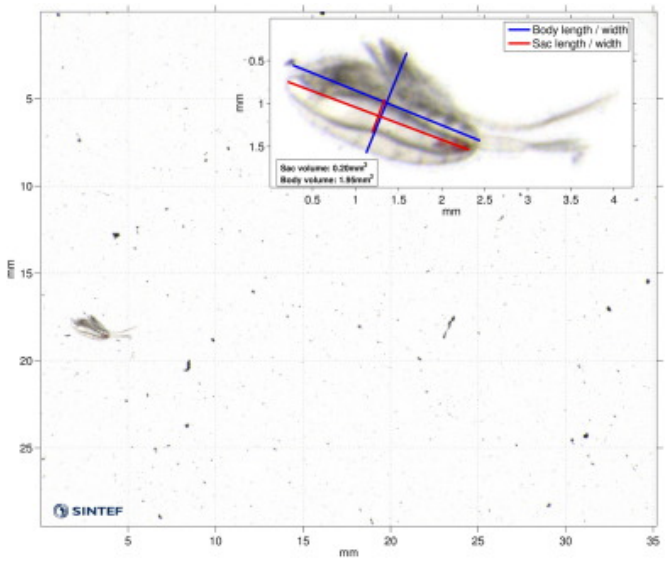

FIGURE 3.5: Example colour image of copepod in Frænfjorden, Norway. Courtesy of Davies et al. (2017).

Spectral transmittance can be calculated through each pixel after a background correction of the raw image. This correction is shown in Equation (3.1) and manages the variation in sensitivity over different wavelengths.

$$C(i,j,\lambda) = \frac{I(i,j,\lambda) - I_D(i,j,\lambda)}{I_0(i,j,\lambda) - I_D(i,j,\lambda)} \tag{3.1}$$

Here, I is the raw intensity in position i,j as a function of wavelength, λ, I_0 is the reference illumination intensity in position i,j as a function of wavelength, and I_D is a dark image.

The post-processing of the SilCam images before any further actions are implemented, such as classification, is quite simple. For each image, several steps are carried out.

1. Noise reduction of the image using a clean background,
2. Binarization of the image so that a logical image consisting of zeros and ones is produced,
3. Counting of detected particles and calculation of particle properties,

4. Calculation of particle size distribution.

FIGURE 3.6: SilCam mounted on LAUV Roald.

As mentioned, SilCam is a complete setup for both imaging and classification of particles. In addition to the imaging system, a software called PySilCam is developed for specifically managing SilCam images. With PySilCam, images are analyzed to provide size distributions and concentrations of OOIs, before machine learning algorithms, more specifically convolutional neural networks (CNN), are used to identify the type of particle. Figure 3.7, also from the Github repository of Silcam, shows how copepods, larvae, and eggs are successfully classified using the method.

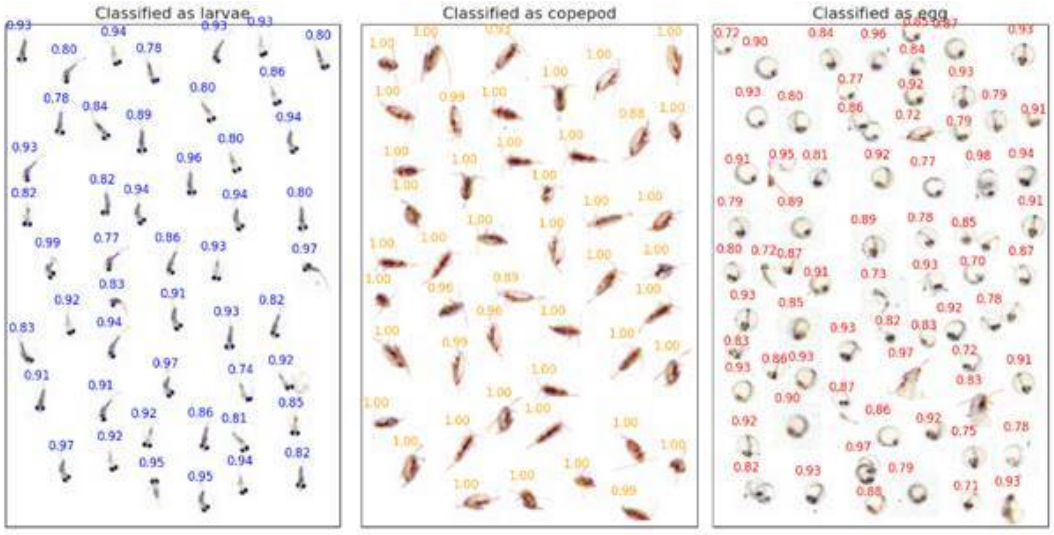

FIGURE 3.7: CNN classification using PySilCam. Courtesy of Davies.

This method for object detection of copepods using SilCam has been tested for several years with promising results. It is shown that copepods can successfully be differentiated from other objects, both using supervised and unsupervised learning methods. Hence, SilCam is already an off-the-shelf solution, and it is, e.g., used in the AILARON project mentioned in Section 1.2.

3.3 Adaptive Sampling

This section is inspired by a lecture in path planning in the module course *TMR09-Underwater Technology*.

As seen in Chapter 1, copepods and krill are likely to appear in enormous swarms distributed over very large ocean areas. Hence, it is not an efficient solution to pre-plan a route for the AUV to sample the organisms, as there is no guarantee for them to be present, and the ocean areas are way too large to sample the entire domain in all three dimensions. Therefore it is necessary with specialized autonomy that can prioritize and select its sampling locations based on what it senses, illustrated in Figure 3.8. This is called adaptive sampling.

This idea introduces a level of autonomy where the agent thinks and learns by itself, adapting to the surrounding dynamic environment. It has to reason about the value of information and make its future decisions based on this information. In Fossum et al. (2019) adaptive sampling is attempted for phytoplankton with promising results, and this method is highly relevant for monitoring plankton projects.

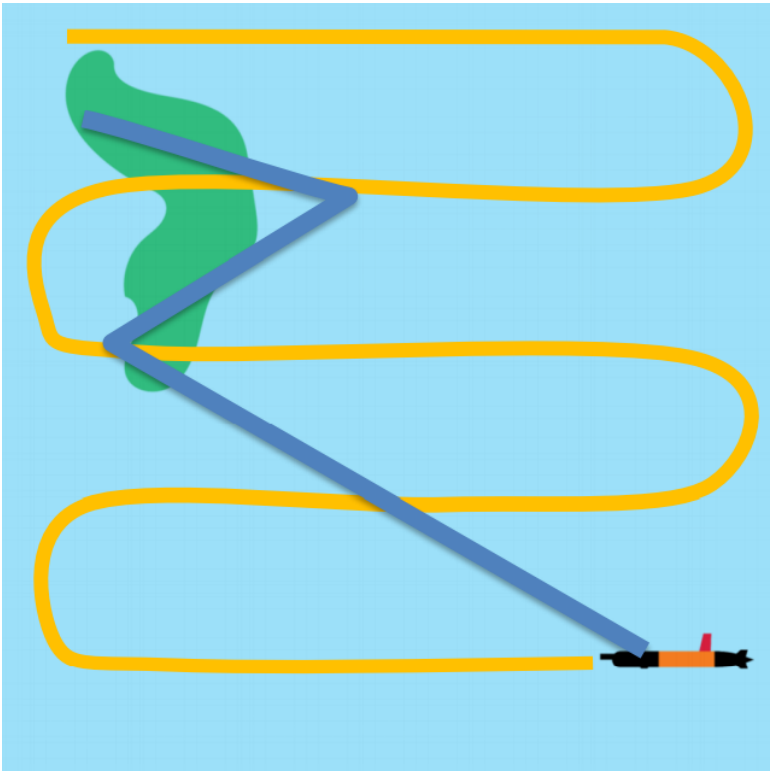

FIGURE 3.8: Illustration of adaptive sampling. Courtesy of lecture notes by Fossum.

Chapter 4

Light and Spectroscopy

The word "light" to most people interprets "visible light". However, there is much more to light than what humans can see. Visible light is just a fraction of the electromagnetic spectrum, containing electromagnetic waves in different forms and with different properties. Visible light also contains properties that can not be detected by the human eye but are of great importance in, for example, imaging. To fully understand the concepts of imaging presented later in this thesis, this chapter presents some basic concepts of the physics of light. Then the foundation is built to introduce spectroscopy, proposing a great tool for investigating materials and animals based on light analysis.

4.1 Fundamentals of Light

This section covers some basic concepts of the physics of light, or more generally, electromagnetic radiation.

4.1.1 Light as a Photon

When describing light as a photon, an atom surrounded by electrons in several energy levels is considered. When this atom receives energy by, e.g., bumping into another atom, an electron can jump to a higher energy level. However, the electron will not necessarily stay in this excited position, and can release the excess energy to go back to its base position. This released energy is what forms a photon. The photon is considered a packet of energy, moving away from the atom with wave-like properties.

4.1.2 Light as a Wave

The photon emitted from an atom is considered as an electrically charged particle surrounded by an electrical field. A magnetic field is generated when the particle moves, and when the particle changes its direction, the electrical and magnetic fields also move. This creates a wave motion, also giving light the properties of a wave. The amplitude of the wave is in Sigernes (2018) defined as

$$E(x,t) = E_0 sin(kx \pm \omega t) \tag{4.1}$$

where E_0 is the maximum amplitude of the wave, k is the wave number defined as $k = 2\pi/\lambda$, λ is the wave-length, ω is the angular frequency defined as $\omega = 2\pi/T$, T is the period defined as $T = \lambda/c$, and c is the speed of light given by 300,000,000 m/s in vacuum.

4.1.3 The Electromagnetic Spectrum

All electromagnetic radiation is included in the electromagnetic spectrum. The radiation frequencies give different properties for several uses, and visible light is only a tiny part of the spectrum. Figure 4.1 presents several types of electromagnetic waves with their respective interval of wavelengths.

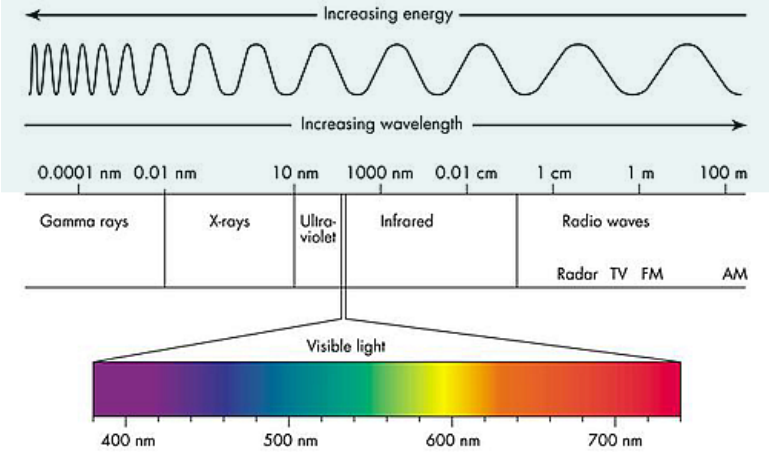

FIGURE 4.1: Components of a hyperspectral imager. Courtesy of Cyperphysics (n.d.)

Radio waves are waves with the longest wavelength. The longest waves can go through most materials and are typically used for wireless transmission of information over long distances, such as radio and television. Shorter radio waves, or microwaves, are used for satellites, mobile telephones, and microwave heating. However, the long wavelength of radio waves makes these unable to travel through water, which is one reason why underwater technology and communication are challenging. Infrared radiation is used in remote controls and equipment for night vision and is closest to visible light wavelength-wise. Visible light is a very small part of the electromagnetic spectrum and travels from red to violet. Wavelengths range between 400 nm to 700 nm. For the following chapters of the thesis, only visible light will be considered. On the other side of visible light, the wavelengths are shorter, and the radiation has more energy. This makes the waves able to penetrate the human body and can cause damage. Ultraviolet radiation is closest to visible light, often divided into UVA, UVB, and UVC. These can penetrate the skin and can cause sun damage and cancer. X-rays go further into the body and are hence widely used for imaging skeletons. However, being exposed to large doses of this type of radiation is also dangerous. Gamma rays are the waves with the most energy in the spectrum. They can cause massive damage, which make them both dangerous and helpful, as it can be used for disinfection, sterilization, and curing cancer.

4.2 Light Interaction with Materials

When a wave meets a boundary between two media of different optical properties, it is split into a transmitted wave proceeding into the second medium, and a reflected wave propagated back into the first medium (Born et al., 2013). Looking at the atoms of the materials, it is in Section 4.1.1 described how photons are generated when excited electrons fall back to their original energy level. However, this is only one of several material reactions when it is subjected to incident light. Every material has its own composition of atoms which will interact with light differently than other materials,

based on the natural frequency of the electrons.

4.2.1 Refraction

When a wave of light enters a medium of a different material, the wave will bend due to the difference of speed of light in the two materials. Each material or medium has a refractive index. It is defined as

$$n = \frac{c}{v} \tag{4.2}$$

where c is the speed of light and v is the phase-velocity in the material. Commonly, a refractive index of 1 is used for air in normal pressure, and 1,333 is used for water. Practically, this means that light travels 1,333 times slower in water than in air. This constant has important properties when Fresnel's equations are introduced. The amount of bending depends on the indices of refraction of the two media and is described quantitatively by Snell's Law. These two concepts are described in Section 4.2.3. Speed of light is reduced in the slower medium, so the part of the wave which hits this medium first will change its direction closer to the normal of the boundary. The rest of the wave will follow as it hits the boundary. The effect of refraction can be seen in figure 4.2, where the transmitted light is a result of refraction.

4.2.2 Reflectance and Transmittance

In cases where the incident wave-frequency matches the natural frequency of the electrons in the atom, the energy is kept inside the atom as kinetic energy, chemical energy or both. This is the phenomenon of light absorption. A black surface absorbs light while a white surface reflects light. An example of this is how the melting of sea ice causes the ocean to get warmer. As the amount of white ice decreases and melts into water, heat is absorbed by the water, which continues to melt more ice. The sea ice of the polar areas of the world is, therefore, crucial to reflect some of the incident sunlight away from the earth's surface to maintain a stable temperature, which is one of the most significant issues with the ongoing climate changes.

As mentioned, when light hits a material, it can either reflect off of the material or enter it. Reflection is a result of wavelengths that are not absorbed in the material. It is hence what causes materials to have colors. The atoms in the material are excited by a specific frequency and emit photons with a specific wavelength which we observe as a color. When struck by white light (containing all colors), a red fish reflects red light and absorbs all other colors. Likewise, grass reflects green light and absorbs all other colors.

Reflectance is the ratio between the intensity of light reflecting off a surface and the intensity of incident light,

$$R = \frac{I_{reflected}}{I_0} \tag{4.3}$$

However, if the material is somewhat transparent, it means that some light is transmitted through the material. Some wavelengths are absorbed or reflected, while some light will pass through. This resulting light can provide information about the penetrated medium through light analysis such as spectroscopy.

The transmittance, T, of the substance, is the ratio between the transmitted intensity, I over the incident intensity, I_0,

$$T = \frac{I}{I_0} \tag{4.4}$$

Figure 4.2 illustrates the concepts described above. Here, I is the light of incidence, and T is the light of transmittance. n_i and n_t are two different refraction indices for their respective mediums. θ_i, θ_t, and θ_r are the incident angle, the transmittance angle, and the reflected angle, respectively.

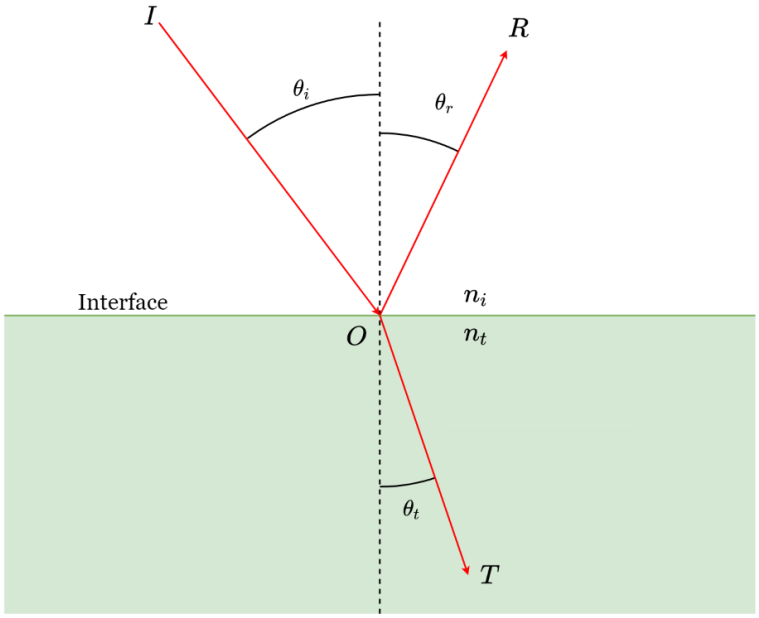

FIGURE 4.2: Figure describing the concepts of refraction, reflectance, and transmittance.

4.2.3 Fresnel's Equations and Snell's law

The properties of light introduced above are mathematically described through Fresnel equations. These equations describe how much light is reflected from, or transmitted through, a surface between materials (SNL, 2018). As seen in Equations (4.7-4.10), reflected and transmitted light are given for both parallel and perpendicular behaviour. This has to do with the polarizing effect Fresnel equations handle, but it is not further described in this thesis. Looking at the light illuminated normally at a surface, with reflective index n, through air (reflective index 1), Fresnel's equations give the reflection ratio as

$$R = (\frac{1-n}{1+n})^2 \tag{4.5}$$

However, light is often illuminated from an angled position, and Snell's law is introduced to handle these angles for transmitted and reflected radiation. Snell's law relates the indices of refraction n of the two media to the directions of the propagation in terms of the angles to the normal, and is defined as

$$n_i sin\theta_i = n_t sin\theta_t \tag{4.6}$$

Combining Fresnel's equations with Snell's law then give the reflection coefficients for parallel and perpendicular behavior in Equations (4.7-4.8), respectively. Transmission coefficients for parallel and perpendicular behavior are given in Equations (4.9-4.10), respectively.

$$r_{\parallel} = \frac{\tan(\theta_i - \theta_t)}{\tan(\theta_i + \theta_t)} \tag{4.7}$$

$$r_{\perp} = \frac{-\sin(\theta_i - \theta_t)}{\sin(\theta_i + \theta_t)} \tag{4.8}$$

$$t_{\parallel} = \frac{2\sin\theta_t \cos\theta_i}{sin(\theta_i + \theta_t)\cos(\theta_i - \theta_t)} \tag{4.9}$$

$$t_{\perp} = \frac{2\sin\theta_t \cos\theta_i}{sin(\theta_i + \theta_t)} \tag{4.10}$$

4.2.4 Beer-Lambert's Law

Beer-Lambert law is a linear relationship between the attenuation of light through a substance and the properties of that substance. It is commonly applied to chemical analysis and physical optics, and is defined as

$$A = \varepsilon c l \tag{4.11}$$

Here, A is unit-free absorbance, ε is the molar absorption coefficient with units of L $mol^{-1}cm^{-1}$, c is the molar concentration with unit $molL^{-1}$, and l is the optical path length, being the length of the sample. The molar absorption coefficient is a measure of how strong an absorber the sample is at a particular wavelength of light. The concentration is simply the moles $L^{-1}(M)$ of the sample dissolved in the solution, and the length is the length of the curvette used for the absorbance measurement.

4.3 Light in Air

Light behaves differently in the air and in a fluid. There is little that will affect the light between the target and the observer or camera in air, and the observed light can be expressed directly by light intensity. The following sections are inspired by Yamashita et al. (2007), including the figures, if not stated otherwise. Light intensity in air is here defined as

$$I_{\lambda}(l, z) = \frac{L_{0,\lambda} \cdot \kappa_{\lambda} \cdot \cos^3\alpha}{z^2} \tag{4.12}$$

Here, I_{λ} represents the reflected light intensity at a given wavelength, λ, $L_{0,\lambda}$ represents the intensity of the light source, l is the distance between the object and the observer, and z describes the distance from the object to the light source. κ_{λ} is the reflectance ratio of the object's surface at a given wavelength, λ, and α is the angle between the ray vector from the light source and the normal vector of the object surface. Figure 4.8 presents a simple representation of a setup for reflectance, where Equation (4.12) can be applied.

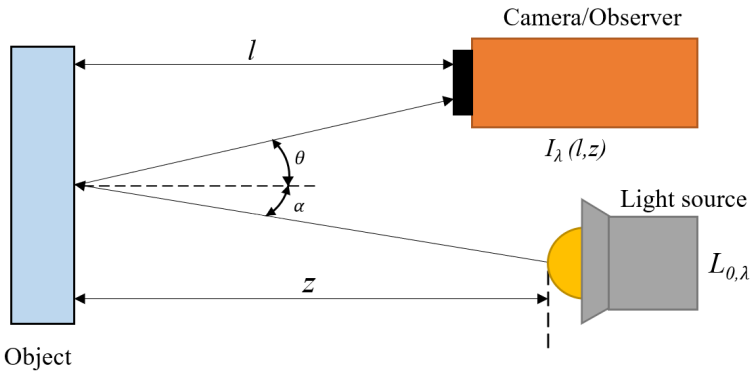

FIGURE 4.3: Setup for measuring reflectance in air

4.4 Light in Fluid

Light behavior in a fluid is different because the intensity of light decreases faster than in air. This effect is called light attenuation and is a composition of absorption and scattering. As mentioned, absorption is when the radiant energy is kept inside the molecule and converted to another type of energy. Scattering happens when photons are dispersed as they penetrate the fluid, which causes the light to change direction. There is, however, a complex and nonlinear relation between absorption and scattering, and there exists no exact solution to their radiative transfer equations (Dahl et al., 2019). Figure 4.4 shows the absorption coefficient for visible light in pure water. This coefficient is important with regard to underwater optics.

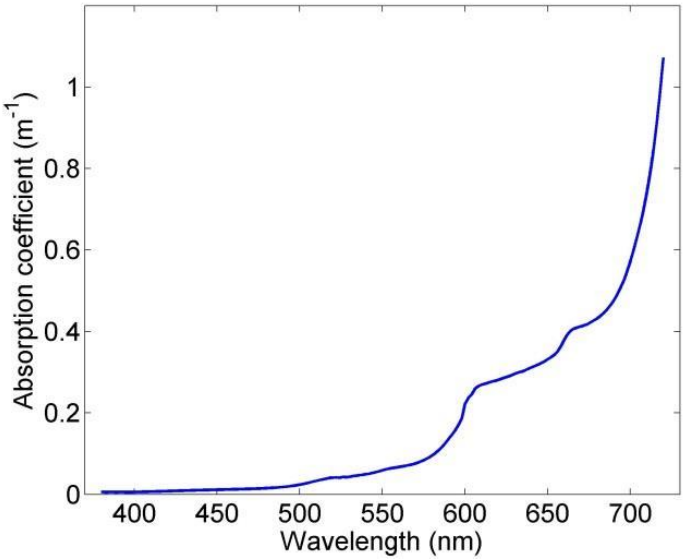

FIGURE 4.4: Pure water optical properties. Courtesy of Shaw et al. (2015)

Recalling Figure 4.1 in Section 4.1, it can be recognized how red light, with the longest wavelength of visible light, is absorbed fastest in water due to having the least amount of energy. Thus, red color is rarely observed below the surface areas when natural light is the only illumination. Having a red color is hence an advantage for protection against predators, and hence, in the deep ocean, red and black animals predominate (Ocean Exploraiton, n.d.). As an example, although blue color hardly changes, red

light disappears at a 20 m distance from the light source (Yamashita et al., 2007). This is an important issue when considering imaging of red-colored zooplankton such as krill and *C.finmarchichus* under water. For remote sensing using only sunlight, imaging will only give results if the swarms are in the surface layers. For investigating the swarms in deeper waters, underwater robots and artificial lighting is necessary.

Artificial lighting is required to obtain satisfactory results in deeper water, but also in shallow water, artificial light is often required to obtain satisfactory resolution of sensor data. Figure 4.5 illustrates how emitted light from a light source is affected by the water. Due to scattering, attenuation, and absorption, only small portions of the emitted light hits the target, and even smaller portions are received by the camera. This makes it challenging for the cameras to obtain the necessary light exposure for high-resolution images.

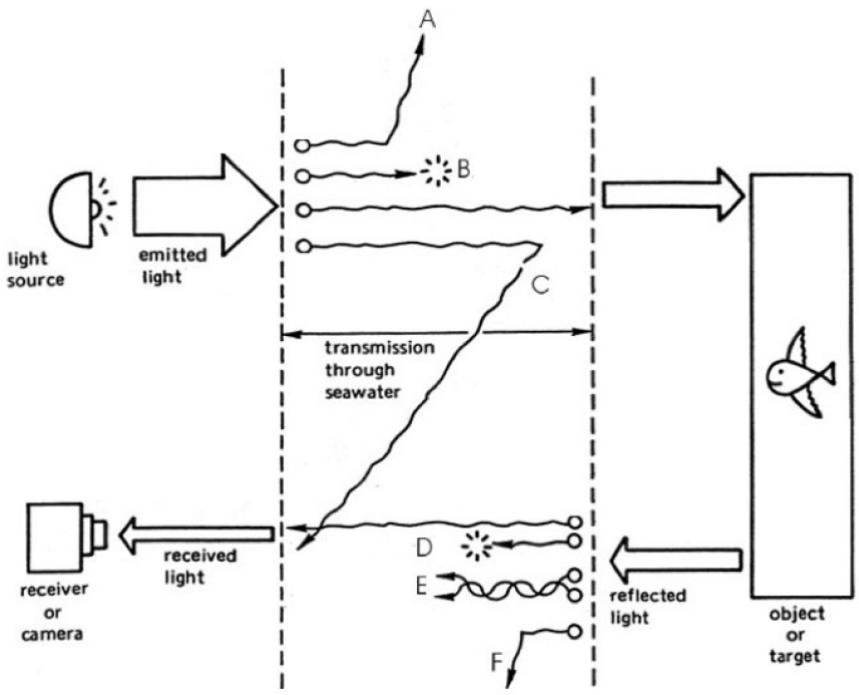

FIGURE 4.5: Artificial light positioned relative to the object and camera. Courtesy of Johnsen, Sørensen and Ludvigsen.

Returning to the definitions of Yamashita et al. (2007), the concepts of light attenuation in a fluid can now be included in the expression for reflected intensity of light in the air in Equation (4.12). First, the diminishing effect of light attenuation is applied to the light source's intensity,

$$L_\lambda(z) = L_{0,\lambda} \exp\left(-c_\lambda z\right) \tag{4.13}$$

Here, λ is the wavelength of light, z is the distance between the camera, $L_\lambda(z)$ is the light intensity of wavelength λ at the light source, and c_λ is the attenuation coefficient of liquid at wavelength λ, respectively. A visual representation of the situation is shown in Figure 4.6

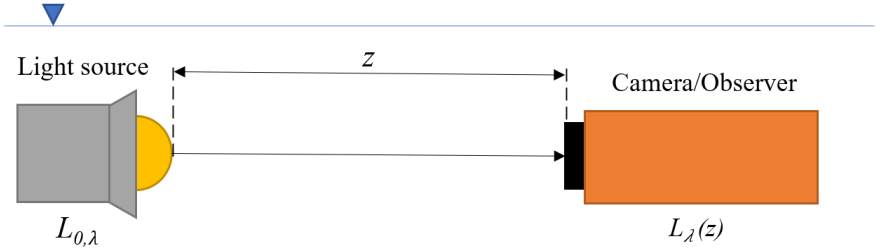

FIGURE 4.6: Measuring light intensity under water

Recalling the visual representation of Figure 4.8, the light intensity $I_\lambda(l, z)$ in fluid can be expressed as in Equation (4.14) by considering the diffuse reflection light in liquid from Equations (4.12) and (4.13).

$$I_\lambda(l, z) = \frac{L_{0,\lambda}\kappa_\lambda \cos^3 \alpha}{z^2} \exp\{-c_\lambda(\frac{z}{\cos \alpha} + \frac{l}{\cos \theta})\} \tag{4.14}$$

Here, I_λ is the reflected light intensity at the given wavelength, λ, $L_{0,\lambda}$ is the intensity of the light source, l is the distance between the object and the observer, and z describes the distance from the object to the light source. c_λ is the attenuation coefficient of liquid, and κ_λ is the reflectance ratio of the object's surface at the given wavelength, respectively. α is the angle between the ray vector from the light source and the normal vector of the object surface, and θ is the angle between the ray vector of light from the object and the optical axis of the lens.

For underwater imaging using underwater robotics, the UUV usually carries all of its imaging tools, including both the camera and the source of illumination. With these placed next to each other, Equation (4.14) can be simplified accordingly. Hence, $z \approx l$, $\alpha \approx \theta \approx 0$, and $\cos \alpha \approx \cos \theta \approx 1$. Hence, Equation (4.14) is simplified to Equation (4.15) (Dahl et al., 2019).

$$I_\lambda(z) = \frac{L_{0,\lambda}\kappa_\lambda}{z^2} \exp\{-c_\lambda \cdot 2z\} \tag{4.15}$$

4.5 Relations of Light through Copepods

In this section it is considered how the concepts presented above can be used with copepods. The copepods are complicated 3D structures with uncontrolled scattering, and complicated models are necessary to correctly describe and measurements observed by the sensor. The aim of this task is not to develop such models, but to observe differences in response across the copepod's spectrum. Thus, complicated mathematical expressions are not derived or used in the thesis. This section, however, presents the assumptions made for the analyzes described in Section 6.4. The system setup of the laboratory experiments is described in detail in Chapter 6, but simply illustrated here for an understanding of the light relations.

The concept of transmission through the copepods is relatively simple. For measuring the transmittance, a simplification of the system is shown in Figure 4.7. A petri dish with an anesthetic and the copepods is placed over the illumination source. For simplicity, the anesthetic is from now on called water.

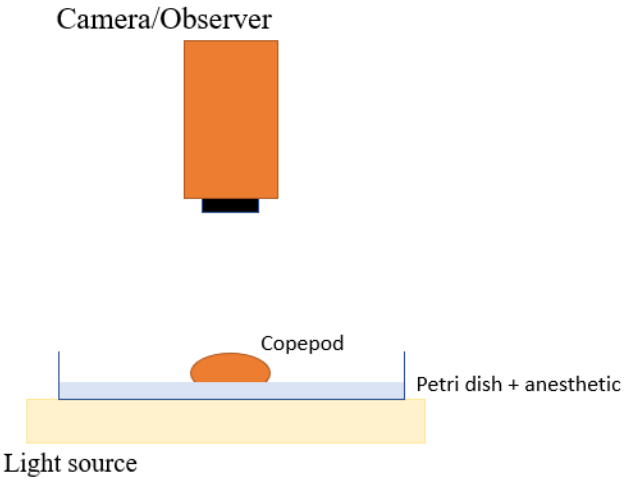

FIGURE 4.7: Simple illustration of measuring transmittance

The radiation observed by the sensor is either passing through just the dish + water, or dish + water + copepod. By neglecting the attenuation in the dish and water, the radiation observed by the sensor is the transmitted light through the copepod, solely influenced by the attenuation of the copepod itself. This attenuation is assumed to be uniform over the copepod's depth. Further neglecting the scattering in the copepods, the attenuation only represent the absorbance, A, in the copepods. The absorbance can be expressed using a percentage transmittance, where $\%T = 100T$. Recalling Equation (4.4) where transmittance is given as $T = I/I_0$, the expression for absorbance is developed in Equation (4.16). Here it is shown how the absorbance is related to the transmittance and incident and transmitted intensities.

$$\begin{aligned} A &= \log_{10} \frac{I_0}{I} \\ &= \log_{10} \frac{1}{T} \\ &= \log_{10} \frac{100}{\%T} \\ &= 2 - \log_{10} \%T \end{aligned} \tag{4.16}$$

For reflectance, things are more complicated, resulting in more assumptions. The simplified setup is illustrated in Figure 4.8.

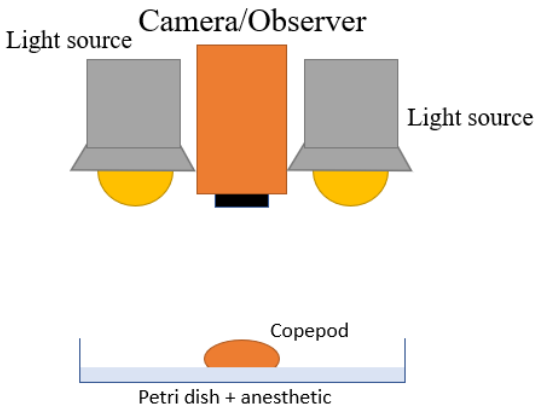

FIGURE 4.8: Simple illustration of measuring reflectance

For these measurements, the reflected light is assumed to be from the reflectance at the copepod's surface solely. This means that the effects of light passing through the copepods and reflected in either the water, the dish, or the stage, are neglected. Considering the system, it is assumed that the camera and light are perpendicular to the imaging surface, neglecting the angular effects introduced.

4.6 Spectroscopy and Classification

All materials reflect, absorb, and emit electromagnetic energy. Like human fingerprints, each material has its own molecular composition, which can be detected by analyzing its light absorption, reflectance, and transmittance over several wavelengths. The result is a spectrum that shows how much light is emitted, reflected, or transmitted from the target, and it is often presented as a graph as a scale of intensity and wavelengths. This is called a spectral signature, and as it can be unique to different materials, it is possible to recognize and identify materials based on it.

In Section 1.3 and the laboratory experiments in Chapter 6, spectral signatures of OOIs are obtained as "ground truths" using a spectrometer and a hyperspectral imager, respectively. This is to know what to look for when performing remote sensing, and to establish the correct answer for classification purposes. In short, classification is the task of categorizing images into one of several predefined classes (Karpathy et al., 2016). It is a supervised learning method, which means that the classifier is trained on data where the correct answer is known. This is where the laboratory results come in handy, as they represent the spectra desired to locate remotely. Hence, if a sensor system is familiar with the spectrum of an OOI through a trained classification model, it can be computed to recognize and classify OOIs autonomously for, e.g., use in adaptive sampling as presented in Section 3.3.

Chapter 5

Hyperspectral Imaging

This chapter presents the concepts of a hyperspectral imager and the imaging process. Sections 5.2 and 5.3 are largely inspired by the lecture notes in the course TTK20 *Hyperspectral remote sensing* (Sigernes, 2018), while the paragraphs describing the hyperspectral imager, Sections 5.1 and 5.4, are based on the information on the website an Youtube channel of Specim (Specim, n.d.[b]).

5.1 Hyperspectral Imager

A hyperspectral imager is a setup of usually three different components; an objective, a spectrometer, and a camera. Figure 5.1 shows a typical hyperspectral imager where the objective is the first, grey part, the spectrometer is the black parts in the middle, and the camera is the final piece. The objective forms an image to the spectrometer, and the camera uses the information from the spectrometer to form a spectral image. The details of how the spectrometer works are described in detail in Section 5.2. A hyperspectral imager can measure up to hundreds of thousands of spectra, and the collected spectra are used to form an image of the target. This means that each pixel in an image includes a complete spectrum of either the incident light, which indicates the portion of incident energy from the sample object as a function of wavelength (Manolakis et al., 2002).

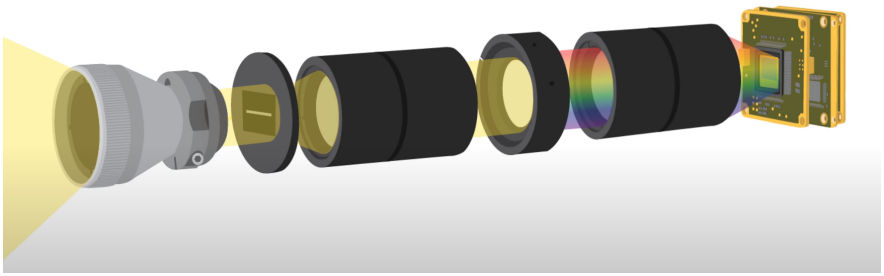

FIGURE 5.1: Components of a hyperspectral imager. Courtesy of Specim (n.d.[b]).

5.2 Spectrometer

When studying how light interacts with a specific target, a spectrometer is typically used. A spectrometer is an instrument that splits the incoming light into a spectrum before the spectral information is collected by a hyperspectral camera.

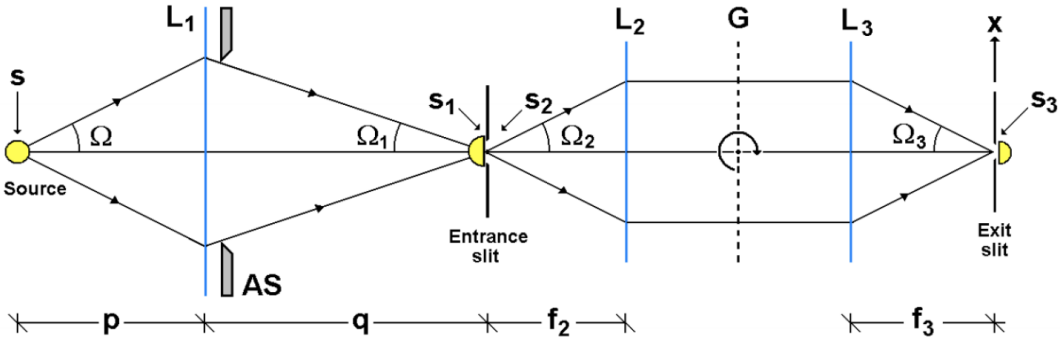

FIGURE 5.2: Optical diagram of a Spectrometer. Courtesy of Sigernes (2018).

Figure 5.2 shows the optical diagram of a spectrometer. In general, the diagram presents a way to describe a ray-tracing through any spectrometer. In this section, several concepts of the spectrometer are described thoroughly. Beginning from the source of light, the ray of light is followed through the spectrometer until it passes through the exit slit.

The source of light varies depending on what the imaging goal is. For this thesis, both effects of reflectance and transmittance are evaluated. For transmittance, the source of light is similar to the presentation in Figure 5.2, however, with the imaging objects in between the source of light and the first lens. For analyzing reflectance effects, the source of light is the imaging object itself, reflecting illuminated light from the illumination source placed beside the imager.

The light from the source first hits lens L_1, which has converging properties. This lens focuses the incoming light onto an entrance slit, which forms the imaging area through interference and diffraction.

5.2.1 Interference

Interference is the result of individual sources interacting with each other in the same medium. When the waves interact, the net effect of the waves at that point leads to a higher or lower amplitude dependant on the phase of the interfering waves. Hence, we have either a *constructive interference* or a *destructive interference*.

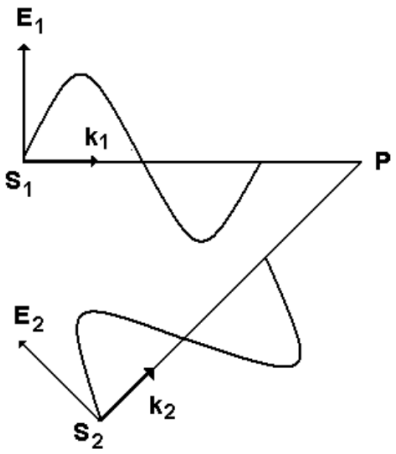

FIGURE 5.3: Interference of two seperate waves

Figure 5.3 displays a simple example of two interacting waves, E_1 and E_2 from two sources S_1 and S_2. The net result at point P is given as the sum of the two vectors $\mathbf{E} = \mathbf{E_1} + \mathbf{E_2}$. If the phases of E_1 and E_2 are perfectly equal at point P, the intensity in this point will be the two amplitudes E_{01} and E_{02} summed, while two perfectly opposite phases will equalize each other.

5.2.2 Diffraction

When a wave is distorted by an obstacle or encounters an opening with dimensions comparable to the wavelength of the wave, diffraction will occur as the waves bend around the corners of whatever is in its way. An example of this is shown in figure 5.4a, displaying ocean waves hitting the entrance wall to a port or harbor.

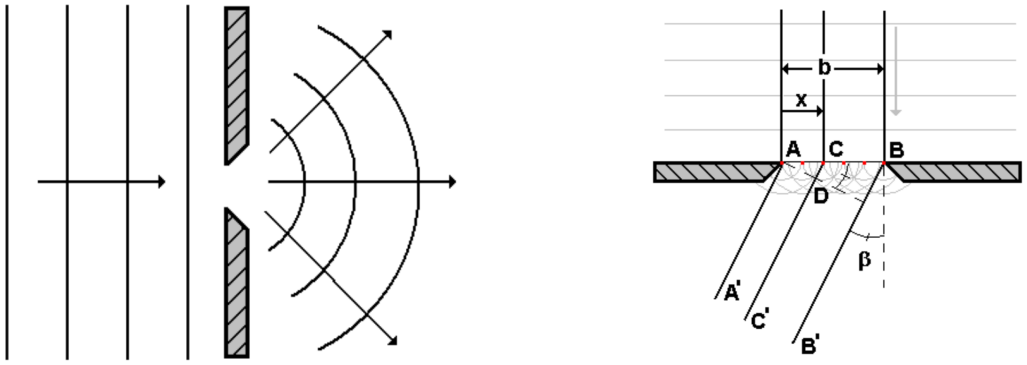

(A) Wall

(B) Principle

FIGURE 5.4: Diffraction

Using the entrance slit in the spectrometer as an example, the effects after passing the entrance slit are described by the principle of Huygens-Fresnel. This principle states that every point on a wave-front is a source of wavelets, which are spread forward at the same speed. These new waves now form a new united wave-front, as shown in Figure 5.4b.

The new wave-front then hits L_2, which is a collimating lens. This lens aligns the incoming light in a parallel fashion and forms a collimated beam towards the diffraction grating.

5.2.3 Diffraction Grating

A diffraction grating is obtained using multiple single slits placed next to each other. The spacing between the slits is a, and the width of each slit is b. Each slit acts as a source with an intensity, and the net intensity is the interference caused by N slits, modulated by the diffraction pattern of one single slit. An illustration of a diffraction grating is shown in Figure 5.5.

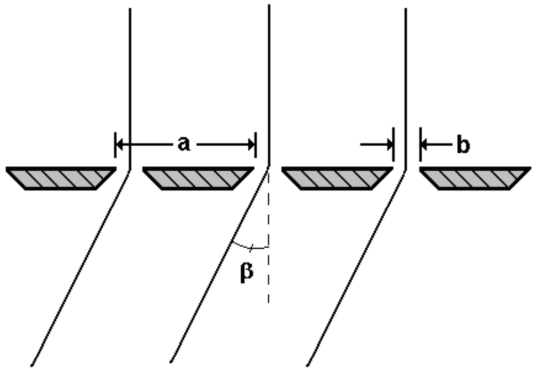

FIGURE 5.5: Diffraction grating

The diffraction grating is a dispersive unit that, on an atomic level, splits the photons by wavelength and spreads the collimated light into a spectrum. An illustration of this is shown in Figure 5.6

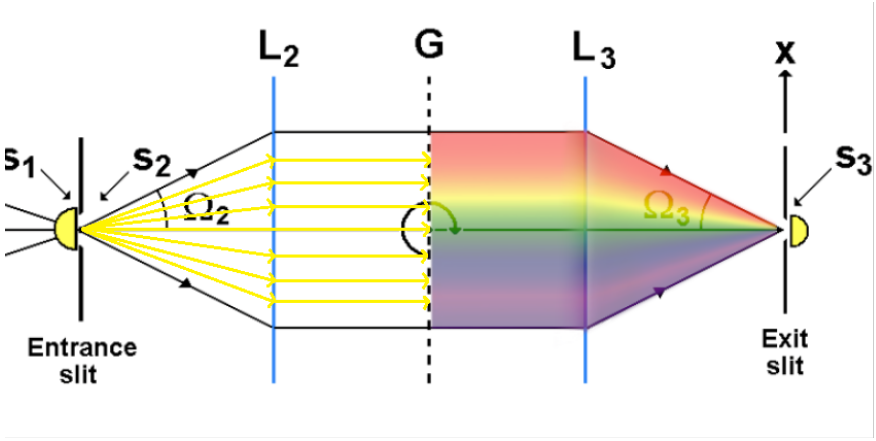

FIGURE 5.6: Illustration of incoming light in a collimating lens with a diffraction grating

Finally, lens L_3 is a focusing lens that focuses the diffracted light from the grating onto the exit slit plane as a function of wavelength. As a result, image area S_3 is the area of diffracted entrance slit image. Each pixel represents a portion of the spectrum that can further be translated and viewed with a spectroscopy software.

5.3 Light Through the Spectrometer

The concepts described in this section determine the amount of light passing through a spectrometer. While the previous section was focused on the wave properties of light, this section focuses on light as energy particles, or photons, as described in Section 4.1.1.

5.3.1 Etendue

Etendue is a geometric property of light that says how much space the light takes up spatially and angularly. Defining the maximum geometric extent allowing traveling photons characterizes an optical system's ability to accept light. For an instrument to

be optimally constructed, it has to ensure that no light is lost, which requires constant etendue throughout the instrument without any reduction from geometrical blocking.

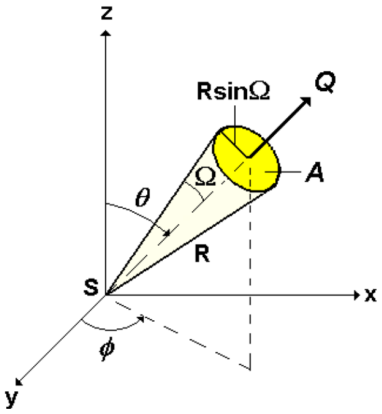

(A) Figure showing the solid angle Q

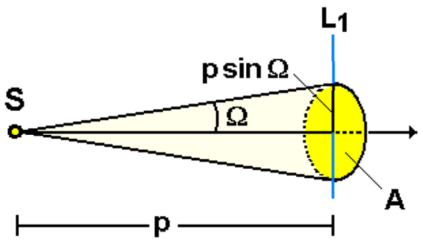

(B) Figure showing front lens etendue

FIGURE 5.7: Etendue. Courtesy of Sigernes (2018)

In Figure 5.7 the concept of etendue is illustrated. S is the source of light, and Q is the solid angle of which the light propagates into or out of. By definition, etendue, G, is then described as:

$$G \equiv \iint dSdQ \tag{5.1}$$

Hence, for a simple spectrometer, the etendue can be simplified to

$$G = S \times Q = \pi S sin^2(\Omega) \tag{5.2}$$

Based on Figure 5.7b, Q can be defined as

$$Q = \frac{A}{p^2} = \frac{\pi(p \sin \Omega)^2}{p^2} = \pi \sin^2 \Omega \tag{5.3}$$

Assuming constant etendue through the elements in the spectrometer, the optimal exit slit width can be calculated. Starting with the entrance slit, the etendue is calculated as

$$G_2 = \frac{G_A \cos(\alpha)}{f_2^2} \cdot w \cdot h \tag{5.4}$$

Similarly, the etendue from the exit slit is calculated as

$$G_3 = \frac{G_A \cos(\beta)}{f_3^2} \cdot w' \cdot h' \tag{5.5}$$

In Equations (5.4-5.5), $G_A cos(\alpha)$ and $G_A \cos(\beta)$ define the illuminated area of the grating as seen from the entrance slit and exit slit, respectively. w, w', h, and h' are their respective widths and heights. By using similarity of form, $h \cdot f_2 = h' \cdot f_3$ is obtained, resulting in the similarity

$$w' = \frac{\cos(\alpha}{\cos(\beta)} = \frac{f_3}{f_2} \cdot w \tag{5.6}$$

With the exit slit expressed as a function of the entrance slit, useful information on the spectral bandpass and resolution can be obtained.

5.3.2 Flux

Flux, Φ, is defined as the number of photons emitted from a source S per unit time [s] into a solid angle Q. This gives the expression

$$\Phi = \frac{photons}{s} \tag{5.7}$$

Flux can then be used to describe both light intensity and radiance, where intensity is calculated as the flux per unit solid angle

$$I = \frac{\Phi}{Q} = \frac{photons}{srs} \tag{5.8}$$

Radiance, B, is photons flux per unit area and solid angle. This also describes the intensity through a unit surface area, A,

$$B = \frac{I}{A} = \frac{photons}{cm^2srs} \tag{5.9}$$

Using the definitions above and the fact that etendue defines the maximum geometric cone and bean an instrument can accept, the photon flux through this cone can be described as a function of the radiance and the etendue

$$\Phi \equiv B \times G \tag{5.10}$$

$$\frac{photons}{s} = \frac{photons}{cm^2ssr} \times cm^2sr \tag{5.11}$$

With Equation (5.10), photon fluxes in and out of a spectrometer system can be evaluated.

5.3.3 Throughput

Throughput is defined as the usable flux at the exit slit, which is the flux available to the detector at the end of the spectrometer. Using Equations (5.4) and (5.5), and assuming that B_2 is the total radiance of the light source, Equation (5.12) calculates the flux entering the entrance slit.

$$\Phi_2 = B_2 \cdot G_2 = B_2 \cdot \frac{G_A cos8\alpha)}{f_2^2} \cdot w \cdot h \tag{5.12}$$

For calculating the flux leaving the exit slit, some new parameters are introduced. The remaining radiance following the exit slit is described by B_r, which comprises the spectral radiance B_λ multiplied by decreasing factors due to loss, E_λ^n and T_λ. E_λ^n determines the efficiency of the utilized grating at spectral order n, while losses caused by the geometry of the components in the spectrometer are described by T_λ. Finally, the flux leaving the exit slit is expressed as

$$\Phi_\lambda = B_r \cdot G_3 = B_\lambda \cdot E_\lambda^n \cdot T_\lambda \cdot \frac{G_A cos(\beta)}{f_3^2} \cdot w' \cdot h' \tag{5.13}$$

5.4 Imaging Method

The hyperspectral imager does not function as a regular digital image, capturing a typical "snapshot" of the object. This is because the input slit inside the spectrometer limits the incoming information. The information obtained at one point represents one line of pixels in the final image, and many lines must be scanned to form the final cube of an image and its spectral characteristics. The technique is called a line scan technique, which is illustrated in Figure 5.8. The narrower the slit, the more accurate spectra are obtained.

FIGURE 5.8: Illustration showing the push-broom technique. Courtesy of Specim (n.d.[b]).

In order to sample the entire object, the target must be moved relative to the recording instrument. This can be done by either moving the imager or the target while keeping the other still, but both can also be moved as long as there is a difference in velocity. This is because the relative velocity between the imager and the target is essential for the imaging resolution. Equation (5.14) describes the requirement of the relative velocity, saying that the length of the measured area, dx, must exceed the distance moved during readout time, τ.

$$\nu \cdot \tau \leq dx \tag{5.14}$$

This method is called the push-broom technique. When the technique is conducted properly, spectrograms for each track of the object are recorded. To obtain the information of the complete image, all samples are summarized. However, if the requirement in (5.14) is not fulfilled, the instrument will miss samples of the target area (undersample), which will lead to missing data in the final image.

There are several parameters necessary in order to obtain a successful data recording. In addition to the hyperspectral camera, proper illumination is important. As the imaging is based on light reflection, absorption, and transmittance, the target should be evenly illuminated, and the light should have a spectral response that matches the hyperspectral camera's wavelength range. To use the information provided by the spectrometer one should also have a reflectance reference, which is a white reference

for most cases.

Chapter 6

Laboratory Experiment and Data Processing

To the our knowledge, there has never been conducted a hyperspectral imaging experiment of copepods before. Hence, by involving several people with knowledge in their specific area, a team was put together to carry out the experiments. The team consisted of one in possession of a hyperspectral imager, one in possession of a culture of copepods, my co-supervisor Løvås, and myself, which makes up four people with interest for the study from different knowledge bases and points of view.

The first of two experiments was conducted in the working period of pre-work of the previous fall. Before this experiment, neither of us had any idea of what to expect, and the primary goal of this experiment was to find out if reasonable results could be obtained. For the second experiment, which was conducted in the working period of the Master's thesis, we had a more specific plan based on the result and knowledge from the first experiment. Each of the experiments is described briefly in this chapter, but Experiment 2 is described in more detail because it provided most of the results used for the data analysis.

6.1 Laboratory Setup

The laboratory experiments are performed at the location of SINTEF Ocen in Trondheim. The setup is nearly identical for both experiments. It consists of a rig and a computer, where the rig holds the moving stage, the lighting, and the hyperspectral imager. The imager used is sCMOS-50-V10E from Specim (Specim, n.d.[a]) which uses the push-broom methodology described in Section 5.1. It operates in the spectral range of 400-1000nm, has a spatial resolution of 2184 pixels, and an image rate of up to 100 images per second. The software used is Lumo Scanner, a data recording application for Specim's hyperspectral scanner systems.

The system consists of two types of lights. The top lights are 2 arrays of 4 LED lights, more specifically CREE Lumia 5.2 70W LED, and one array is placed on each side of the imager. A backlight is used to investigate the copepods' transmittance characteristics.

Between the two experiments, only some adjustments are made. For the first experiment, a piece of card is placed between the samples and the light, shown in Figure 6.1b, for the backlighting recordings. This was done for three reasons;

1. While scanning the image, the output is a row of pixels and not a full 2D image, making it difficult to tell whether or not the copepods are in the focus area.

Hence, the card with the small opening is there to position the copepods at the same place for each scan.

2. The card blocks out light from areas that are not directly beneath the sample. Otherwise, this light might leak into the sensor and reduce the image contrast.

3. The third reason is simply for comfort, as it is unpleasant to look at a very bright square in a dark room for long periods.

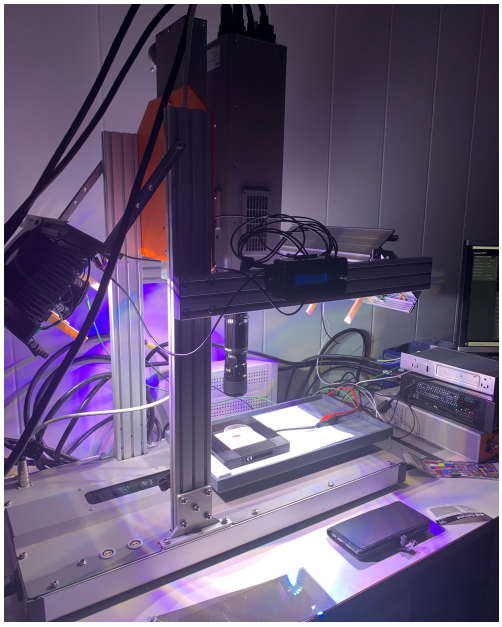

(A) System setup using top lights

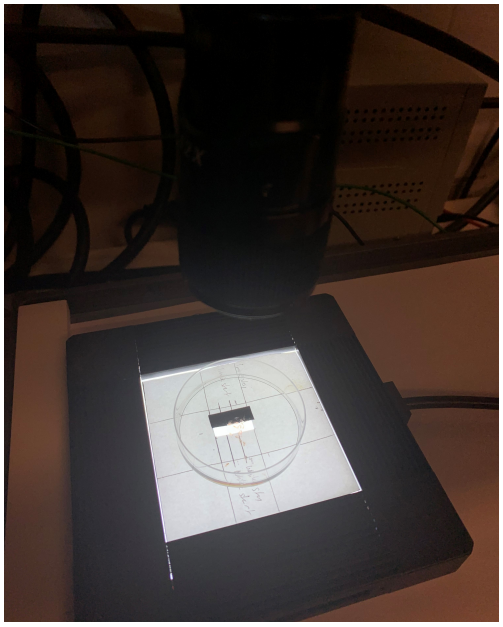

(B) Back-lighting with the out-holed card

FIGURE 6.1: Hyperspectral imaging setup

For the second experiment, however, a slightly different approach is tested. This time we want to separate the copepods more in order to avoid any overlay of the individuals. Hence, the out-holed card is removed, and the copepods are more spread in the petri-dish. To capture enough copepods in the image to obtain satisfactory results, the objective is further away from the individuals in this experiment. Otherwise, the same lighting and setup are used. We also want to introduce a measuring scale for visualizing the size of the copepods in the images. To do this, we use standard 230-micron spherical particles for detemining the pixel size in the across track and along track direction. The size-comparison can be seen in image 6.2b

6.2 *C.finmarchichus* Individuals

At SINTEF, a culture of copepods is stored and controlled by Altin. For both experiments, individuals from this culture are used. This culture was isolated from Trondheimsfjorden outside Munkholmen in 2004, from a depth of approximately 400 meters. In the laboratory, they are kept at a constant temperature of 10 °C. Each individual lives for about half a year, and four and a half generations are reproduced annually. They are fed with a mix of two microalgae, *Rhodemona Spaltica* and *Dynaliella Tertiolecta*, which has a red and green color, respectively. This culture is DNA-tested to ensure that the species is *C. finmarchichus*.

For the second experiment, we also want to image individuals recently isolated from the ocean (April, 2021). This is in order to see if their spectra are similar to the spectra of the lab-individuals or if there could be significant differences. The individuals were isolated from Trondheimsfjorden a week before the second experiment and kept isolated from the lab-individuals. They were caught using a WP3 plankton net with a standard mesh size of 1000 μm and a diameter of 113 cm. The net was pulled with a vertical pull from a depth of 300 meters to the surface. In order to have their characteristics as genuine as possible, they were not fed after isolation from the ocean. It must also be stated that since these individuals are not DNA-tested, it is not possible to ensure that the individuals are of the species *C.finmarchichus* or another *Calanus* species.

For the imaging process, the copepods are carried in a bucket inside a small freezer with ice cubes to maintain a stable temperature for the samples. To perform imaging, some samples are picked up using a pipette and put on a petri dish filled with a small amount of an anesthetic. The anesthetization of the copepods is necessary for a controlled experiment and to obtain data, as the copepods typically move around with quick movements. The size of the copepods, being up to four millimetres, led to skepticism before the first experiment. It was exciting to see how well the object lens could focus on the copepods and what kind of resolution would be obtained on the resulting image. A regular image of the copepods from the laboratory culture in the petri dish taken with an iPhone is shown in Figure 6.2a, while the comparison to the 230-micron particles is seen in Figure 6.2b.

(A) Copepods in petri dish

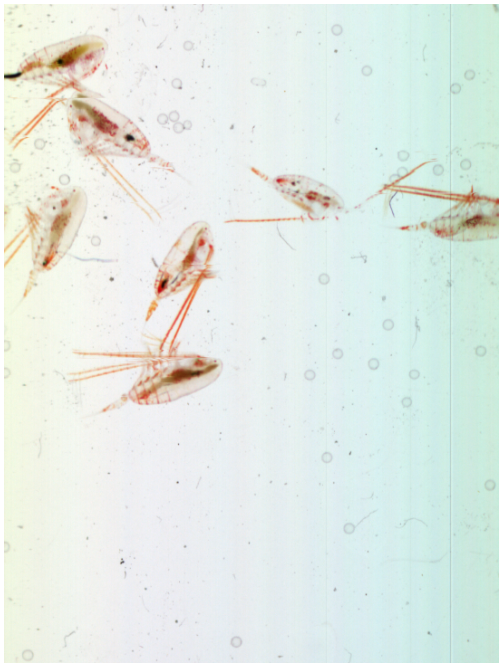

(B) Copepods with backlighting, next to 230 micron particles

FIGURE 6.2: Copepods size measurement

6.3 Imaging Settings and Process

When the setup is complete, the imaging process can begin. First, several test scans are done to ensure the samples are both in the imaging area and in focus. The focusing is a quite challenging task as the speed of the HSI is very low, and that, as mentioned

earlier, the camera output is only rows of pixels and not a 2D image. However, using the push-broom technique over the samples, more lines of pixels are scanned, and the image is slowly obtained, previewed at the computer. The scanning data is stored in a folder containing both the resulting image and the parameters used for that specific scan. These initial scans are performed in both experiments, as the camera objective is put in a different distance from the individuals.

As the goal of the first experiment is to simply test hyperspectral imaging of copepods, several adjustments are tried to see what results are obtained. One of the most important differences is the use of light. First, the scans are carried out using only backlighting. This means that the light captured by the imager is the transmitted light through the sample, resulting in a transmittance spectrum. Secondly, the backlight are turned off and the top lights are used. Now, the light captured was the reflectance light, resulting in a reflectance spectrum. Some parameters are also varied through the experiment to see how it affected the results. These are the frame rate, the spatial binning, the spectral binning, and the moving speed of the imager.

With the knowledge we have from the previous experiment, we conduct the second experiment with a more specified plan considering what will work best this time in terms of settings and desired results. We also know what we want the results for and do not spend any time changing frame rates, spatial- or spectral binning, or moving speed of the imager. Our main focus is obtaining a couple of good clear images using both different light settings and several different copepods. We also try to diminish the effect of shadows in the reflectance images using less anesthetic. These shadows contribute to much noise in the images making the resolution seem poorer. This can be seen in both the iPhone image in Figure 6.2a, and the cropped reflectance image in Figure 6.5b.

However, as the copepods are more widespread and the objective is further away compared to the first experiment, it still takes some time to find the suitable settings to obtain satisfactory results. With the proper focus obtained, we are experimenting with motor speed, which is a parameter that was not noted last time. A detailed description of the imaging process is included in Appendix A.

6.4 Data Processing

The results from the laboratory experiment are here presented as visual presentations of the imaged spectra of the organisms. However, some data processing is necessary to present this correctly, and this will be described thoroughly in this section. The processed data are used in mainly two different analyzes, one with analyzing specific areas of the copepods and one where the copepods are analyzed as an average to represent a more realistic point of view.

6.4.1 The Data File

As mentioned, the software Lumo Scanner is used for data recording and visualizing of the data in the laboratory. The scanner makes it possible to save the recorded files locally on the computer. When the files are captured, they are saved as an ENVI image format, which is a popular commercial software package for processing and analyzing geospatial imagery (Boggs, n.d.). The data in the ENVI format is stored as a binary system of bytes and in one of three formats; the band sequential(BSQ), the Band-interleaved-by-pixel (BIP) format, or the Band-interleaved-by-line (BIL) format,

which is the one used in this thesis. This format stores the first line of the first band, followed by the first line of the second band, followed by the first line of the third band, interleaved up to the number of bands. Hence, the format provides a compromise in performance between spatial and spectral processing (Geospatial, n.d.).

6.4.2 Reference Conversion

Figure 6.3 shows some examples of the reference frames used for processing the spectra. Each image has a reference frame-recording, except in the circumstances described below. As mentioned, the dark frame represents the noise of the imager, with no entering illumination, while the white frame shows the intensity of pure reflected or transmitted illumination. Some "get-arounds" are implemented to manage some incomplete measurements;

- For all transmittance images, the white-reference is calculated as an average of an empty area of the petri dish. While the correct white frame should be the pure illumination itself, it is instead disturbed by the dish and anesthetic. However, as the experiment's goal mainly is to discover differences in the spectra, the small attenuation-error obtained from the dish and the anesthetic is accepted.
- For the first laboratory experiment, no reference frames were recorded. For the transmittance image, however, white frame is calculated as described above to obtain a result. The dark frame is expected to be similar as the ones recorded in Experiment 2, as the same imager is used, In addition, comparing the values for dark frame with the ones for white frame, they are of little significance, and small differences are assumed to be negligible. Thus, the dark frame in Experiment 1 is actually the dark frame from Experiment 2. However, with no measurements of the reflectance tile, no reflectance results are obtained from this experiment.

The reference frames are used to scale the image to exclude all other effects on the spectra than the copepods themselves. Hence, a reference pixel is plotted with the results to show how the spectrum of an empty pixel looks in comparison.

Figure 6.3a shows an example of a dark frame. The dark frames are very similar for all images, as they are unaffected by illumination and solely represent imager noise. For the scaling conversion, the dark frame represents the minimal intensity. Figure 6.3b shows an example of a reflectance measurement of the white calibration tile. The tile reflects all light and the plot shows the pure reflected illumination. In other words, the plot represents the wavelength distribution of the illumination source. The same applies to the transmittance white frames, shown in Figures 6.3c-6.3d. Neglecting the attenuation-effect from the anesthetic and dish, the plots represent the pure illumination from the backlight.

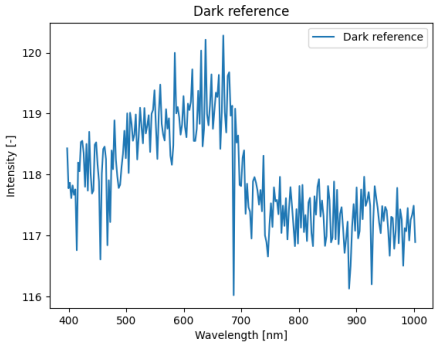

(A) Dark frame from Experiment 2

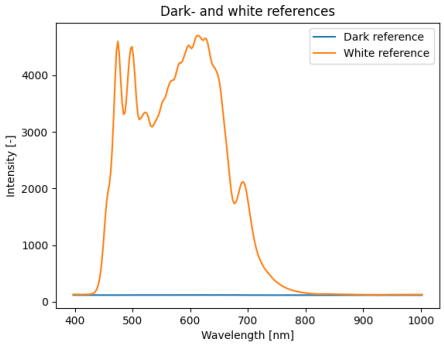

(B) Reflectance references plot from Experiment 2

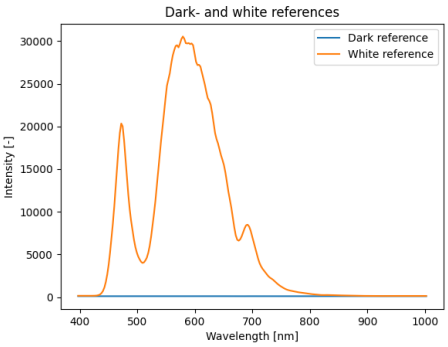

(C) Transmittance references plot from Experiment 1.

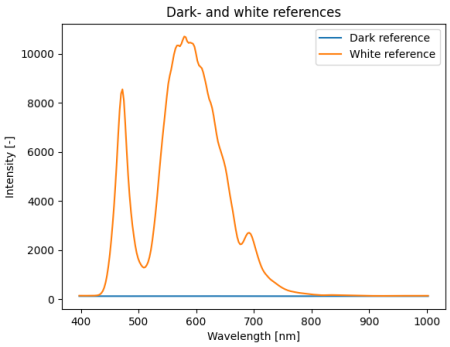

(D) Transmittance references plot from Experiment 2

FIGURE 6.3: White- and dark-frames for both Experiment 1 and 2. These plots show the pure reflected or transmitted radiation, representing the respective light source.

6.4.3 Processing

For simple information-extraction of the image, the BIL file is transformed to a 3-dimensional hypercube. Here, x and y represent the spatial dimensions of the image, while the third dimension is the spectral dimension. This way, it is compatible with displaying the image, where the 2D image is shown, and the spectra can be shown by choosing one specific pixel. This property is important for this task because it is desired to obtain single spectra at specific points in each image, representing different parts of the individuals. The spectra are, at this point, a total representation of the amount of light entering the hyperspectral imager. As the light intensity for both transmittance and reflectance light is large compared to the effects of absorption by the copepods, the spectra need to be scaled with the reference frames to show the desired result. The frames are images captured in the same manner as the actual image and are hence transformed to a hyper-cube similarly. When all cubes are of the same format, the scaling of the image is done using the normalizing equation first presented in Section 3.2.3 and repeated here,

$$C(i,j,\lambda) = \frac{I(i,j,\lambda) - I_D(i,j,\lambda)}{I_0(i,j,\lambda) - I_D(i,j,\lambda)} \tag{6.1}$$

Again, I is the raw intensity in position i,j as a function of wavelength, λ, I_0 is the white frame, being the reference illumination intensity in position i,j as a function of wavelength, and and I_D is the dark frame.

6.4.4 Spectral Measurements of Copepod Areas

Copepods are relatively transparent creatures, but the main internals do have a color. However, these small areas of color are not evenly distributed but concentrated in specific parts of the body. One of these parts is a bag of astaxanthin in the back of their body, which is a small bag containing a high concentration of the pigment. The antennas are also expected to contain high concentrations of the pigment, and it is this bag and the antennas which are most likely to match the astaxanthin spectrum. As the astaxanthin is a red-like pigment, it means that this color is what is reflected of the copepods in natural light. Considering the principles described in Chapter 4, this means that other colors than red are absorbed in their body, and this can be shown in an absorption spectrum.

Figure 6.4 shows how different wavelengths are absorbed in pure astaxanthin. Being a red-orange colored compound, it absorbs wavelengths of approximately 500 nm. The spectra of the parts containing a high concentration of astaxanthin are hence assumed to show lower intensity in the same area, as reflectance - and transmittance -spectra will show the opposite of an absorption spectrum.

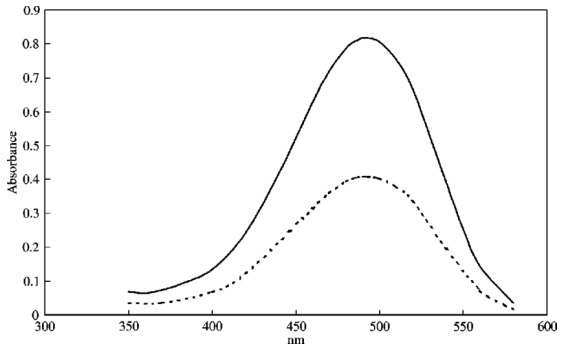

FIGURE 6.4: Absorbance spectrum of astaxanthin. Courtesy of Rønsholdt et al. (2001).

Other colored parts of the body are the head, or brain, and the stomach if the copepod has eaten. The color of the stomach is then based on what algae it has eaten and its color, while the head also is influenced by astaxanthin. Pixels are chosen manually to obtain spectra from the specific areas. Then, the process described above is applied to the pixel to obtain the correct, scaled format for displaying the results. Figure 6.5 shows two images captured in the first laboratory experiment, using both reflectance light and backlighting. The copepods are marked with numbers as an example of where pixels can be chosen from.

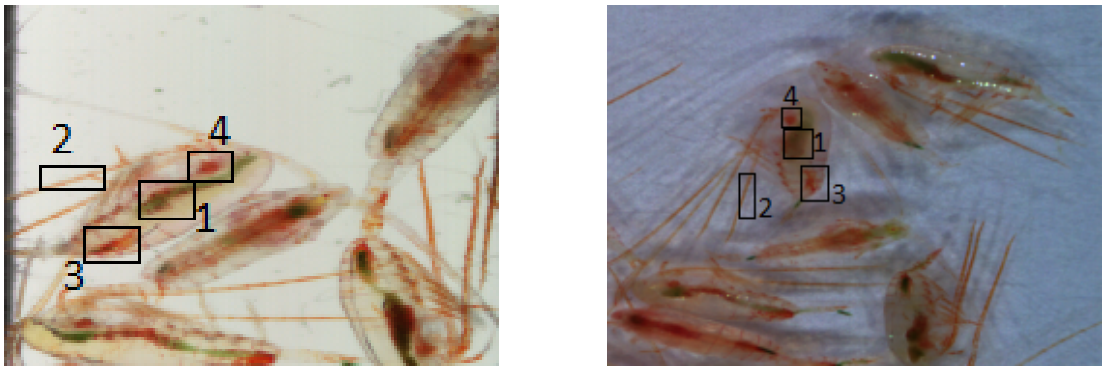

(A) Cropped transmittance image with areas.

(B) Cropped reflectance image with areas.

FIGURE 6.5: Images from Experiment 1 with marked areas as an example for where pixels are chosen from. More specifically, 1 = brain, 2 = digested algae, 3 = astaxanthin-bag, and 4 = antenna.

6.4.5 Masked Copepods

The spectra from the previous approach can provide knowledge of the copepods in a laboratory environment. However, for realistic imaging of the animals in the wild, the size of the copepods will make it challenging to separate the different parts of the copepod for recognition and identification. Based on the assumption that astaxanthin is the dominating pigment of the copepods, a calculated average spectrum of several copepods could provide a spectrum that is more likely to be observed remotely from patches with a high density of copepods. Hence, the average spectrum for each copepod is calculated using binary masks. The masks are created by marking each copepod manually from the original image in the image processing program ImageJ.

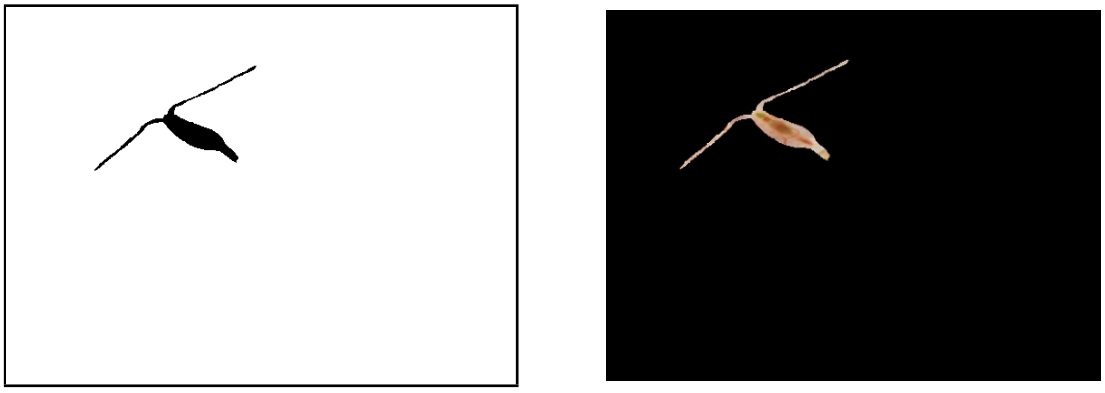

(A) Binary mask

(B) Mask applied to original image

FIGURE 6.6: Masks of copepods

Figure 6.6a shows how the plain mask, while the outcome of applying the mask on the original image is shown in Figure 6.6b. The copepod's average is now calculated as the average of the third dimension, the bands, of all non-black pixels.

6.4.6 Plotting of Copepods

The results in this thesis are mainly plots from different images, showing the results from the two explained methods. The X-axis of the plots represents the wavelength with unit of measurement $[nm]$, and the intensity of the wavelength captured by the

imager is shown on the Y-axis. This is a common representation when describing effects such as absorbance, reflectance, and transmittance, and is, e.g., used to describe the absorbance spectrum of astaxanthin in Figure 6.4. Keep in mind that the spectra are scaled with the reference frames, representing a min/max conversion of the intensity.

The hypercube of data makes it possible to generate several plots showing the information in different comparisons. While the results from Expeirment 1 are all from one transmittance-image, the second experiment is performed with four different scenarios. They are:

- Imaging with reflectance light- wild copepods
- Imaging with transmittance light- wild copepods
- Imaging with reflectance light- lab copepods
- Imaging with transmittance light- lab copepods

The highlights of the results are shown and described in Chapter 7, while all results are in the Appendix.

Chapter 7

Results

In this chapter the results obtained in the laboratory experiments are presented. They consist of both images and spectra, and are shortly described for understanding of the results. A thorough discussion of the results is found in Chapter 8. Additional plots not presented in this chapter are found in the Appendix.

7.1 Results of Spectral Measurements of Copepod Areas

The following figures show the results from the method described in Section 6.4.4.

7.1.1 Transmittance with Laboratory Copepods, Experiment 1

The results from Experiment 1 are all from the image shown in Figure 7.3a. Figure 7.1 shows the spectra from four different places in four different copepods.

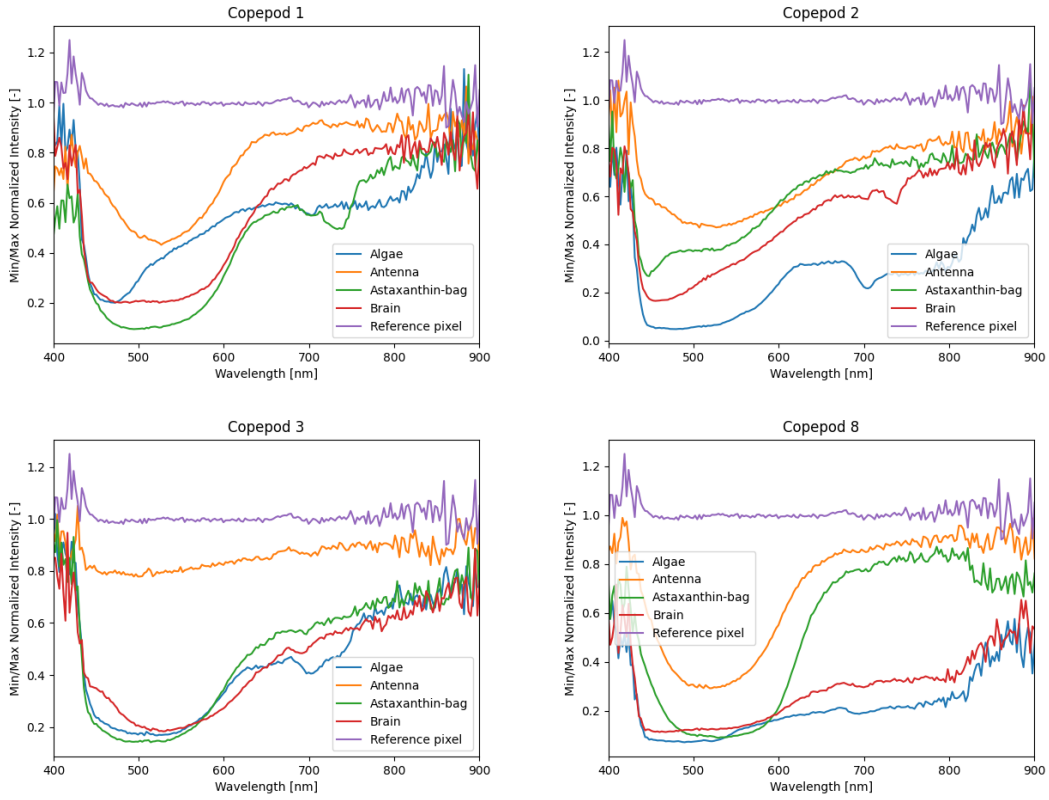

FIGURE 7.1: Areas in four different copepods. Some differences are seen between the copepods, but overall, the spectra show similarities with the absorbance spectrum of astaxanthin in Figure 6.4. The reference pixel is an empty pixel for comparison.

Figure 7.2 shows the spectra divided into the specific areas of the copepods. In this plot, it is easier to see the general pattern of each of the areas.

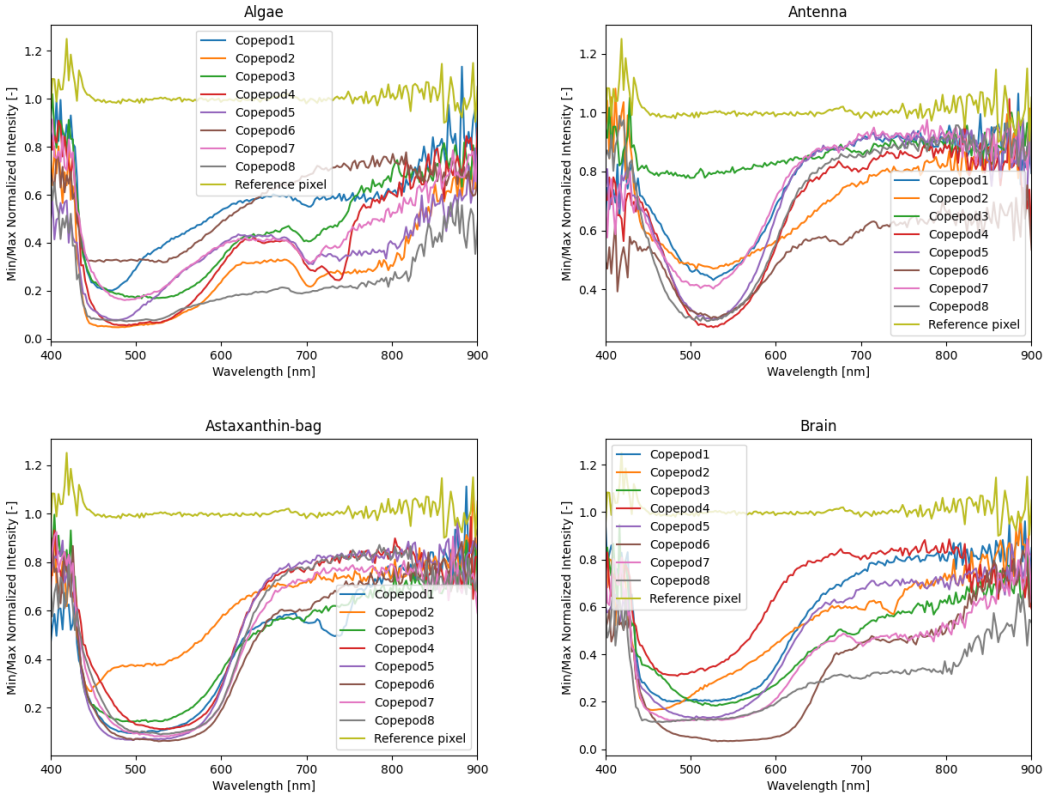

FIGURE 7.2: The same areas in each copepod plotted together. The similarities in the same areas are significant, especially for the astaxanthin-bag.

In Figure 7.3 two figures are shown. The image is the 2D representation of the scanned data-cube. Figure 7.3b shows the calculated average of the different areas in all copepods.

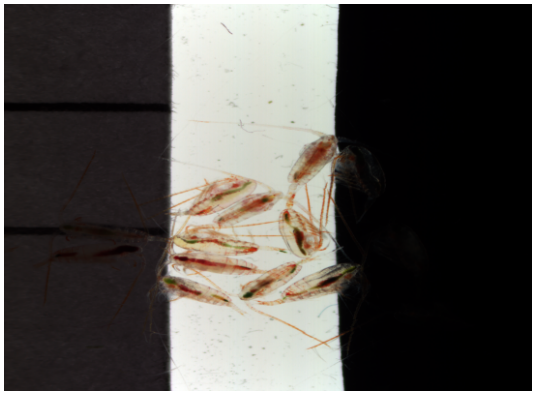

(A) 2D image of the copepods with backlighting. Internals and digested algae can be seen clearly.

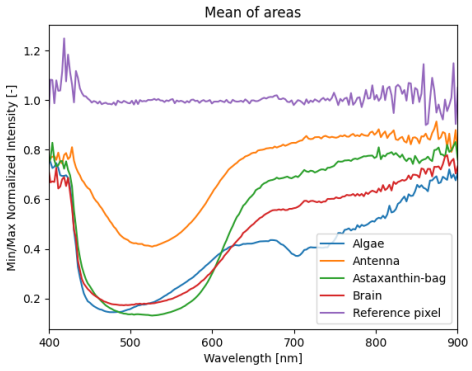

(B) Average spectra of the different areas in a copepods.

FIGURE 7.3: Image and transmittance spectra from Experiment 1. The antenna does not absorb as much light as the others, but the connection to astaxanthin is still clear.

7.1.2 Transmittance with Wild Copepods, Experiment 2

From now on, only the plots with spectra divided into the specific areas of the copepods are included in this chapter, while all results can be found in the Appendix.

The wild copepods are not fed since they came to the lab to have them as close to natural as possible, and there is hence no digested algae in their body. Therefore, Figure 7.4 shows only three areas of all copepods. Figure 7.5 shows the 2D image and the average spectra for all areas.

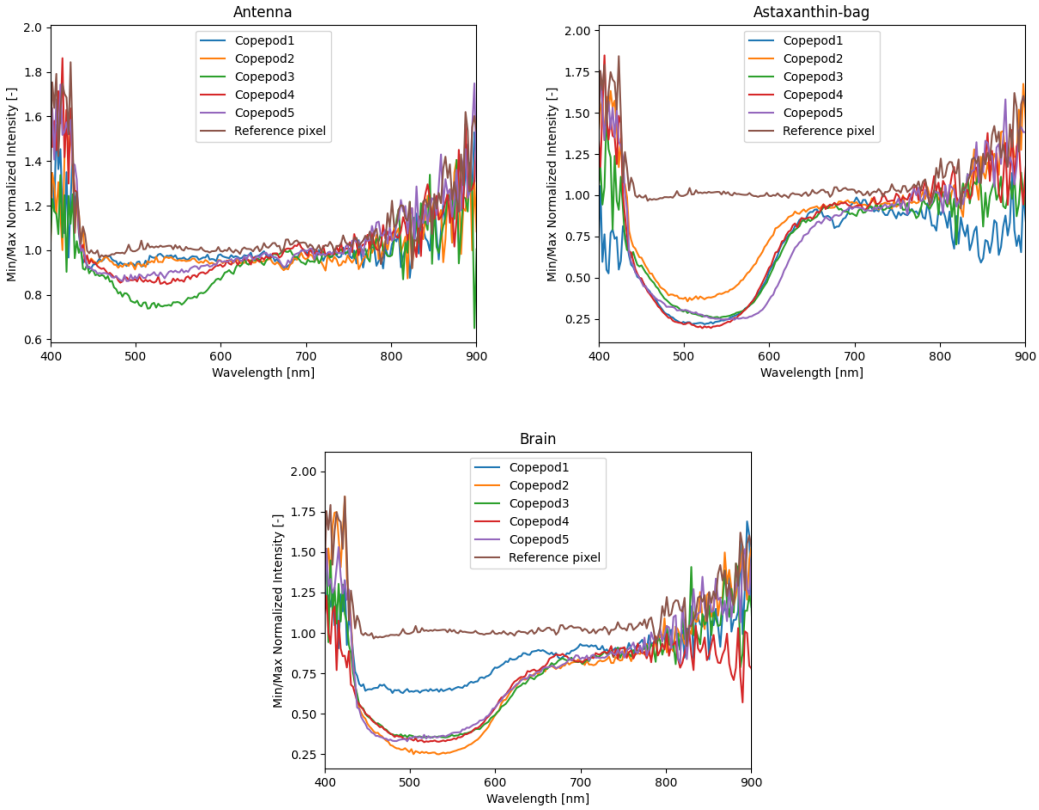

FIGURE 7.4: The same areas in each copepod plotted together. The antennas' spectra are nearly unrecognized by the imager, while the spectra of the astaxanthin bags again are significant. The brain is also significant, but with slightly different spectra than the bag.

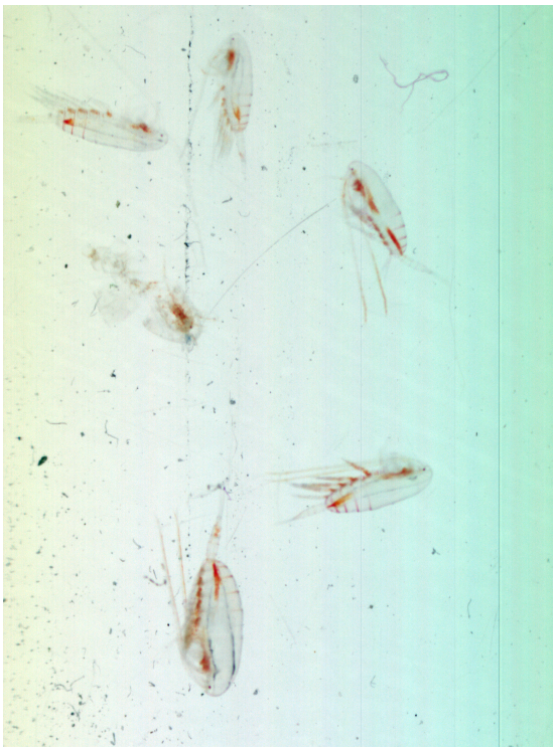

(A) 2D image of the wild copepods with backlighting. Nearly no algae can be seen here.

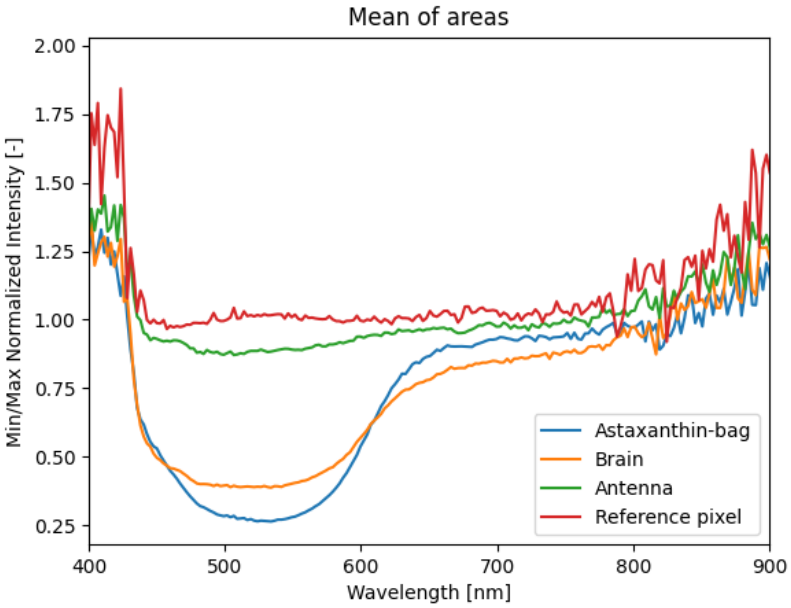

(B) Average spectra of the different areas in the copepods.

FIGURE 7.5: Image and transmittance spectra from Experiment 2, using backlighting and wild copepods.

7.1.3 Transmittance with Laboratory Copepods, Experiment 2

Figure A.5 shows the spectra obtained using the backlighting on the laboratory copepods. Figure 7.7 shows the 2D image and the average spectra for all areas.

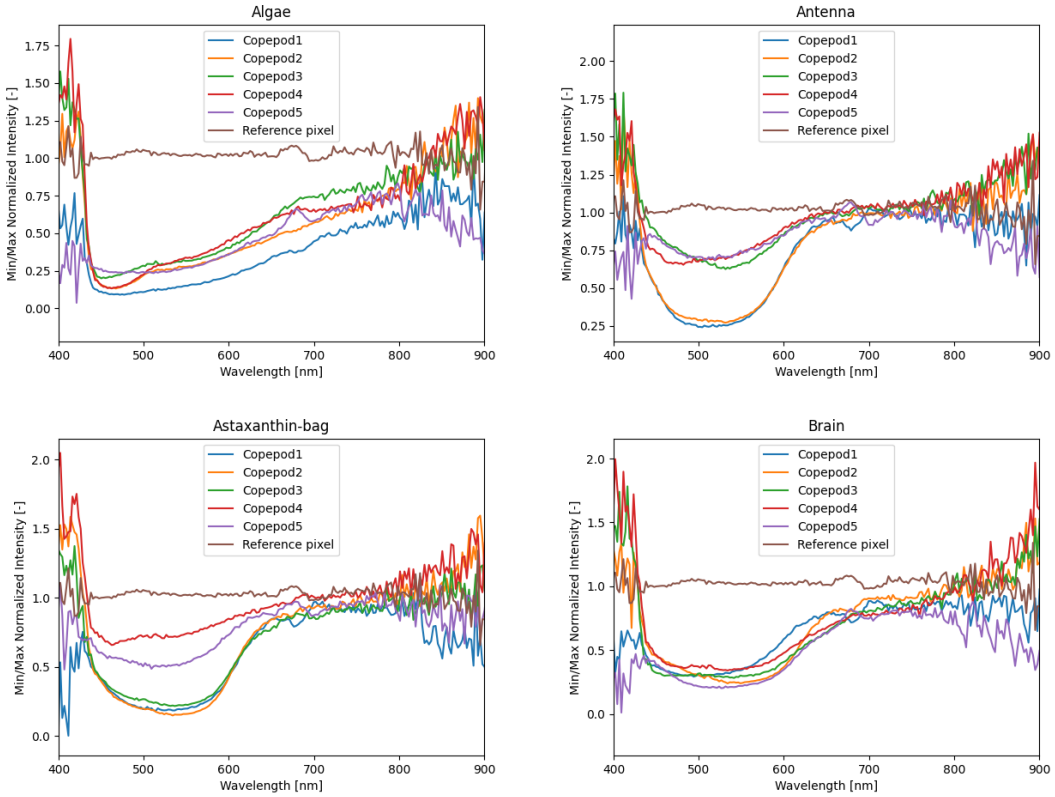

FIGURE 7.6: The same area in each copepod plotted together. The most similar spectra are the algae spectra, but with significant differences from the other spectra.

(A) 2D image of the laboratory copepods. Here we see digested algae inside the copepods

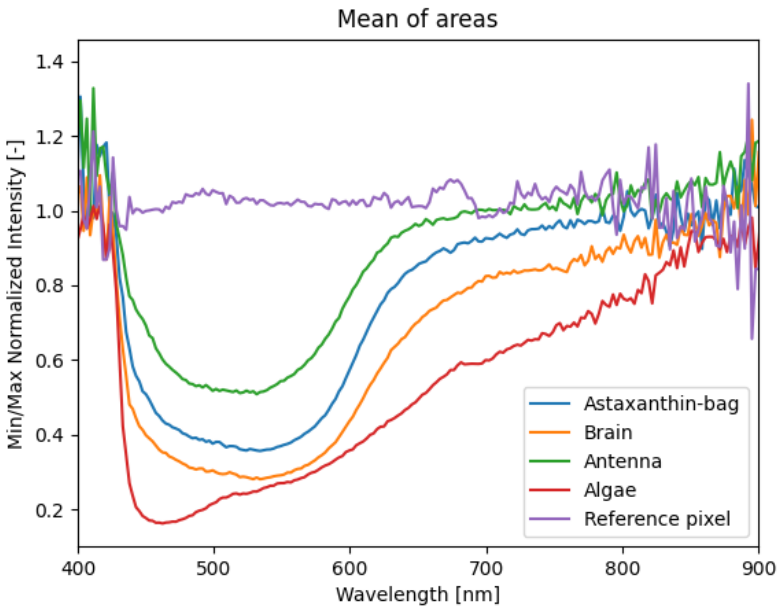

(B) Average spectra of the different areas in a copepods

FIGURE 7.7: Image and transmittance spectra from Experiment 2, using backlighting and laboratory copepods.

7.1.4 Reflectance with Wild Copepods, Experiment 2

With reflectance measurements we use the lights placed next to the imager to obtain a reflectance situation as shown in Figure 4.8 Wild copepods are used here, and Figure 7.8 shows the spectra for the different areas, while Figure 7.9 shows the 2D image and the average spectra for all areas.

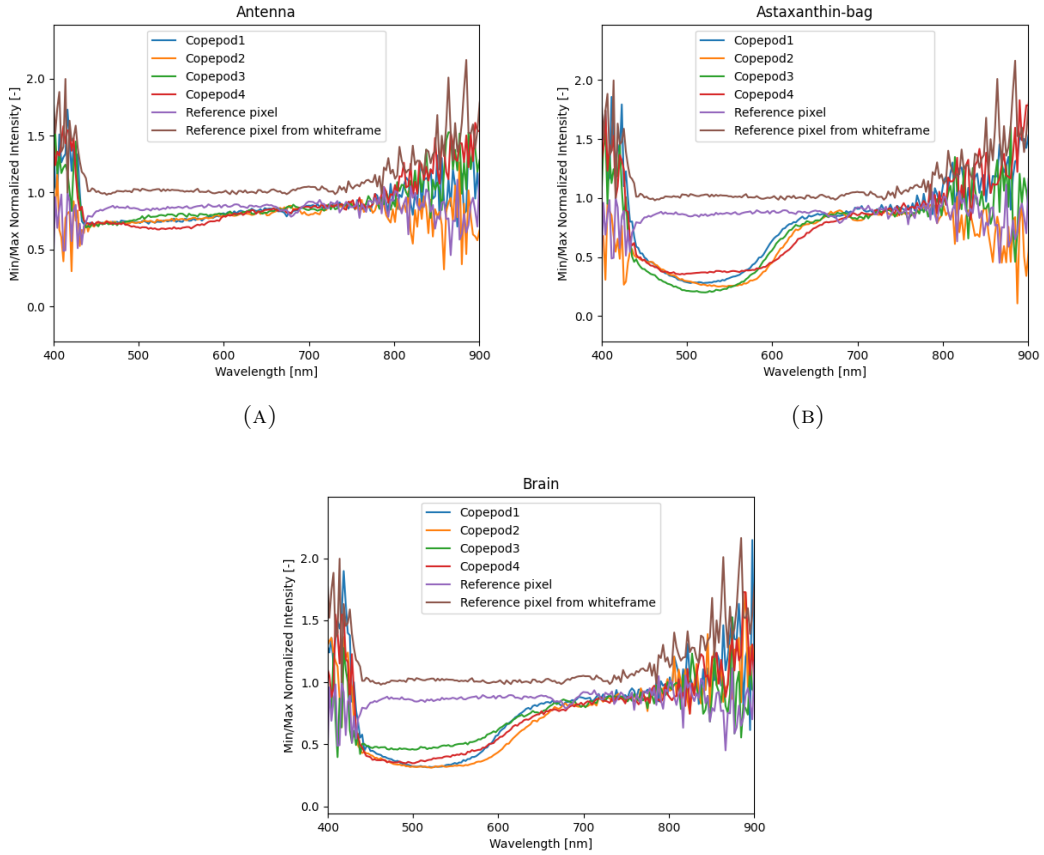

(A) (B)

(C)

FIGURE 7.8: The same areas in each copepod plotted together. The reflectance spectra show weaknesses with noise. The reference pixel shows the effect of light attenuation in the dish and anesthetic. Again, the spectra of the antennas are nearly unrecognized by the imager.

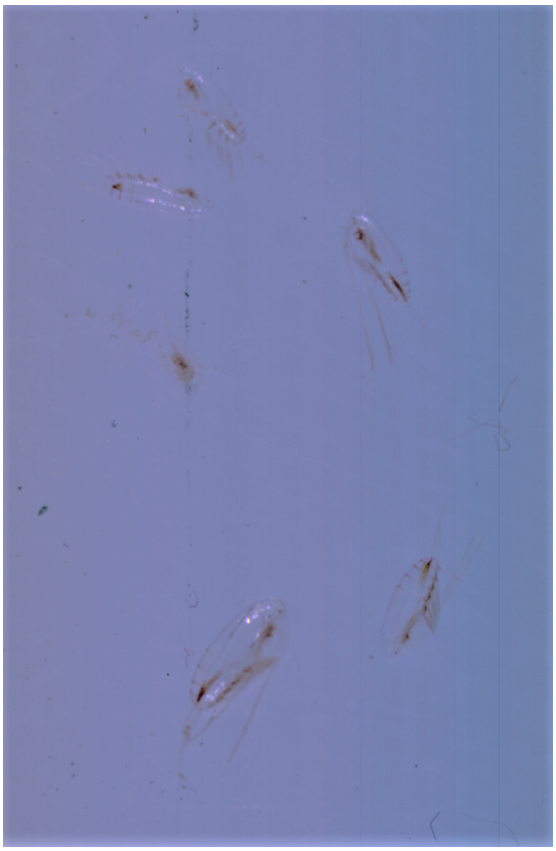

(A) 2D image of the wild copepods with lights placed next to the imager. No algae can be seen here.

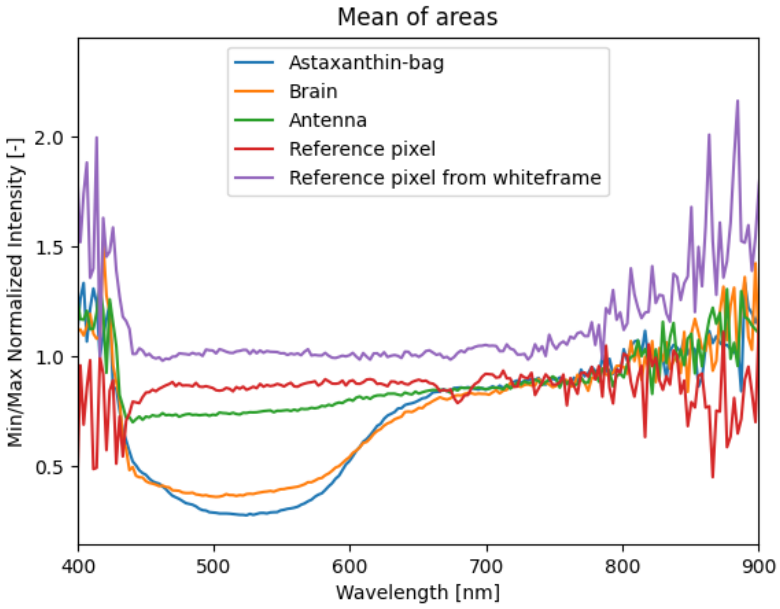

(B) Average spectra of the different areas in a copepods

FIGURE 7.9: Image and reflectance spectra from Experiment 2, using reflectance lighting and wild copepods

7.1.5 Reflectance with Laboratory Copepods, Experiment 2

Finally, we use laboratory copepods for reflectance measurements. Figure 7.10 shows the spectra for the different areas, while Figure 7.11 shows the 2D image and the average spectra for all areas.

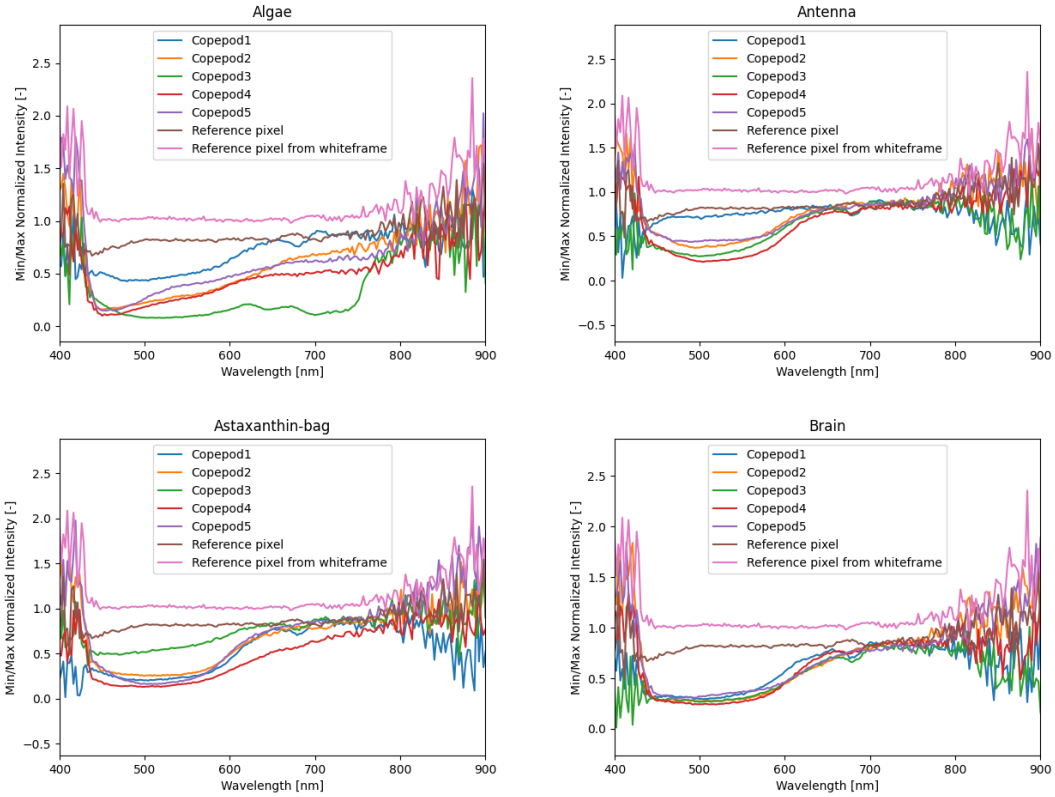

FIGURE 7.10: The same areas in each copepod plotted together. Again, algae is the area that differs the most from the other areas, but these measurements also reveal a large internal variation between the different copepods.

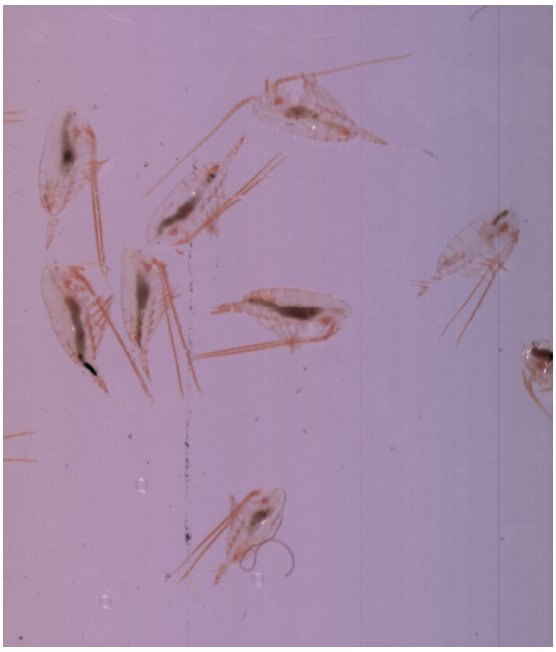

(A) 2D image of the laboratory copepods with lights placed next to the imager. Here we see digested algae inside the copepods.

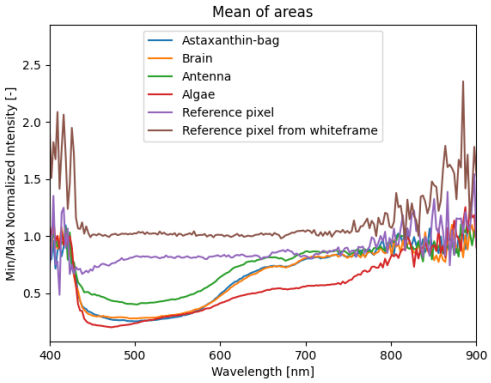

(B) Average spectra of the different areas in a copepods

FIGURE 7.11: Image and reflectance spectra from Experiment 2, using reflectance lighting and laboratory copepods copepods

7.2 Masked Copepods

In the following subsections the results from the method described in Section 6.4.5 are presented. The images used are the same as for the marked areas.

7.2.1 Transmittance with Laboratory Copepods, Experiment 1

Figure 7.12a shows the average over each of the copepod in Image 7.1. The average of these are shown in Figure 7.12b

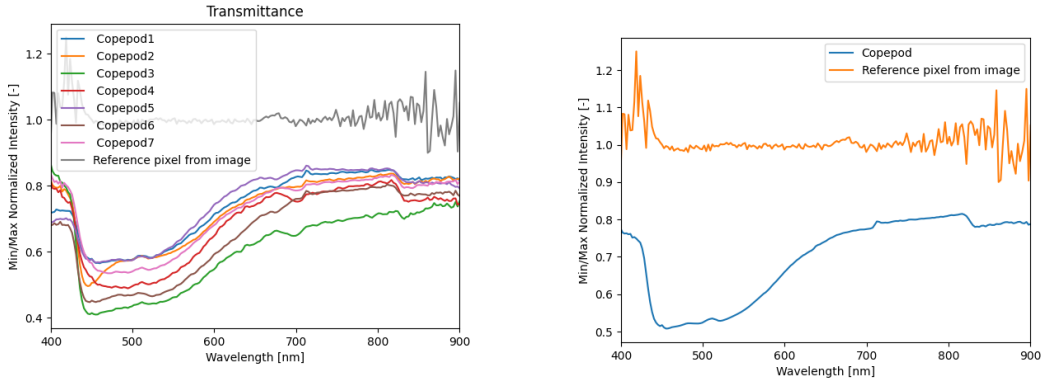

(A) Average spectra of all copepods separately compared to reference pixel

(B) Final average spectrum of all copepods

FIGURE 7.12: Average transmittance spectra of all copepods. The general absorption over all wavelengths are higher with the average, but there is still a significant increased absorption around the expected wavelengths.

7.2.2 Transmittance with Wild Copepods, Experiment 2

Figure 7.13a shows the average over each of the copepod in Image 7.5a. The average of these are shown in Figure 7.13b

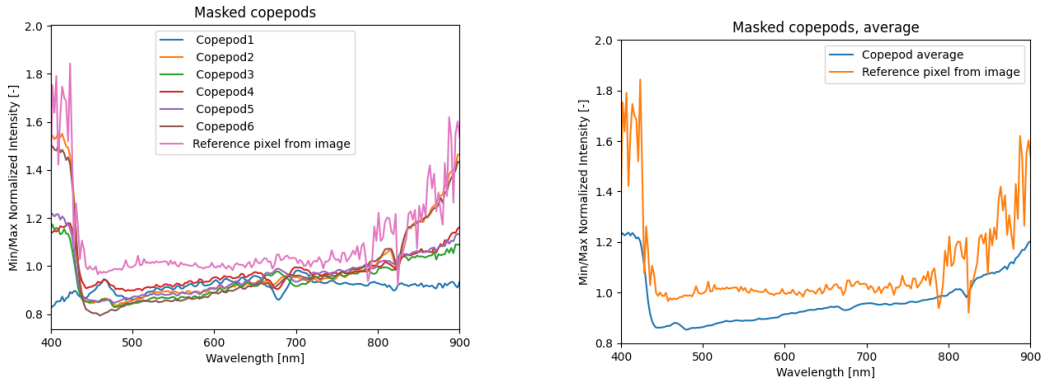

(A) Average spectra off all copepods compared to reference pixel.

(B) Final average spectrum of all copepods

FIGURE 7.13: Average transmittance spectra of all wild copepods. A significantly weaker spectrum is observed, mostly representing a general higher absorption, and not a spectral signature.

7.2.3 Transmittance with Laboratory Copepods, Experiment 2

Figure 7.14a shows the average over each of the copepod in Image 7.7a. The average of these are shown in Figure 7.14b

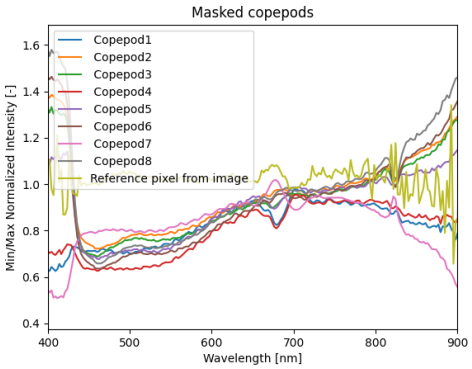

(A) Average spectra of all copepods compared to reference pixel

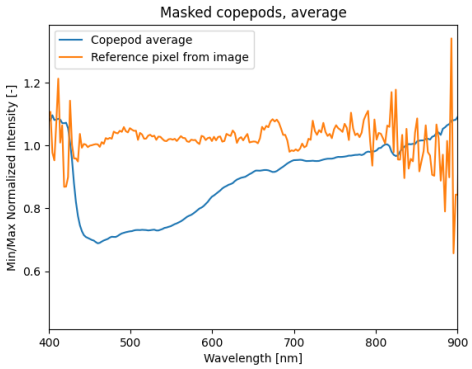

(B) Final average spectrum of all copepods

FIGURE 7.14: Average transmittance spectra of all laboratory copepods. A significant spectral signature is shown here, similar as for the same method in Experiment 1.

7.2.4 Reflectance with Wild Copepods, Experiment 2

Figure 7.15a shows the average over each of the copepod in Image 7.9a. The average of these are shown in Figure 7.15b

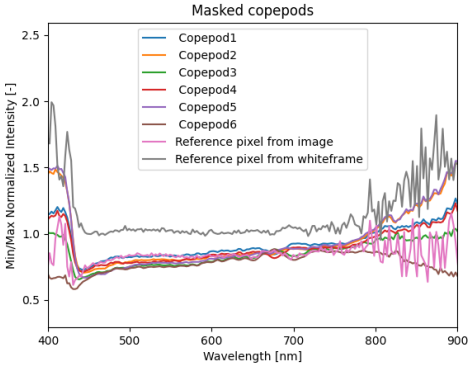

(A) Average spectra of all copepods

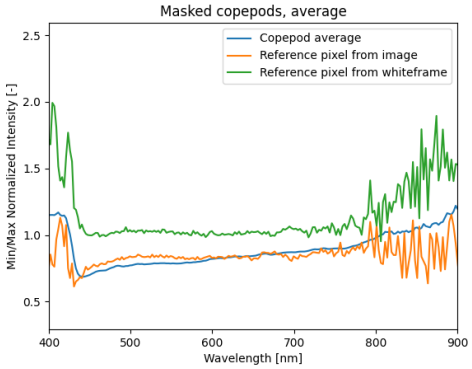

(B) Final average spectrum of all copepods

FIGURE 7.15: Average reflectance spectra of all wild copepods. In this plot there is nearly no absorption, and clearly no spectral signature.

7.2.5 Reflectance with Laboratory Copepods, Experiment 2

Figure 7.16a shows the average over each of the copepod in Image 7.11a. The average of these are shown in Figure 7.16b

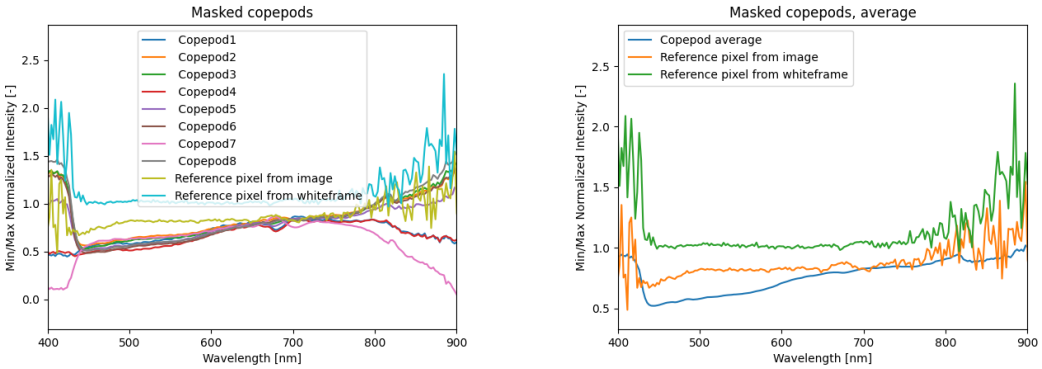

(A) Average spectra of all copepods

(B) Final average spectrum of all copepods

FIGURE 7.16: Average reflectance spectra of all laboratory copepods. Again, a spectra showing higher absorption than the reference pixel, but no clear spectral signature.

Chapter 8

Discussion

In this chapter, the imaging process and the following results are discussed. The discussion is mainly divided into the experimental approach and results.

8.1 Imaging Approaches

The first laboratory experiment was performed during the pre-work for the thesis conducted the previous fall. The primary purpose of this experiment was to figure out if reasonable results could be obtained using the imaging approach. With the knowledge from this experiment, the second experiment was conducted in the spring, which provided most of the results presented in the thesis.

8.1.1 Laboratory Experiment 1

Other than what was necessary to perform the experiment, there was no plan or procedure for the imaging process of the first experiment. As it was not clear what the possible results could be used for, several approaches were tested. This resulted in a lot of time in calibration, test images, and rather pointless scans. As a reminder, the images are not captured like regular "snapshot"-images, but with the scanning method described in Section 5.4. As an example, to obtain the resolution shown in Figure 7.3a from Experiment 1, a scanning time of over a minute was necessary.

When optimal settings were found, some of the results were surprisingly satisfactory. Considering the small size of the copepods, approximately 2 mm long, the resolution of the imaging itself is quite impressive. The scanning method makes the imaging highly sensitive to movement, and any minor disturbances of the stage will be visible in the scan. The copepods are anesthetized in order to stay calm during the imaging, and this is fully necessary for the imaging in the laboratory. Although this is not representative of a real situation, remote sensing is not sensitive to this kind of small movements. However, if hyperspectral imaging is to be used *in situ*, e.g., in combination witch SilCam, these movements are crucial, and the same resolution of images would be challenging to obtain outside the laboratory environment.

There were several faults with the first laboratory experiment in terms of lack of measurement, which were corrected in the second experiment. One of these issues was that it was not recorded reference frames with the images. This is especially an issue for the reflectance images because there is no reference to normalize the result. Hence, the results are not a representation of the copepods solely, but a combination of the copepods and the incident light. Also, shadows from the copepods in the anesthetic were a problem, contributing to noise and incorrect measurements. With these faulty results, the images were not further used, but the findings provided knowledge used in

the second experiment.

The situation is a little different for the transmittance images. Here, the reference from a tile would make no sense, and the true white reference is the pure illumination from the light source below the copepods. There were not performed any scans with only this light, but it is assumed that the attenuation effects from the glass and the anesthetic can be neglected. Another problem with these scans is that the copepods are very close or lying on top of each other. This could possibly be a source of error for the results, as different parts are affected by other copepods. Although it is not a too big of an issue, it was still taken care of for the second experiment.

8.1.2 Laboratory experiment 2

For the second experiment, we had a larger idea of what to do and what to expect. However, even though we knew which settings provided the best results the last time, it took quite some time to have a sufficient focus of the copepods. To have a wider spreading of the animals, the camera objective was further away from the copepods, which made it challenging to obtain sharp images. The black cover with the small square was not used this time, because it would leave the copepods too close to each other. We made sure to use less anesthetic this time to minimize the effect of shadows when using the reflecting light.

There were several problems with the new approach, some discovered in the lab and some discovered during the data processing. The spreading of the copepods also meant that larger areas would have to be scanned. While each scan in Experiment 1 consisted of 400 lines, the scans now consisted of 2138 lines. Hence, the scanning time took five times the time of the scans in the first experiment, and likewise for the amount of data.

To obtain this scanning area, the camera objective was, as said, further away from the individuals. The scans covered larger areas, and the edge of the glass was included in the images. For the reflectance measurements, this affected the images to a large degree. The resulting 2D image is scaled with the different light intensities, and as the edges reflect a large amount of light, everything else in the image appears dark. Cropping the data cube in the processing diminishes this effect to a small degree, but we are far away from obtaining the same resolution and "true color" effect as we did in Experiment 1. However, the effect this has on the spectral measurements is critical.

In general, the assumptions made in Section 5.3 can be of significance for the results. While it is assumed that the overhead lighting is perpendicular to the camera, it is in practice angled, causing angular effects which should, if more complex modelling was intended, be handled by implementing calculation of Snell's law and Fresnel's equations. It is also assumed that scattering can be neglected inside both copepods, anesthetic, and petri dish, which does not reflect the true situation. While the transmittance measurements are little affected by this, reflectance measurements are affected by both transmission, absorption, and scattering effects. Hence, the real situation is quite different from the ideal situation, where it is assumed that the reflected light is pure reflectance of the copepods' surface. In addition, these effects are squared for reflectance measurements to account for that the light rays enter everything except the stage, which we assume to be opaque, twice.

8.2 Spectral Measurements in Specific Areas

The objective of this approach was to see if significant spectral signatures could be obtained for different parts of the copepods and if they would match the absorption spectrum of astaxanthin.

8.2.1 Transmittance

First of all, for all images, it is observed that the scaling function works as it should, as the reference pixel is constant at approximately 1. There is still some noise affecting the signals, however, and this is of a significant matter before 400 nm and after 700 nm for all images. This noise is assumed to be a result of a weaker signal of the light source in these boundaries. However, the interesting area relatively unaffected by this.

First, the plots of the different copepods in Figure 7.1 from Experiment 1 are considered. These four plots are chosen out of eight for being the spectra with the most significant differences. The overall impression is that most of the areas show clear similarities in effects of absorption in the corresponding area of absorbance in astaxanthin. The differences in between the copepods can be of several reasons, many of these as a result of the simplifications described in Section 5.3. As the copepods are differently positioned relative to the imager, angular effects are introduced. To avoid this, the copepods would have to be placed at a line along track, which extremely challenging due to their size and floating position. Internal differences are also present, as the copepods may be of different age and composition.

Considering the plots of the different areas in Figure 7.2, more similarities are shown. Except for 1 copepod, all spectra for the astaxanthin-bag are highly consistent in the considered area. They show a clear connection to the absorption spectrum of astaxanthin, and surely confirm the potential of the task. The spectra of digested algae show a larger variation between the copepods, but also significantly different signatures than the astaxanthin. The digested algae may be of either red or green color, impacting the color of the internals. The molecular composition may differ based on the type of algae or how far in the digesting process it has come, affecting the spectral signatures. The same holds for the brain, as the molecular composition here is different than for the more pure astaxanthin found in the astaxanthin-bag. It must be noted that even though components contain astaxanthin, different compounds of the pigment may result in different spectral signatures.

The spectra of the antennas reveal an important weakness of this method. All pixels used to obtain these spectra are chosen manually by locating one pixel in the selected area and plotting its spectrum. This pixel may not be representative for the complete area, or may show a significant color due to unknown factors. The small size of the antennas makes them nearly impossible to see with the human eye, and also the imager struggles to obtain sufficient resolution of these pixels to obtain their spectrum. Hence, some of the pixels containing parts of the antennas show higher intensity than others as the registered absorbance is weaker. However, there are also clear correspondence with the absorption spectrum of astaxanthin for the spectra of high resolution. This confirms that the areas with the expected highest levels of astaxanthin, astaxanthin-bag and antennas, show spectral signatures matching the known absorption spectrum of astaxanthin.

For the subsequent transmittance measurements captured in the second experiments, similar results are observed. However, the plots showing the digested algae of the laboratory copepods in Figure A.5 are more consistent compared to the previous experiment. This may result from that all copepods are recently fed with the same algae, but it can also result from poorer resolution of the image. Nevertheless, the spectral signature is different from astaxanthin as expected, revealing a distinct molecular composition. Again, the astaxanthin-bag spectra are consistent. The antennas of the wild copepods, however, show surprisingly weak signatures. It is unknown whether this is because of a smaller amount of astaxanthin or the image resolution. As seen in the corresponding 2D image in Figure 7.5a, it is challenging to see the antennas of some of the copepods, which can result in poorly chosen pixels. If this can be used to determine whether the wild copepods truly are of the species *C.finmarchichus* or not, goes beyond the analyzes of this thesis and would require additional expertise from biologists.

8.2.2 Reflectance

Overall, the reflectance measurements show similar spectral signatures as for the transmittance images, as expected. The spectra of the astaxanthin-bag and brain are still relatively consistent, with minor differences. The spectra of digested algae, however, are quite different from the transmittance images. This indicates that the very similar transmittance spectra to a larger degree is a result of imager resolution rather than the feed. Again, the antennas show nearly no spectral signature for the wild copepods, and the reasons considered for the transmittance images still hold.

In general, the reflectance measurements are weaker than the transmittance measurements, and several reasons for this are discussed in the imaging approach. The results may show that too many assumptions are made and that they are not representative of the real situation of the complex relations. An example is the neglecting of the scattering and absorption of the anesthetic and petri dish, which is of significance considering the reference pixel (not from the white frame). However, the results are satisfactory both due to consistency and correspondence with the absorption spectrum of astaxanthin, showing large potential for future purposes.

8.3 Copepod Masks

The processing with the copepods masks intends to obtain an average spectrum over the whole copepod, which is more likely to be observed remotely. If remote sensors and UAVs are able to detect a significant change in the spectrum it scans, it can be a sign of patches of the zooplankton it searches for, whether it is krill, copepods, or similar.

The spectra obtained in the experiments are both from transmittance and reflectance images. Because they both will measure light entering the imager, they are both likely to show a similar spectrum opposite to the astaxanthin absorption spectrum. However, outside the lab, these two sources of light change the mission significantly. The transmittance-lighting depends on an illumination behind the OOIs, which is not a natural situation. This is only possible to achieve for a mission using sensors like SilCam, where the water flows between the illumination source and the imager. For remote sensing, however, the reflectance spectrum is interesting.

8.3.1 Transmittance

The image from the first experiment is of high resolution, and body internals are clearly observed. A significant change in the desired area, around 500 nm, is observed. As this is an average over all parts of the copepods, the similarities with astaxanthin are not as clear as for some of the specific parts, but the spectra are consistent over all the copepods, confirming a general average spectrum for these individuals. Considering the results for the laboratory copepods, the shape of the average spectra is similar to the results from the first experiment. This indicated a common average spectrum of the species, even though camera settings and image resolution is different.

The results are remarkably worse from the experiment with wild copepods. There is almost no spectral signature observed other than a general weaker intensity over all wavelengths. The assumed primary reason to this is that they have no absorption due to digested algae, and appear more transparent than the laboratory copepods. Another reason could be that they in general contain a smaller amount of astaxanthin, corresponding to being a different species.

8.3.2 Reflectance

The average reflectance measurements are also weak, both for wild and laboratory copepods. The spectral signature observed in the transmittance spectra is not recognized here, other than a general weaker intensity in the interesting area for the laboratory copepods. This could be of several reasons, both experimental faults or a challenging technological task. Without similar results from the first experiment, it is not possible to compare these measurements with measurements of other camera settings, which should be further analyzed before a conclusion is made upon this approach.

Although the laboratory environment is advantageous for spectral analyzes, it does not necessarily represent how remote sensing would perform. The individuals in the laboratory are separated and analyzed one by one, while large patches of copepods would be observed as a significant change in ocean color, e.g., as presented in the mentioned study by Basedow et al. (2019). Hence, the method has a lot of potential for remote investigation and should be further explored with the use of aerial vehicles.

Chapter 9

Conclusions and Further Work

9.1 Conclusions

This thesis has investigated methods that can contribute to obtaining more knowledge and increased mapping and monitoring of species in lower trophic levels, focusing on zooplankton. This study was done through presenting a brief review of the existing technology of sensor-carrying platforms and sensors, which all complement each other for the purpose. Both well-known concepts and new developments were described and evaluated for their potential in zooplankton mapping.

The scientific contribution of the thesis is hyperspectral imaging of copepods, namely the species *Calanus finmarchichus*. Through two different laboratory experiments, spectral signatures of alive individuals were obtained. Both spectra from specific areas in the copepods and average spectra were achieved through data processing, suitable for various purposes. One group of individuals were from a laboratory stock of DNA-tested copepods, while the other group was newly isolated from Trondheimsfjorden. For both groups, both transmittance and reflectance measurements were performed.

The imaging process and following results exceeded our expectations. Most 2D images were of high resolution despite the copepods' small size and the imaging method. The majority of the spectral measurements were also satisfactory, revealing interesting information unnoticeable for the human eye. The results for the specific areas show significant spectral signatures. The areas were evaluated for consistency in all individuals and compared to the absorption spectrum of the red pigment *astaxanthin*. The areas that were assumed to contain high contents of the pigment also proved this with their spectral signature, confirming the task's potential. Wild and laboratory copepods were in general similar, but with some significant differences. It is, however, not sure whether this is for biological reasons or due to inaccurate imaging or data analysis.

The results of each copepod's average spectra were weaker than the measurements of the specific areas. However, for transmittance spectra with laboratory copepods, a consistent spectral signature was obtained using different imager settings. This reveals a potential for determining a general spectral signature of *Calanus finmarchichus* species. However, there is a large room for improvement in both the imaging approach, mathematical modeling of the complex system, and data analyses, proposing many opportunities for further work.

9.2 Further Work

This thesis presents some ideas as small steps towards mapping and monitoring of zooplankton in large ocean areas. Hence, further work would include an improvement of the work presented in this thesis, as well as new contributions to bring us closer to the goal.

Several weaknesses of the performance of the laboratory experiments are discussed, and there is revealed room for improvement when it comes to the imaging procedure. More complex models for the copepods can be developed for extensive analyzes, providing more information about the species in general. With these improvements, the spectral signatures can be used to identify similar spectra and further identify the exact species observed. For instance, to differentiate some of the *Calanus* species in Norwegian coastal areas, DNA analyzes are today the only solution. Spectroscopy may suit as an alternative to this solution. As an example, different spectra were in this thesis obtained for the DNA-verified individuals of *C.finmarchichus* and the unverified, wild individuals. If this was due to biological differences or faulty measurements is unsure and could be interesting to continue with.

The hyperspectral images obtained in the laboratory can serve as a "ground truth" for imaging of copepods, in this case especially the *C.finmarchichus*. They were satisfactory in terms of spectra with similarities with the absorption spectrum for astaxanthin and can be used in additional improvements, such as Artificial Intelligence (AI) and Machine Learning. These concepts are highly interesting for mapping large ocean areas. Computer programs can be taught to recognize significant spectra for a zooplankton species and tell the difference between spectra from zooplankton and other spectra from the ocean. With such algorithms, many interesting technologies can be further developed. For instance, real-time object detection can be used on AUVs to perform adaptive sampling, shortly described in the thesis. If AUVs can follow and measure large patches of zooplankton autonomously, information can be collected more effective, more correctly, and safer than ever before.

In general, there are endless possibilities for technological improvements to increase knowledge about zooplankton and other pivotal species of our ecosystem. Each step contributes to ensuring more sustainable harvesting, improving ocean health, and possible positive effects of climate change. Through previous developments and the results of this thesis, optical imaging has proven to provide a large potential in the work towards future solutions and should be given a lot more attention in the future.

Bibliography

Aker Biomarine (n.d.). *The power of tiny krill*. URL: https://www.akerbiomarine.com/the-power-of-tiny-krill-0. (accessed: Sept. 10, 2020).

Asner, G. P. et al. (2007). "Carnegie airborne observatory: in-flight fusion of hyperspectral imaging and waveform light detection and ranging for three-dimensional studies of ecosystems". In: *Journal of Applied Remote Sensing* 1.1, p. 013536.

Basedow, S. L. et al. (2019). "Remote sensing of zooplankton swarms". In: *Scientific reports* 9.1, pp. 1–10.

Bazilchuk, N. (2021). *Sporhunden som lukter mikroalger*. URL: https://gemini.no/2021/05/lauv-sporhunden-som-lukter-mikroalger/?fbclid=IwAR13b_h4ftiL8YIErsNy3mxOuxS8r9T84qRaYrCOQ3zqLT9Qv1uLJki93UY. (accessed: June. 04, 2021).

Beddington, J. R. and R. M. May (1982). "The harvesting of interacting species in a natural ecosystem". In: *Scientific American* 247.5, pp. 62–69.

Berge, J., G. Johnsen, and J. H. Cohen (2020). *POLAR NIGHT Marine Ecology: Life and Light in the Dead of Night*. Springer Nature.

Birkeland, R. (2009). *Satelitt*. URL: https://snl.no/satellitt. (accessed: May. 10, 2021).

BluEye (n.d.). *BluEye*. URL: https://www.blueye.no/?gclid=CjwKCAiAt9z-BRBCEiwA_bWv-Fv6J-A-kSYbNTgcc78jpvDSJR-jBec2dhKOp66aJGnkcFSge3WfpBoCiDMQAvD_BwE. (accessed: Dec. 14, 2020).

Boggs, T. (n.d.). *Spectral Python 0.21 Documentation*. URL: https://www.spectralpython.net/index.html. (accessed: May. 25, 2021).

Borge, L. (2017). *Vil åpne for høsting av nøkkelart i Norge*. URL: https://www.aftenposteninnsikt.no/klimamilj/vil-pne-h-sting-av-n-kkelart-i-norskehavet. (accessed: March. 08, 2021).

Born, M. and E. Wolf (2013). *Principles of optics: electromagnetic theory of propagation, interference and diffraction of light*. Elsevier.

Broms, C. et al. (2016). "Vitenskapelig bakgrunnsmateriale for forvaltningsplan for raudåte". In:

Calanus (n.d.). *Calanus Finmarchichus*. URL: https://calanus.no/resource/. (accessed: Mar. 19, 2021).

Cuzin-Roudy, J et al. (2014). "Southern Ocean Euphausiids". In: *Biogeographic Atlas Southern Ocean*, p. 510.

Cyperphysics (n.d.). *The Electromagnetic spectrum: the familiy of light*. URL: https://www.cyberphysics.co.uk/topics/light/emspect.htm. (accessed: April. 26, 2021).

Dahl, E. M. H. and A. Ø. Stien (2019). "Identification of Marine Plastics using Hyperspectral Imaging and Raman Spectroscopy". MA thesis. NTNU.

Dalamagkidis, K. (Jan. 2015). "Classification of UAVs". In: pp. 83–91. ISBN: 978-90-481-9706-4. DOI: 10.1007/978-90-481-9707-1_94.

Davies, E. J. et al. (2017). "The use of wide-band transmittance imaging to size and classify suspended particulate matter in seawater". In: *Marine pollution bulletin* 115.1-2, pp. 105–114.

ESA (n.d.). *SENTINEL-3*. URL: https://sentinel.esa.int/web/sentinel/missions/sentinel-3.

Everson, I. (2008). *Krill: biology, ecology and fisheries*. John Wiley & Sons.

fishfarmingExpert (2020). *Study finds multiple benefits of krill diet for salmon*. URL: https://www.fishfarmingexpert.com/article/study-finds-multiple-benefits-of-krill-diet-for-salmon/. (accessed: Sept. 14, 2020).

Fossum, T. O. et al. (2019). "Toward adaptive robotic sampling of phytoplankton in the coastal ocean". In: *Science Robotics* 4.27.

Funk, V. A. and L. A. Hobson (1991). "Temporal variations in the carotenoid composition and content of Euphausia pacifica Hansen in Saanich Inlet, British Columbia". In: *Journal of experimental marine biology and ecology* 148.1, pp. 93–104.

Geospatial, L. (n.d.). *ENVI Image Files*. URL: https://www.l3harrisgeospatial.com/docs/enviimagefiles.html. (accessed: May. 25, 2021).

Geyer, R., J. R. Jambeck, and K. L. Law (2017). "Production, use, and fate of all plastics ever made". In: *Science advances* 3.7, e1700782.

Giske, J. (2018). *Det er på tide å tenke nytt om hvordan vi skal høste fra havet*. URL: https://fiskeribladet.no/tekfisk/nyheter/?lukk_cookieinfo=ja&artikkel=62052. (accessed: Sept. 07, 2020).

Greenpeace International (2018). *License to Krill*. URL: https://www.greenpeace.org/international/publication/15255/licence-to-krill-antarctic-krill-report/. (accessed: Sept. 10, 2020).

Hegrenæs, Ø., T. O. Sæbø, P. E. Hagen, et al. (2010). "Horizontal mapping accuracy in hydrographic AUV surveys". In: *2010 IEEE/OES Autonomous Underwater Vehicles*. IEEE, pp. 1–13.

IUCN (n.d.). *Marine plastics*. URL: https://www.iucn.org/resources/issues-briefs/marine-plastics. (accessed: 06. 07, 2021).

Jambeck, J. R. et al. (2015). "Plastic waste inputs from land into the ocean". In: *Science* 347.6223, pp. 768–771.

Johnsen, G. et al. (2013). "Underwater hyperspectral imagery to create biogeochemical maps of seafloor properties". In: *Subsea optics and imaging*. Elsevier, 508–540e.

Johnsen, G. et al. (2016). "The use of underwater hyperspectral imaging deployed on remotely operated vehicles-methods and applications". In: *IFAC-PapersOnLine* 49.23, pp. 476–481.

Jones, C., S. Kawaguchi, and K. Reid (2015). *Krill- biology, ecology and fishing*. URL: https://www.ccamlr.org/en/fisheries/krill-%E2%80%93-biology-ecology-and-fishing. (accessed: Sept. 14, 2020).

Karpathy, A. et al. (2016). "Cs231n convolutional neural networks for visual recognition". In: *Neural networks* 1.1.

Kebkal, K. and A. Mashoshin (2017). "AUV acoustic positioning methods". In: *Gyroscopy and navigation* 8.1, pp. 80–89.

Krafft, B. (2019). *Tema: Krill - Antarktisk krill*. URL: https://www.hi.no/hi/temasider/arter/antarktisk-krill. (accessed: May. 11, 2021).

Lotocka, M and E Styczynska-Jurewicz (2001). "Astaxanthin, canthaxanthin and astaxanthin esters in the copepod Acartia bifilosa (Copepoda, Calanoida) during ontogenetic development". In: *Oceanologia* 43.4.

Mahmoud, M. S., M. O. Oyedeji, and Y. Xia (2021). "Chapter 10 - Path planning in autonomous aerial vehicles". In: *Advanced Distributed Consensus for Multiagent Systems*. Ed. by M. S. Mahmoud, M. O. Oyedeji, and Y. Xia. Academic Press, pp. 331–362. ISBN: 978-0-12-821186-1. DOI: https://doi.org/10.1016/B978-0-12-821186-1.00018-0. URL: https://www.sciencedirect.com/science/article/pii/B9780128211861000180.

Manolakis, D. and G. Shaw (2002). "Detection algorithms for hyperspectral imaging applications". In: *IEEE Signal Processing Magazine* 19.1, pp. 29–43. DOI: 10.1109/79.974724.

McRee, G. J. (1977). *The Role of Aerospace Technology in Agriculture: 1977 Summer Faculty Fellowship Program in Engineering Systems Design, NASA-Langley Research Center, American Society for Engineering Education, Old Dominion Research Foundation*. National Aeronautics and Space Administration.

Melle, W. et al. (2014). "The North Atlantic Ocean as habitat for Calanus finmarchicus: Environmental factors and life history traits". In: *Progress in Oceanography* 129, pp. 244–284.

Miller, D. and I Hampton (1989). "Krill aggregation characteristics: spatial distribution patterns from hydroacoustic observations". In: *Polar biology* 10.2, pp. 125–134.

Mogstad, A. A. et al. (2020). "Mapping the historical shipwreck figaro in the high arctic using underwater sensor-carrying robots". In: *Remote Sensing* 12.6, p. 997.

Myrbakken, P. S. (2021). *Å fiske etter raudåte – Havets nyeste kontrovers?* URL: https://www.kystogfjord.no/nyheter/forsiden/AA-fiske-etter-raudaate-Havets-nyeste-kontrovers. (accessed: March. 19, 2021).

NASA (n.d.). *Remote Sensors*. URL: https://earthdata.nasa.gov/learn/remote-sensors. (accessed: May. 11, 2021).

National Geographic (n.d.). *Krill*. URL: https://www.nationalgeographic.com/animals/invertebrates/group/krill/. (accessed: Sept. 10,2020).

Nicol, S, A James, and G Pitcher (1987). "A first record of daytime surface swarming by Euphausia lucens in the Southern Benguela region". In: *Marine Biology* 94.1, pp. 7–10.

NTNU (2020). *omega-3-fettsysrer*. URL: https://sml.snl.no/omega-3-fettsyrer. (accessed: March. 12, 2021).

— (n.d.). *Ailaron*. URL: https://www.ntnu.edu/web/ailaron. (accessed: June. 04, 2021).

Ocean Exploraiton (n.d.). *Why are so many deep-sea animals red in color*. URL: https://oceanexplorer.noaa.gov/facts/red-color.html. (accessed: April. 23, 2021).

Oceana (n.d.). *Open Ocean*. URL: https://oceana.org/marine-life/marine-science-and-ecosystems/open-ocean. (accessed: June. 07, 2021).

Ødegård, Ø. et al. (2016). "A new method for underwater archaeological surveying using sensors and unmanned platforms". In: *IFAC-PapersOnLine* 49.23, pp. 486–493.

Ødegård, Ø. et al. (2018). "Underwater hyperspectral imaging: A new tool for marine archaeology". In: *Applied optics* 57.12, pp. 3214–3223.

Pedersen, A. M. (2007). "Olje fra raudåte (Calanus finmarchicus). Oksidativ stabilitet, fettklasser og karotenoidinnhold." MA thesis. Universitetet i Tromsø.

Pettersen, R. et al. (2014). "Development of hyperspectral imaging as a bio-optical taxonomic tool for pigmented marine organisms". In: *Organisms Diversity & Evolution* 14.2, pp. 237–246.

Prado-Cabrero, A. and J. M. Nolan (2021). "Omega-3 nutraceuticals, climate change and threats to the environment: The cases of Antarctic krill and Calanus finmarchicus". In: *Ambio*, pp. 1–16.

Repstad, T. (2019). *5 Things You Probably Didn't Know About Krill*. URL: https://www.superbakrill.com/blog/5-things-you-probably-didnt-know-about-krill. (accessed: June. 5, 2021).

Ritchie, H. (2019a). *Food production is responsible for one-quarter of the world's greenhouse gas emissions*. URL: https://ourworldindata.org/food-ghg-emissions. (accessed: Oct. 21, 2020).

Ritchie, H. (2019b). *Half of the world's habitable land is used for agriculture*. URL: https://ourworldindata.org/global-land-for-agriculture. (accessed: Oct. 21, 2020).

Rønsholdt, B. and E. McLean (2001). "Determination of total carotenoid content in rainbow trout muscle by multivariate calibration of VIS reflectance spectra". In: *Journal of Food Composition and Analysis* 14.4, pp. 345–357.

Sakshaug, E., G. H. Johnsen, and K. M. Kovacs (2009). *Ecosystem Barents Sea*. Tapir Academic Press.

Selding, P. B. de (2016). *Europe's Sentinel-3A Earth observation satellite successfully launched*. URL: https://spacenews.com/europes-sentinel-3a-earth-observation-satellite-successfully-launched/. (accessed: May. 11, 2021).

Shahidi, F. and P. Ambigaipalan (2018). "Omega-3 polyunsaturated fatty acids and their health benefits". In: *Annual review of food science and technology* 9, pp. 345–381.

Shaw, J., P. Nugent, and M. Vollmer (Dec. 2015). "Colors of the Yellowstone thermal pools for teaching optics". In:

Sigernes, F (2018). "Basic hyperspectral imaging". In: *TTK20 Hyperspectral remote sensing-lecture notes, Norwegian University of Science and Technology, Trondheim*.

SNL (2018). *Fresnels Likninger*. URL: https://snl.no/Fresnels_ligninger. (accessed: April. 26, 2021).

Sørensen, A. J. et al. (2020). "Sensor-Carrying Platforms". In: *POLAR NIGHT Marine Ecology*. Springer, pp. 241–275.

Specim (n.d.[a]). *sCMOS-50-V10E*. URL: https://www.specim.fi/products/scmos-50-v10e/. (accessed: Dec. 05, 2020).

— (n.d.[b]). *Specim FX10*. URL: https://www.specim.fi/products/specim-fx10/. (accessed: Dec. 05, 2020).

Swerdloff, A. (2016). *What If We Had All Listened to NASA ans Started Eating Krill?* URL: https://www.vice.com/en/article/aeakvb/what-if-we-had-all-listened-to-nasa-and-started-eating-krill. (accessed: May. 12, 2021).

Throndsen, J. (2018). *Planteplankton*. URL: https://snl.no/planteplankton. (accessed: 06. 07, 2021).

USGS (n.d.). *What is remote sensing and what is it used for?* URL: https://www.usgs.gov/faqs/what-remote-sensing-and-what-it-used?qt-news_science_products=0#qt-news_science_products. (accessed: June. 05, 2021).

Van Sebille, E. et al. (2015). "A global inventory of small floating plastic debris". In: *Environmental Research Letters* 10.12, p. 124006.

Wiborg, K. and K. Hansen (1974). "Fiske og utnyttelse av raudåte (Calanus finmarchicus Gunnerus)". In:

Yamashita, A., M. Fujii, and T. Kaneko (2007). "Color registration of underwater images for underwater sensing with consideration of light attenuation". In: *Proceedings 2007 IEEE International Conference on Robotics and Automation*. IEEE, pp. 4570–4575.

Yoerger, D. R. et al. (2018). "Mesobot: an autonomous underwater vehicle for tracking and sampling midwater targets". In: *2018 IEEE/OES Autonomous Underwater Vehicle Workshop (AUV)*. IEEE, pp. 1–7.

Ytreberg, R. (2019). *Fant 10 millioner tonn mer krill*. URL: https://www.dn.no/fiske/krill/aker-biomarine/havforskningsinstituttet/fant-10-millioner-tonn-mer-krill/2-1-656979. (accessed: Sept. 07, 2020).

Appendix A

Appendix

A.1 Description of Imaging Process

Table A.1: Description of process

Time	Action	Purpose
11.24	Turning off lights in the room, turning on the system	We want as little noise and light disturbance as possible.
11.27	Setting binning and FPS parameters	We use the parameters that performed best in our last test. This is a spectral and spatial binning of four, and five frames per second.
11.44	Obtaining focus	The focus precision is essential as the organisms are tiny.
11.55	Experimenting with motor speed	The motor speed is changed to obtain the most precise images. A slower motor speed gives sharper, undistorted images, but takes a long time. The optimal balance between sharpness and scanning time is sought.
12.00	Applying micron particles for size measurements	To obtain a visual measurement of the organisms, we use standard 230-micron spherical particles for size comparisons.
12.29	Changing field of view	We change the field of view to image more copepods. Ideally, 7-10 copepods should be sharp and in focus in the image.
12.30	Increasing motor speed to 0.10 mm/s	We change motor speed to have faster scans. The impact on the resulting sharpness is unnoticeable.
12.45	Increasing field of view	Field of view is increased again to have as many copepods as desired.
12.46	Settings OK	We are satisfied with the settings, and run a couple of scans. The scans include both a dark frame and a white frame for later processing of the data.
12.56	Transmittance scans	We change light but use the same settings. Copepods are moved between scans to ensure satisfactory results.
12.14	Lights are changed again	We run a last scan using reflectance light. This is to have the same position of the copepods also with the reflectance light.
13.48	We change to wild copepods	We put in-situ copepods in the petri-dish. We only have six, so it is challenging to place them in the image area.
13.58	We change to backlighting	We run a couple of scans of the in-situ copepods in reflection light
14.09	We change to reflectance light	We run a couple of scans of the in-situ copepods in transmittance light

A.2 Additional Results

A.2.1 Transmittance with Laboratory Copepods, Experiment 1

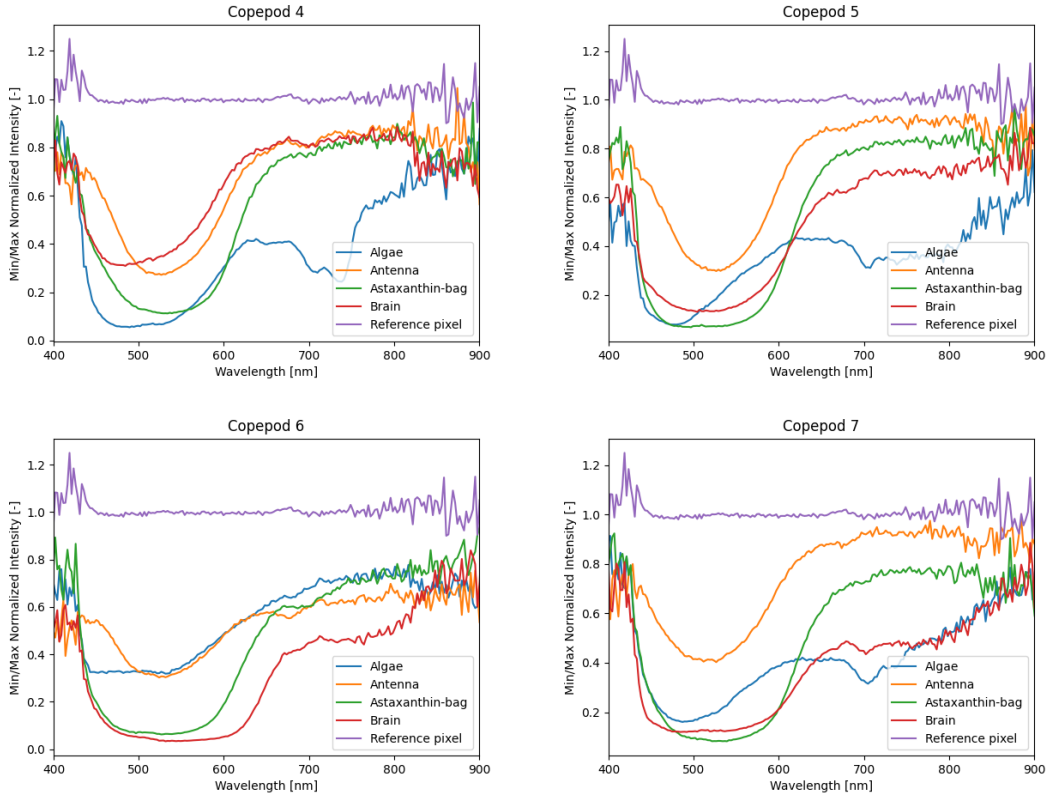

FIGURE A.1: The same area in each copepod plotted together.

A.2.2 Transmittance with Wild Copepods, Experiment 2

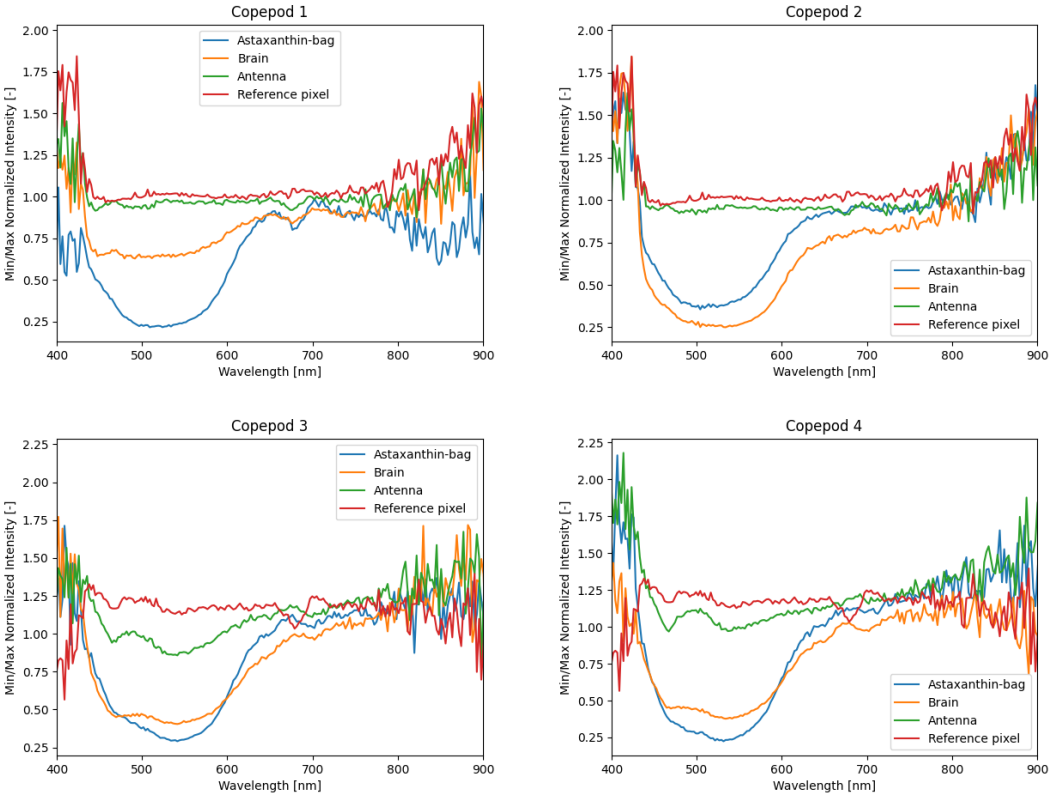

FIGURE A.2: The same area in each copepod plotted together.

A.2.3 Transmittance with Laboratory Copepods, Experiment 2

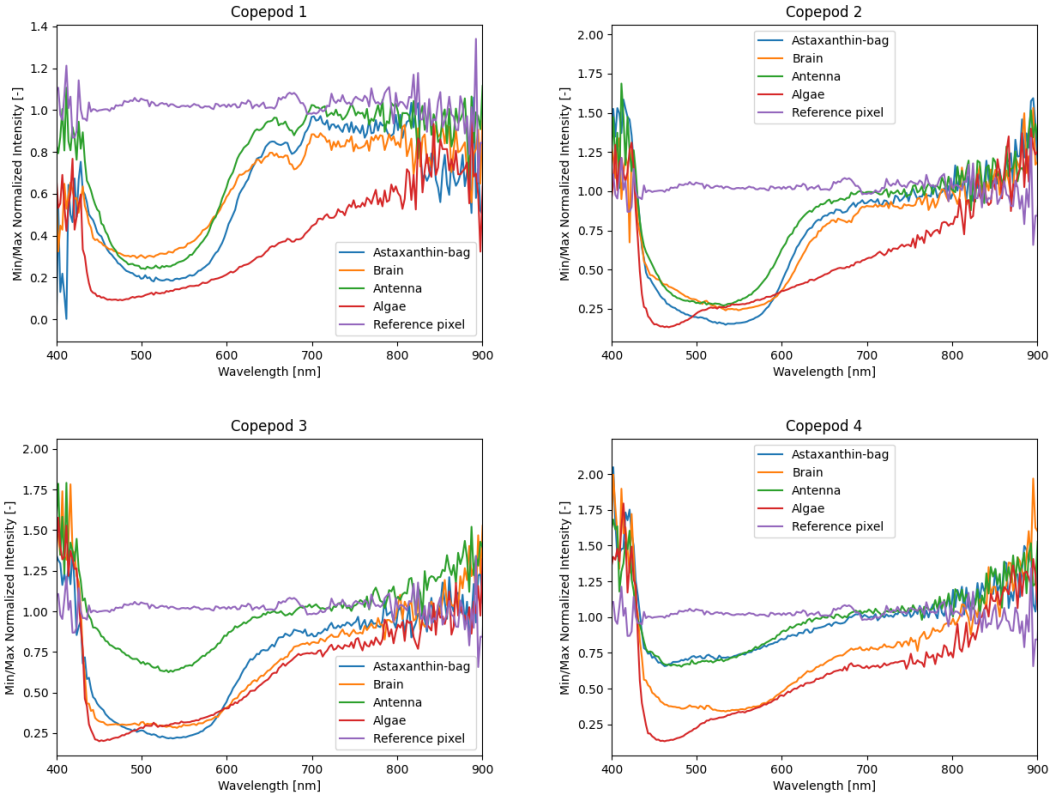

FIGURE A.3: The same area in each copepod plotted together.

A.2.4 Reflectance with Wild Copepods, Experiment 2

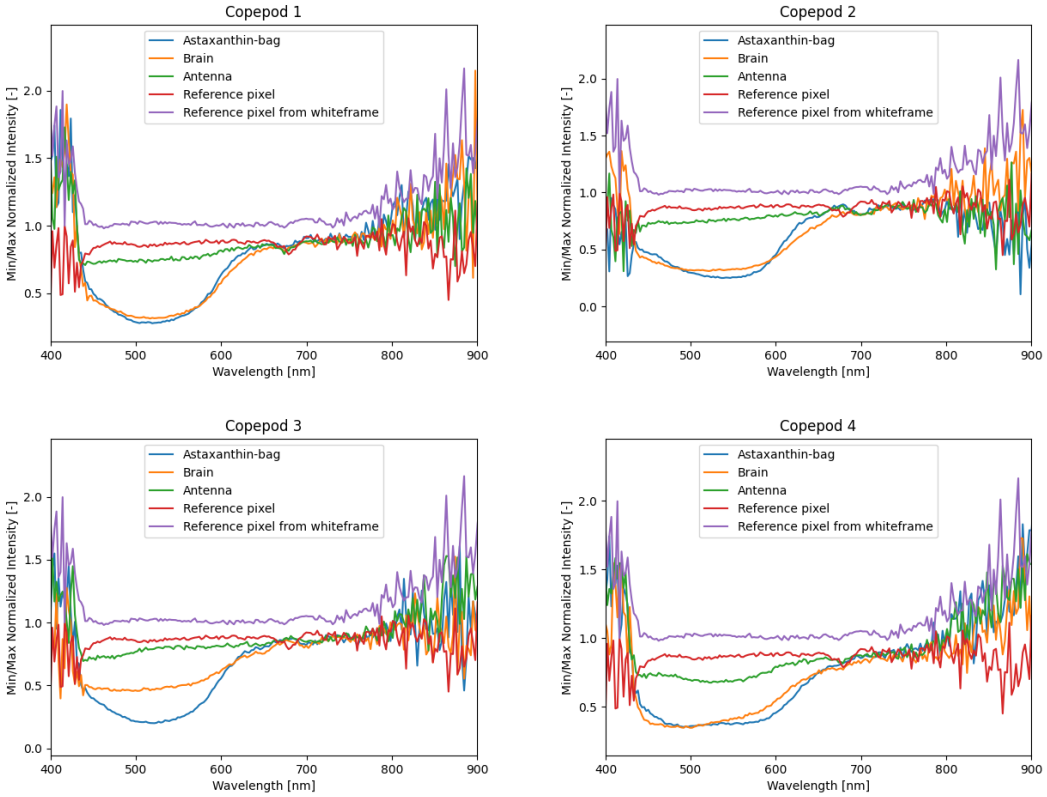

FIGURE A.4: The same area in each copepod plotted together.

A.2.5 Reflectance with Laboratory Copepods, Experiment 2

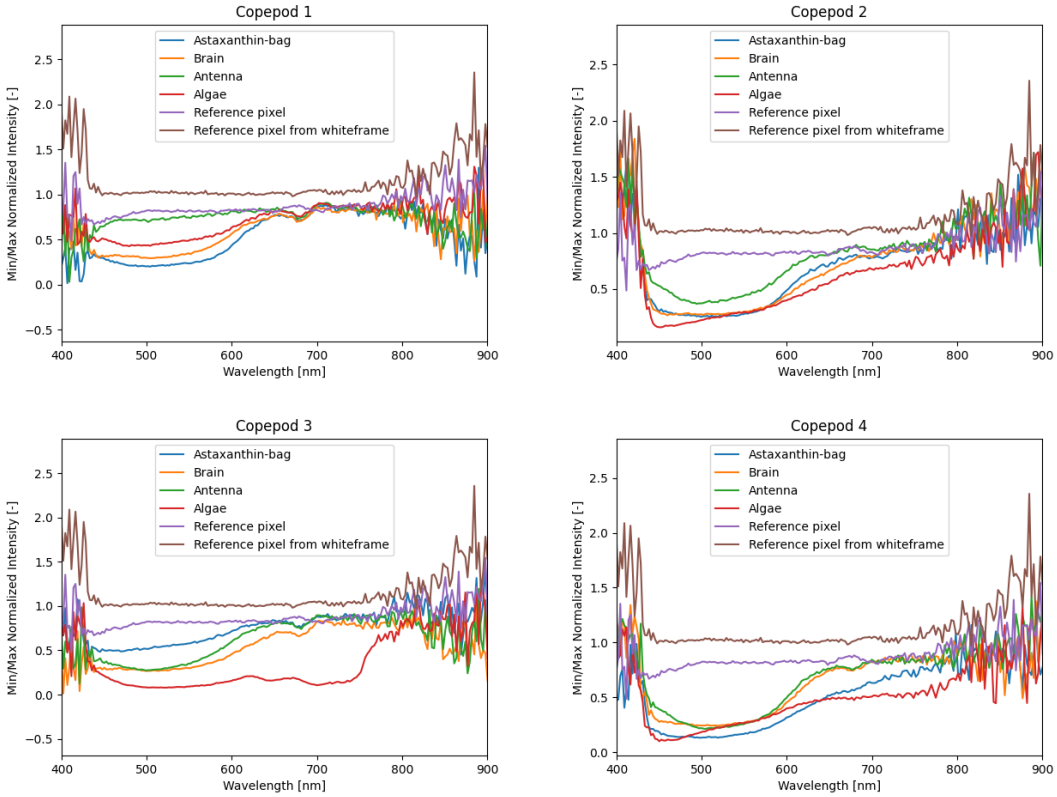

FIGURE A.5: The same area in each copepod plotted together.

Nora Solheim Stuedal

Methods for Mapping of Zooplankton using Optical Sensor Technology

NTNU
Norwegian University of
Science and Technology